

Congenital Disorders of the Brain and Spine

TIMING OF FORMATION OF CONGENITAL LESIONS

It is very important to understand the timing of congenital lesions in the brain and spine and how it is that one can get multiple spinal, supratentorial, and infratentorial anomalies all in the same individual. To put things very simply, the central nervous system (CNS) goes through a five-stage process that includes dorsal induction (3 to 4 weeks' gestation), ventral induction (5 to 8 weeks' gestation), neuronal proliferation/differentiation/histogenesis (8 to 18 weeks' gestation), migration (12 to 22 weeks' gestation), and myelination (5 months fetal age to years postnatal age). The cortex goes through stages of cell proliferation, cell migration, and cortical organization in utero at 2 to 4 months, 3 to 5 months, and at 5 months to 2 years postgestation, respectively.

Dorsal Induction

Under the rubric of dorsal induction, the brain undergoes primary and secondary neurulation; that is, turning a flat bed of cells into a round piece of brain and spinal cord.

Disorders of primary neurulation predominantly affect the spinal cord and include those due to adhesions between the inwardly oriented endoderm and the outer ectoderm. This is the presumed etiology for neurenteric cysts and diastematomyelia. If there is premature separation of the neuroectoderm and the cutaneous ectoderm, it is usually the fat that is left behind and fuses with the neuroectoderm. This produces the lipomyelocele, lipomyelomeningocele, and the intradural lipoma. If the separation never occurs, one gets persistent communication of the CNS with internal or external structures, hence cephaloceles, myeloceles, meningomyeloceles, anencephaly, exencephaly (brain outside the skull), craniorachischisis (congenital fissure of the skull and spine), and dermal sinus tracts. These entities may be associated with the Chiari II malformation because the posterior fossa calvarium is developing at the same time.

Disorders of secondary neurulation generally affect the conus medullaris, filum terminale, and cauda equina. Lipomas of the filum, short thickened tethered fila and tethered cords, and caudal regression syndrome with sacral agenesis are usually listed under this category.

Ventral Induction

Holoprosencephaly represents the signature anomaly associated with failure of ventral induction. Because the premaxillary facial structures are formed in association with ventral induction, it is not uncommon to see cyclopia and probosci in patients with ventral induction failures. Septo-optic dysplasia and pituitary anomalies are also disorders of ventral induction.

Cerebellar development also occurs at the 5- to 15-week period of fetal development. Just as there is cerebral hemispheric development from neural tissue derived from the germinal matrix around the lateral ventricles, so too is cerebellar development dependent on the germinal matrix about the fourth ventricle. Because hemispheric development occurs before vermian development and the superior vermis forms before the inferior vermis, it is rare to see hemispheric anomalies without vermian maldevelopments or superior vermian lesions without associated inferior vermian anomalies. Inferior vermian hypoplasia may be

seen in isolation. Those entities associated with vermian dysgenesis include the Dandy-Walker complex lesions (Dandy-Walker malformation, Dandy-Walker variant, and giant cisterna magna), rhombencephalosynapsis, and Joubert syndrome.

Disorders of hemispheric development include hemispheric hypoplasia, but this is a rare bird more commonly seen with other supratentorial and vermian anomalies.

Neuronal Proliferation, Differentiation, and Histogenesis

Disorders of neuronal proliferation, differentiation, and histogenesis are disorders that occur because of abnormal proliferation, such as microencephaly, macroencephaly, neurocutaneous syndromes, and aqueductal stenosis. Microencephaly and micro-lissencephaly occur because of too few neurons, less brain tissue. In megalencephaly, one has marked overproduction of neurons. Primary causes include achondroplasia, Soto syndrome, and Beckwith-Wiedemann syndrome.

Neuronal Migration

Neuronal migrational anomalies are based on the centrifugal movement of neuroblasts and glioblasts along radial glial fibers. From the periventricular region, the neuroblasts are first to migrate and they take up residence in the molecular layer of cortical zone 1, the most peripheral of the gray matter zones. Cells (glioblasts and neuroblasts) from the intermediate zone then migrate in fan-like waves along radial glial fibers out to the periphery and then double back on themselves to first fill the sixth deepest layer of the cortex, followed by cortical zones 5, 4, 3, and 2. Somehow, this is supposed to result in cortical organization, creating the many layers of the brain and mind. When this gets mixed up, one has classic lissencephaly, heterotopia, pachygyria, polymicrogyria, schizencephaly, and the like.

Myelination

White matter, when myelinated, is bright on a T1-weighted image (T1WI) and dark on a T2WI. The development of myelination is a complicated process but proceeds from posterior to anterior and from central to peripheral (Table 9-1 and Box 9-1). Barkovitch has done a good job in mapping normal myelination dates in term babies. In general, the white matter is seen to be myelinated earlier on T1WI than on T2WI for reasons that have to do with water content versus lipid content. It then takes a bit of wizardry to apply this to the premature infant. Table 9-1 is a good start for determining if there is delayed myelination.

Then along came fluid-attenuated inversion recovery (FLAIR) imaging. The signal intensity of white matter on FLAIR initially is dark because of the marked water content, turns brighter as the "watery brain" of infancy resolves, then again becomes dark as the white matter myelinates. The timing of these stages, summarized in Table 9-1, varies from structure to structure. The cerebellar peduncle and the posterior limb of the internal capsule show high signal intensity relative to gray matter at birth. Thereafter, the white matter loses signal intensity with time and shows low signal intensity at age 50 weeks and beyond. The unmyelinated white matter, including the frontal deep white matter, the occipital deep white matter, and the centrum semiovale, shows low signal

TABLE 9-1. Timing of Myelination

Structure	T1-weighted Scans	T2-weighted Scans	FLAIR Scans
Posterior limb internal capsule (posterior portion)	Birth	Birth–2 mo	3 mo
Dorsal brain stem	Birth	2–4 mo	3–5 mo
Cerebellar peduncles	Birth	Birth–2 mo	1–3 mo
Precentral and postcentral gyrus	Birth	2–3 mo	
Posterior limb internal capsule (anterior portion)	Birth–1 mo	4–7 mo	3–8 mo
Anterior limb internal capsule	2–3 mo	5–11 mo	8–11 mo
Cerebellar white matter	3 mo	3–5 mo	
Splenium	3–4 mo	4–6 mo	5 mo
Genu callosum	4–6 mo	5–8 mo	5 mo
Occipital white matter (central)	3–5 mo	9–14 mo	1, 12 mo
Frontal white matter (central)	4–6 mo	11–16 mo	2, 14 mo
Occipital white matter (peripheral)	6 mo	11–15 mo	
Frontal white matter (peripheral)	7–11 mo	13–18 mo	
Normal maturation	8–11 mo	14–18 mo	24 mo

Box 9-1. Trends in Myelination

Posterior to anterior
 Central to peripheral
 Motor to sensory
 Inferior to superior
 T1WI to T2WI
 Immature to mature

intensity at birth, converts to high signal intensity at age 20 to 30 weeks, and back to low signal intensity after age 2 to 3 years.

It is useful to separate congenital disorders of the brain into those involving the supratentorial structures and those involving the infratentorial structures, because radiologists think in terms of anatomy rather than embryology. We synthesize information based on imaging findings and then think about developmental issues later.

Naturally, disorders can affect both spaces, but as an initial classification scheme, this may be helpful. In addition, in a newborn infant, separating the lesions into those that are cystic and those that are solid is of some help in arriving at a differential diagnosis. Clinical information is also useful in distinguishing among various congenital abnormalities, because several disorders also have associated cutaneous, ocular, or metabolic abnormalities.

— SUPRATENTORIAL CONGENITAL LESIONS**Arachnoid Cysts**

If you had to have a congenital lesion in the brain, this would be the lesion of choice. The arachnoid cyst is the most common congenital cystic abnormality in the brain. It consists of a cerebrospinal

fluid (CSF) collection within layers of the arachnoid. The cyst may distort the normal brain parenchyma.

The arachnoid cyst is typically a serendipitous finding and may not be symptomatic. The most common supratentorial locations for an arachnoid cyst are (in decreasing order of frequency) (1) the middle cranial fossa, (2) parasellar cisterns, and (3) the subarachnoid space over the convexities (Fig. 9-1). Infratentorially (see Infratentorial Abnormalities later in this chapter), arachnoid cysts commonly occur in the (1) retrocerebellar cisterns, (2) cerebellopontine angle cistern, and (3) quadrigeminal plate cistern. Intraventricular cysts are rare but favor lateral and third ventricles (Fig. 9-2).

Computed tomography (CT) scans demonstrate a CSF density mass that typically effaces the adjacent sulci and may remodel bone. The mass measures from 0 to 20 Hounsfield units (HU) and shows no enhancement. In those difficult cases where an arachnoid cyst and a dilated subarachnoid space must be distinguished, one can instill intrathecal contrast to differentiate the cyst (which does not immediately fill with contrast) from the subarachnoid space (which immediately fills) (Fig. 9-3). Be careful though. In time, the arachnoid cyst will imbibe contrast.

On magnetic resonance (MR) imaging the most common appearance is that of an extra-axial mass that has signal intensity identical to CSF on all pulse sequences. Occasionally, the signal intensity may be greater than that of CSF on proton density-weighted images (PDWI) because of the stasis of fluid within the cyst as opposed to the pulsatile CSF of the ventricular system and subarachnoid space. FLAIR and diffusion-weighted imaging (DWI) usually show a dark mass similar in intensity to CSF (again pulsation effects may cause some higher intensity). Rarely, the fluid within the arachnoid cyst may be of higher protein content than CSF, accounting for the difference in signal intensity.

The differential diagnosis of an arachnoid cyst is limited and generally revolves around three other diagnoses: a subdural hygroma, dilation of normal subarachnoid space secondary to underlying atrophy or encephalomalacia, and epidermoid (Table 9-2; see also Fig. 6-1). Although subdural hygromas have been thought to be due to chronic CSF leaks through traumatized leptomeninges, in most cases the trauma results in sufficient blood deposited within the “hygroma” so that the signal intensity on

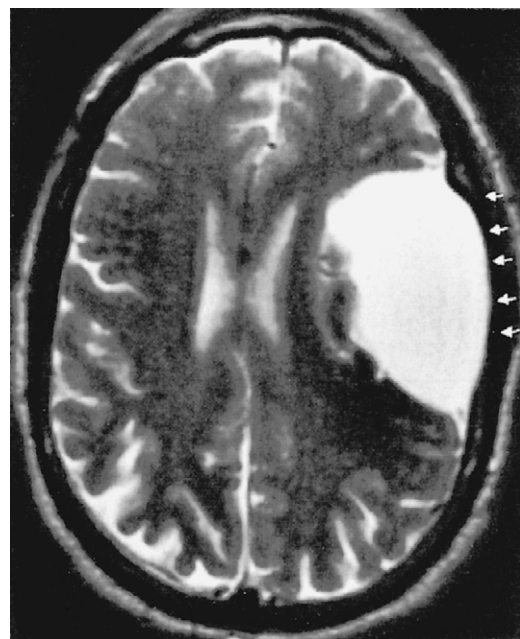


FIGURE 9-1. Arachnoid cyst. T2-weighted image at the level of the lateral ventricle shows a cerebrospinal fluid intensity collection that remodels the bone (arrows) and causes mild midline shift.

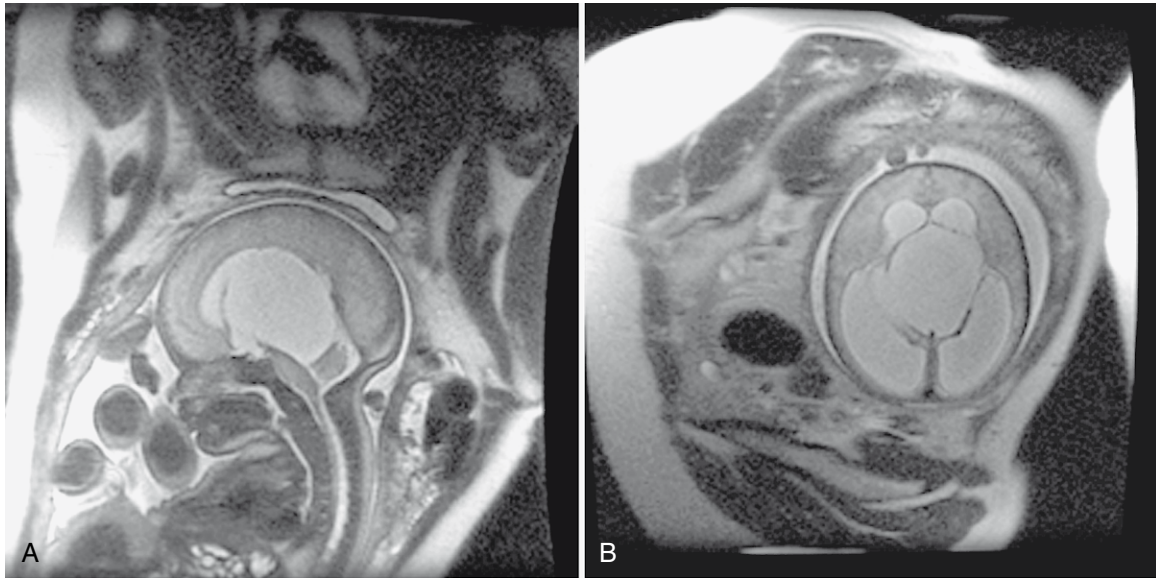


FIGURE 9-2. Fetal imaging of an arachnoid cyst. **A,** The in utero magnetic resonance image defined an arachnoid cyst of the third ventricle, which was misinterpreted as hydrocephalus. Treated intrauterine and baby did well. **B,** There was hydrocephalus, but the ballooning of the third ventricle was the cyst itself.

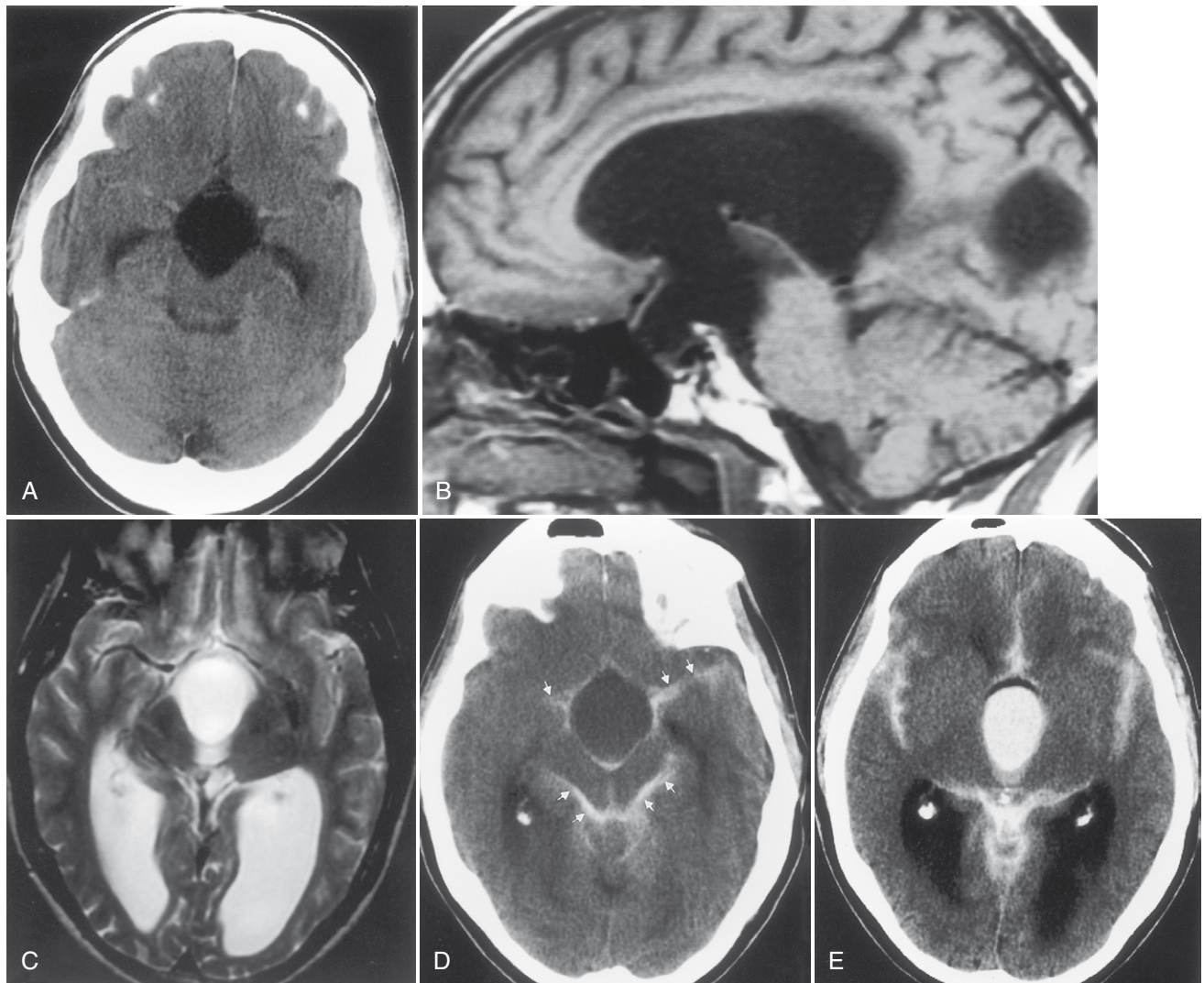


FIGURE 9-3. Arachnoid cyst of third ventricle. **A,** Initial unenhanced computed tomography (CT) scan showed a cystic mass widening the third ventricle. **B,** Sagittal T1-weighted image (T1WI) showed a mass with the same intensity as cerebrospinal fluid (CSF) that appears to communicate with the lateral ventricular system and extend into the sella. **C,** T2WI showed the lesion to have the same signal intensity as CSF. **D,** Intrathecal contrast was administered from a lumbar approach, and the contrast was allowed to flow superiorly to the intracranial compartment. The initial CT scan showed minimal filling of the cyst. Contrast material is in the subarachnoid space (*arrows*). **E,** On delayed axial scans the cyst filled with contrast. This is characteristic of an arachnoid cyst.

TABLE 9-2. Arachnoid Cyst vs. Subdural Hygroma, Epidermoid, Encephalomalacia

Feature	Arachnoid Cyst	Subdural Hygroma	Epidermoid	Widened CSF Spaces as a Result of Atrophy*
Intensity	Isointense to CSF on all sequences	Hyperintense to CSF on T1WI	Hyperintense on FLAIR, slightly hyperintense to CSF on T1	Isointense to CSF on all sequences
Vein location	Pushed inward	Pushed inward	Nondisplaced; epidermoids envelop vascular structures	Coursing through CSF
Mass effect	Positive	Positive	Positive	Negative
Bone remodeling	Present	Absent	Intradural epidermoids slowly remodel bone; intradiploic epidermoids have beveled edges	Absent
Sulci	Flattened	Flattened	Grows into sulcal space	Enlarged
Intrathecal contrast	Delayed opacification	Does not opacify	Outlines mass	Immediate opacification
DWI	Dark	Variable	Bright	Dark
Ca ⁺⁺ /Fat	(-/-)	(+/-)	(±/±)	(-/-)

CSF, cerebrospinal fluid; DWI, diffusion-weighted imaging; FLAIR, fluid-attenuated inversion recovery; T1WI, T1-weighted image.

*Includes large cisterna magna.

T1WI and FLAIR is different from that of CSF. In addition, subdural hygromas are typically crescentic in shape, whereas arachnoid cysts tend to have convex borders. Both efface sulci and show mass effect. In contradistinction, dilation of the subarachnoid space secondary to underlying encephalomalacia does not demonstrate mass effect and the adjacent sulci are enlarged. Another distinguishing feature is the fact that the cerebral veins in the subarachnoid space are seen to course through the CSF in the case of underlying encephalomalacia, as opposed to the subdural hygroma and arachnoid cyst, where the veins are displaced inward. An epidermoid may simulate an arachnoid cyst on CT and T2WI; however, FLAIR and DWI nicely show higher signal intensity than CSF. In fact, the T1WI will often also be brighter than CSF and will be obvious.

A feature, often seen in association with arachnoid cysts, that may suggest the diagnosis is bony scalloping. The bone may be thinned or remodeled, probably because of transmitted pulsations or slow growth. This would not be seen with hygromatous collections or atrophy. However, the finding may be seen occasionally in epidermoids or with porencephaly, where the ventricular pulsations may be transmitted through the porencephalic cavity to the inner table of the skull (see Fig. 8-21). When arachnoid cysts are seen in the middle cranial fossa, the temporal lobe may be hypoplastic. Absence of soft-tissue intensity or density, calcification, or fat distinguishes arachnoid cysts from those of the dermoid-epidermoid line.

Pineal cysts are discussed in Chapter 3.

Rathke Cleft Cysts

Rathke cleft cysts are embryologic remnants of Rathke's pouch, the neuroectoderm that ascends from the oral cavity to the sellar region to form the pituitary anterior lobe and pars intermedia. These cysts are lined with a single layer of cuboidal or columnar cells and may arise within the sella, the suprasellar region, or most commonly both. They occur in up to 13% of autopsy studies of the sella. The cysts can compress normal posterior or anterior pituitary tissue to cause symptoms of hypopituitarism, diabetes insipidus, headache, and visual field deficits but are usually asymptomatic. The cysts are well-defined masses that on MR may have high or low signal intensity on T1WI and high signal intensity on T2WI, and on CT are hypodense and most often nonenhancing (see Fig. 11-31). Intracystic, yellow waxy solid nodules have recently been reported in Rathke cysts containing

cholesterol or mucinous proteins probably accounting for the bright signal on T1WI in some cysts. The differential diagnosis is a craniopharyngioma or hemorrhagic pituitary gland; the presence of calcification, soft-tissue mass, or areas of enhancement would lead one away from Rathke cleft cyst as the diagnosis (see Chapter 11). Treatment is cyst aspiration or removal with little chance of recurrence.

Meningoencephaloceles

A meningocele is a congenital malformation in which the meninges protrude through the bony confines. As opposed to encephaloceles, meningoceles do not include brain tissue within the protrusion. Usually, an encephalocele also contains meninges, so it should really be called a *meningoencephalocele*. In fact, clinicians have become resigned to use the shortened noun *cephalocele*. The terms are used interchangeably in this chapter. Meningocele is rarer than encephalocele. The most common location for meningoencephaloceles associated with Chiari III malformations is the occipital region. These may also be associated with holoprosencephaly and aqueductal stenosis (Fig. 9-4). In the United States, parietal (10%) and frontal (9%) meningoencephaloceles are the next most common locations for this abnormality. Vietnamese and Southeast Asian women have a propensity for nasofrontal or sphenothmoidal meningoencephaloceles (Fig. 9-5). Recent descriptions of meningoceles of Meckel's cave account for the marked CSF enlargements sometimes seen in these locations. The diagnosis of meningoencephalocele is often made clinically when the protrusion is through the occipital, parietal, or frontal region. On the other hand, nasofrontal or sphenothmoidal encephaloceles may be clinically occult and may have a wide clinical differential diagnosis when seen through a nasoscope. Otorhinolaryngologists will love you if you let them know that the polyp they plan to remove from the nasal vault is actually the frontal lobe. The anterior meningoencephaloceles have a higher rate of associated anomalies, such as agenesis of the corpus callosum, colobomas, and cleft lips.

Encephaloceles may also be suspected when one sees enlargement of a basal neural foramen. An MR study will usually discern that there is herniated brain or CSF in the hole (Fig. 9-6). There often is a distortion of the adjacent brain tissue with maloriented white matter tracts.

On CT the meningocele is seen as a CSF density protrusion through a bony defect in the calvarium (Fig. 9-7). MR scans



FIGURE 9-4. Occipital encephalocele. Axial T2-weighted image shows protrusion of meninges (*arrow*) at the foramen magnum–C1 region. Patient had this lesion at birth.

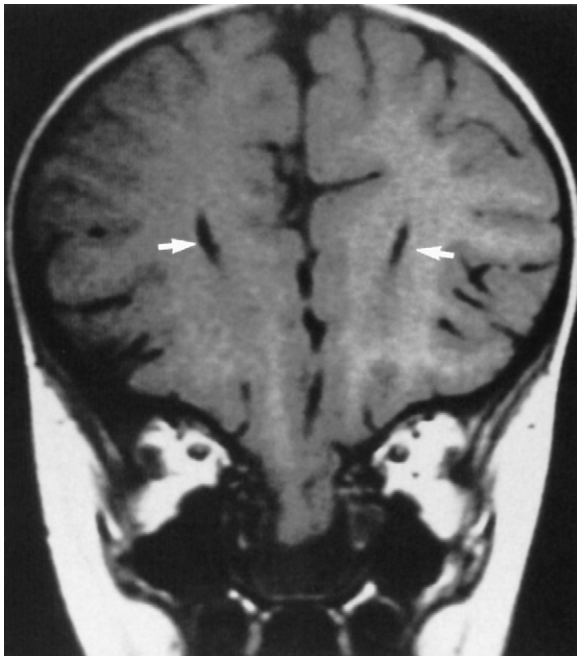


FIGURE 9-5. Anterior basal encephalocele. Coronal T1-weighted image demonstrates inferior displacement of the medial frontal lobes and gyrus rectus into the nasal cavity with hypertelorism. Wide frontal horns (*arrows*) suggest corpus callosum agenesis.

demonstrate continuity of the meningocele with the underlying leptomeninges. The critical task is to find the abnormality; secondarily one should tell the surgeons whether brain tissue is protruding through the defect. For this reason MR, with its superior soft-tissue resolution, is the primary study in this evaluation.



FIGURE 9-6. Basal cephalocele. Seizures were the presenting symptom in this patient with a right temporal encephalocele, which was herniating (*arrows*) into the basisphenoid.

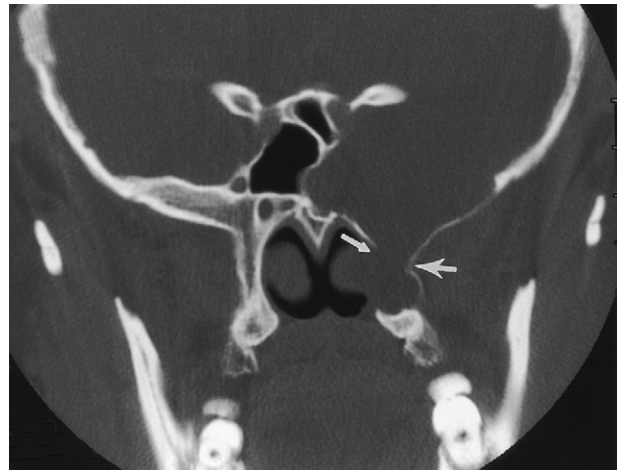


FIGURE 9-7. Meningocele. Coronal computed tomography demonstrates a defect in the skull base on the left side (*arrows*) with remodeling of the bone, indicative of a long-standing process. This represented a meningocele coming from the floor of the left middle cranial fossa.

The brain tissue within the meningoencephalocele typically has the signal intensity of normal brain. However, occasionally one may see heterotopic or disorganized brain tissue, which has a more heterogeneous signal intensity.

Neuroepithelial Cysts

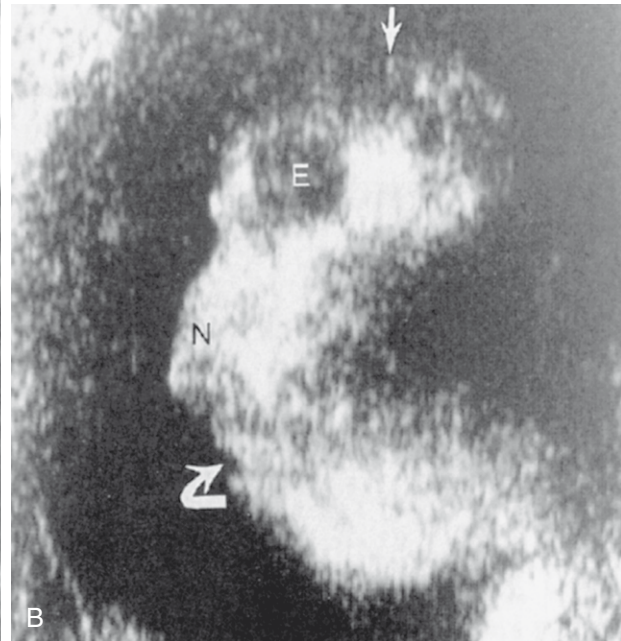
Neuroepithelial cysts may arise within the ependyma of the ventricular system. Although lateral ventricular cysts are most common, often associated with the glomus of the trigone, they may also occur in the other ventricles. Typically, they follow CSF intensity; however, they may be bright on T1WI owing to high protein, mucin, cholesterol, or viscous content. The lining of this cyst is epithelial, and they are thought to arise from ectoderm. Occasionally one may see these cysts randomly in the brain parenchyma, where they may simulate cystic lacunar infarctions in atypical locations. Differential diagnoses might include epidermoid cysts, cysticercosis, or echinococcal cysts.

Anencephaly

Anencephaly means no brain. Anencephaly should now be a diagnosis made prenatally because most women are screened relatively early in pregnancy for elevated levels of serum



FIGURE 9-8. Anencephaly. **A**, Obstetric ultrasound shows lack of development of the cranial vault (*arrow*) in this fetus. Eyes are marked by *asterisks*. **B**, Profile view of the face of the fetus shows nondevelopment of the skull (*arrow*) above the eye (E). N, nose; *curved arrow*, mouth. (Compliments of Peggy Brennecke, MD.)



α -fetoprotein, a marker of neural tube defects. The diagnosis by obstetric ultrasound (US) is made when the cranial vault is seen to be small, with only the fetus's face and posterior fossa well seen (Fig. 9-8). Only a nubbin of tissue is seen at the skull base on US, and amniotic fluid α -fetoprotein levels are elevated. These babies do not do well and may be allowed to die if the diagnosis is not made prenatally. An association with spinal dysraphism exists.

Hydranencephaly

Hydranencephaly has the appearance of absence of that part of the brain supplied by anterior and middle cerebral arteries. The parts of the brain supplied by the posterior circulation are preserved, so the posterior temporal lobes, occipital lobes, thalami, and infratentorial structures are well formed. The brain stops there. In place of the remainder of the brain is a CSF-contained space (Fig. 9-9). The chief differential diagnosis is termed "*maximal*" hydrocephalus (severe hydrocephalus with a thin cortical mantle plastered against the sides of the calvarium) (Fig. 9-10). This will also usually affect the occipital region as opposed to hydranencephaly. To detect this thin rim of cortical tissue, MR is probably more accurate than CT. Shunting is the treatment for maximal hydrocephalus; some return of function may occur with shunting. With hydranencephaly, no treatment is effective. Bad brain: bad prognosis.

Holoprosencephaly

Holoprosencephaly (Table 9-3) refers to a constellation of congenital abnormalities where separation of the right and left cerebral hemispheres is incomplete (Fig. 9-11). The range of this disorder includes a minor form, lobar holoprosencephaly, in which separation of the cerebral hemispheres and lateral ventricles is near normal but formation of an inter-hemispheric fissure and cerebral falx is incomplete. Even in



FIGURE 9-9. Hydranencephaly. Axial computed tomography shows absence of brain tissue in the anterior and middle cerebral artery distributions with preservation of the brain stem and cerebellum.

the mildest of forms you may see fusion of the hypothalamus, cingulum, and caudate nuclei. The frontal horns are closely apposed to each other, with partial fusion of frontal lobes. The most severe form is designated *alobar holoprosencephaly*, which demonstrates almost no separation of the cerebral hemispheres



FIGURE 9-10. Maximal hydrocephalus. The presence of a cortical mantle peripherally and bilaterally suggests that this case represents maximal hydrocephalus and NOT hydranencephaly.

and ventricles. One is left with a single large ventricle with a horseshoe-shaped appearance (monovertricle) (Fig. 9-12). No interhemispheric fissure, falx, or significant separation of the hemispheric structures is identified. The basal ganglia and thalami are fused, and the septum pellucidum and corpus callosum are absent. Because one needs an interhemispheric

TABLE 9-3. Holoprosencephaly Variants

Feature	Lobar	Semilobar	Alobar
Facial deformities (cyclopia)	None	None to minimal	Yes
Falx cerebri	Anterior tip missing or dysplastic	Absent	Present posteriorly
Thalami	Separated	Partially fused	Fused
Interhemispheric fissure	Formed	Present posteriorly	Absent
Dorsal cyst	No	No	Yes
Frontal horns	Yes, but unseparated	No	No
Septum pellucidum	Absent	Absent	Absent
Vascular	Normal	Normal except rudimentary deep veins	Azygous anterior cerebral artery, absent venous sinuses and deep veins
Splenium	Present	Posterior; may be present without genu or body	Absent
Third ventricle	Normal	Small	Absent
Occipital horns	Normal	Partially formed	Absent

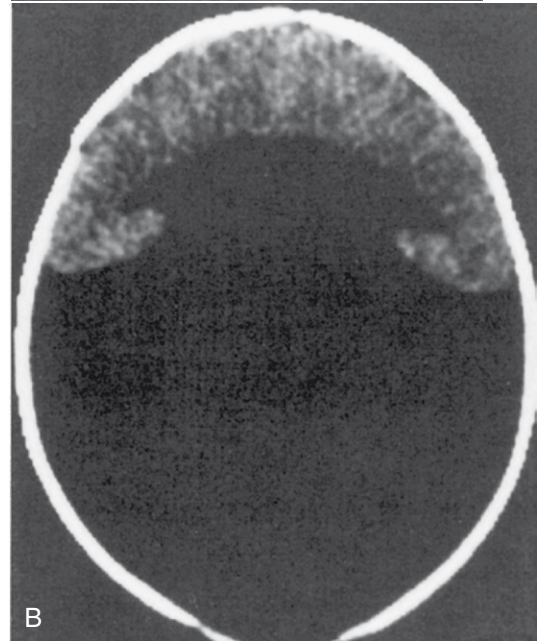


FIGURE 9-11. Holoprosencephaly. **A,** Interhemispheric fissure anteriorly is well formed; however, posteriorly the ventricles expand into a monoventricle with a shunt tube within it. Relatively well-developed anterior hemispheric fissure (*arrows*) suggests lobar holoprosencephaly. Note that no falx is seen. **B,** Monoventricle with no septum pellucidum or interhemispheric separation in a patient with alobar holoprosencephaly.

fissure to form the corpus callosum, it is not surprising that this is commonly absent in patients with holoprosencephaly. Similarly, a dorsal cyst will interfere with callosal formation in holoprosencephaly. Between the two extremes of lobar and alobar holoprosencephaly is semilobar holoprosencephaly, in which there is partial development of the falx and the interhemispheric fissure (with partial separation of the lateral ventricles) (Fig. 9-13). The basal ganglia and thalami are still fused. These abnormalities are associated with rather severe mental retardation, microencephaly, hypotelorism, and abnormal facies. The finding of a solitary median maxillary central incisor is also indicative of holoprosencephaly.

The CT findings in cases of holoprosencephaly include the absence or partial formation of the falx, interhemispheric fissure, and lateral ventricles. Patients typically have absence of the

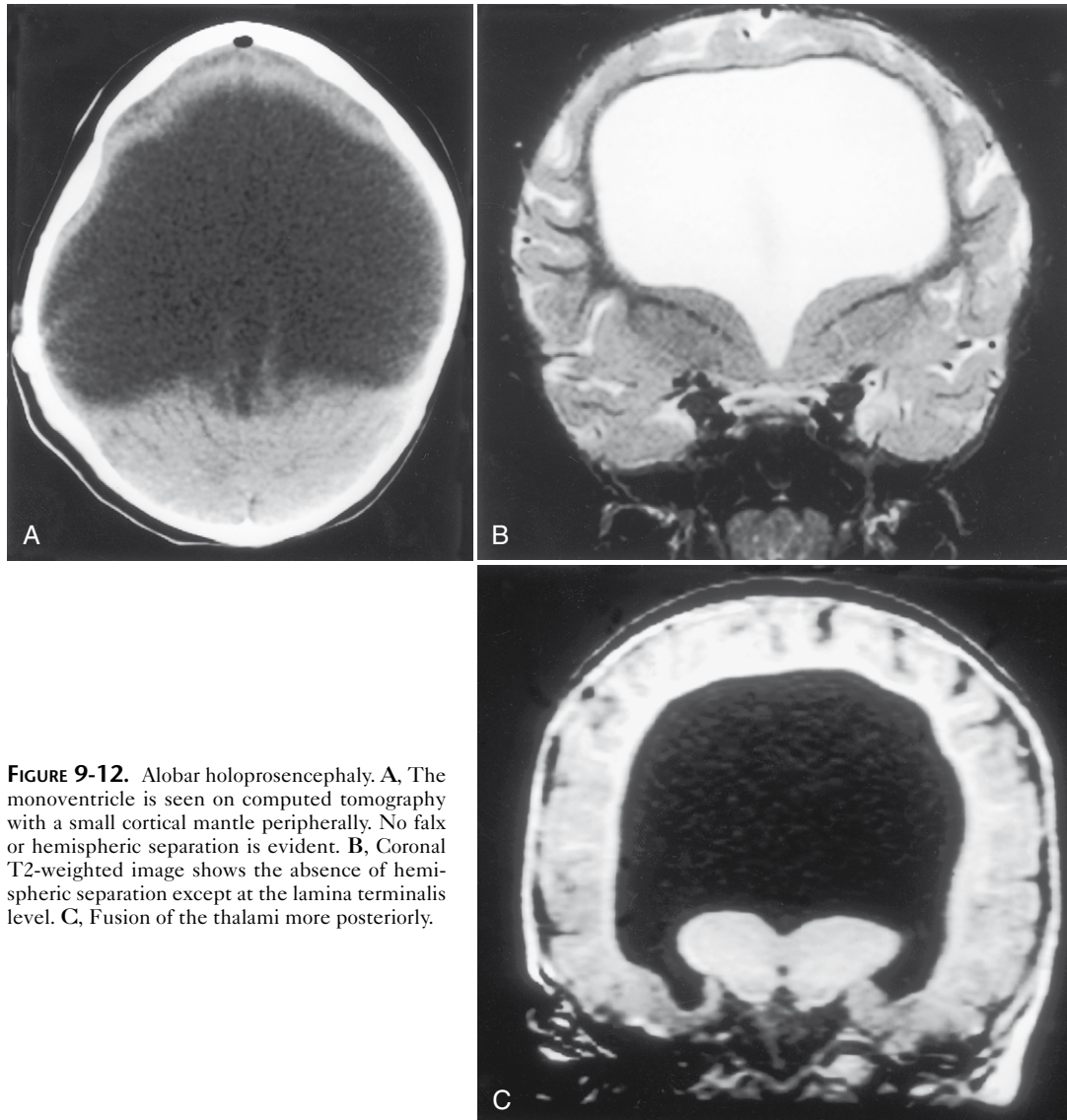


FIGURE 9-12. Alobar holoprosencephaly. **A**, The monovertricle is seen on computed tomography with a small cortical mantle peripherally. No falx or hemispheric separation is evident. **B**, Coronal T2-weighted image shows the absence of hemispheric separation except at the lamina terminalis level. **C**, Fusion of the thalami more posteriorly.

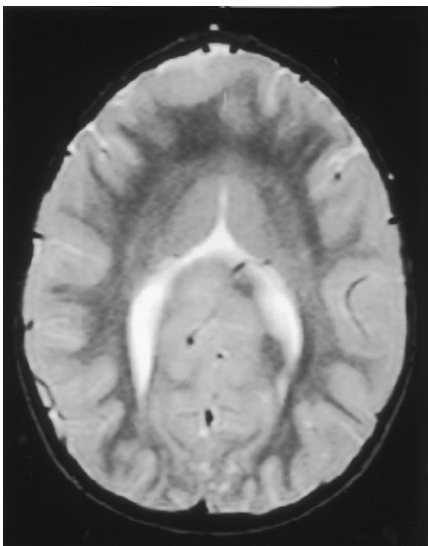


FIGURE 9-13. Semilobar holoprosencephaly. The posterior hemispheres are separated and the falx is implied to be present. The posterior ventricles look nearly normal but there is no development of the frontal horns. Fusion across the midline is seen anteriorly.

corpus callosum and an abnormally formed third ventricle. MR is a useful first study to examine patients with holoprosencephaly, because the evaluation of the corpus callosum, third ventricle, venous sinuses, vascular abnormalities, and septum pellucidum are better evaluated with MR. The olfactory bulbs and tracts are usually absent with lack of development of olfactory sulci and flat gyri recti. Associations with holoprosencephaly are listed in [Box 9-2](#).

Often you must distinguish alobar holoprosencephaly from hydranencephaly and “maximal” hydrocephalus. If no cortical mantle is discernible around the dilated CSF space centrally, the diagnosis is hydranencephaly, especially if all that can be seen is a nubbin of occipital or posterior temporal cortex remaining with a falx present. If you see a well-formed falx,

Box 9-2. Associations with Holoprosencephaly

- Caudal agenesis
- DiGeorge syndrome
- Fetal alcohol syndrome
- Kallmann syndrome
- Maternal diabetes
- Trisomy 13, 15, 18

cortical mantle, and separated ventricles with a septum pellucidum, consider maximal hydrocephalus. If the thalami are fused, septum pellucidum or falx is absent, a cortical mantle is seen, and the ventricles have lost their usual shape, diagnose alobar holoprosencephaly.

A pearl: Holoprosencephaly is the one lesion in which the splenium and posterior portions of the corpus callosum may be formed, but the anterior corpus callosum is absent. Exception to this exceptional rule: The rostrum normally forms after the splenium.

Septo-optic Dysplasia (De Morsier Syndrome)

Septo-optic dysplasia is best considered as part of the spectrum of holoprosencephaly. As such, it represents a minor form of holoprosencephaly. The septum pellucidum is either absent (64%) or partially absent (36%), causing a squared-off appearance to the frontal horns of the lateral ventricles (Fig. 9-14). When the septum pellucidum is partially absent, usually the anterior portion is present. This is best seen on coronal MR. Agenesis of the corpus callosum and white matter hypoplasia may be associated with this abnormality. In general, patients with septo-optic dysplasia demonstrate small hypoplastic optic nerves and a small optic chiasm resulting from the dysplastic optic pathways. In some cases that dysplasia may be limited to the optic disk and the nerves/chiasm may not be small. Patients often (60%) have hormonal abnormalities (usually diminished levels of growth hormone) related to the hypothalamic-pituitary axis abnormality. Check for pituitary gland hypoplasia. Seizures coexist. Effects on the visual pathway may range from blindness to normal vision, nystagmus to normal eye movements.

Schizencephaly (see section below) and neuronal migrational disorders may accompany septo-optic dysplasia in 50% of cases. Paradoxically, patients with the combination of schizencephaly and septo-optic dysplasia are more likely to have normal-sized ventricles, portions of the septum pellucidum spared, normal optic radiations, and seizures as a presentation. If schizencephaly does not coexist with septo-optic dysplasia, hypoplasia of the white matter (evidenced by corpus callosum thinning and ventricular enlargement), complete absence of the septum pellucidum, and worse hypothalamic-pituitary dysfunction usually are present.

Congenital Optic Nerve Hypoplasia

Congenital optic nerve hypoplasia commonly accompanies isolated growth hormone deficiency and multiple pituitary hormone deficiency syndromes. The absence of an anterior pituitary gland, a truncated pituitary stalk, and ectopic or absent posterior pituitary bright spot may also be found in this condition. Small optic nerves are a mandatory feature.

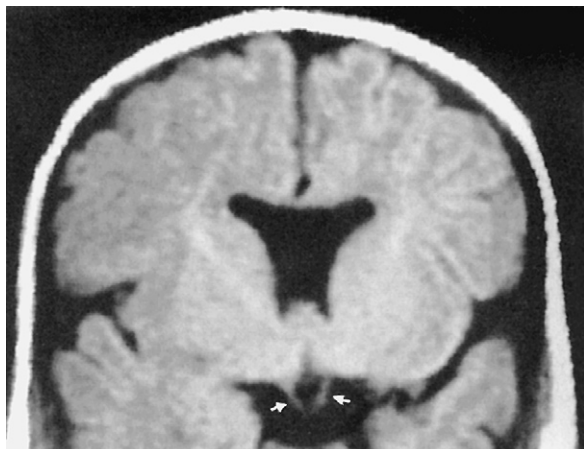


FIGURE 9-14. Septo-optic dysplasia. Coronal T1-weighted image shows absence of the septum pellucidum with small optic tracts (arrows).

Schizencephaly

Schizencephaly refers to an abnormality of neuronal migration at the fifth to seventh week of gestation in which a cleft is seen coursing from the ventricular ependyma to the pial surface of the brain. This cleft has a gray matter lining (usually from polymicrogyric brain) and is usually seen in the supratentorial space (near the sylvian fissure) coursing to the lateral ventricles. The lips of the cleft may be apposed (closed-lipped) (Fig. 9-15) or gaping (open-lipped). The closed-lipped variety may be missed if the clefts are tightly apposed, but a dimple at the ventricle-cleft interface should suggest the diagnosis. At the ventricular junction there often is associated nodular heterotopia. Schizencephaly occurs most commonly in the frontal (44%), frontoparietal (30%), and occipital (19%) lobes. Bilateral involvement (35% to 67%) is associated with seizures, worse developmental delay, and developmental dysphasia. Motor dysfunction is more common with frontal lobe schizencephaly, open-lipped varieties, and wider gaps in the open lips. Anomalous venous drainage may also be associated with schizencephalic brain. The cause of this disorder is thought to be an ischemic watershed insult in utero that leads to infarction of the germinal matrix and radial glial fibers near the ventricles. If there is failure of the germinal matrix to form, there will be fusion of the pia and the ependymal lining of the ventricles. Normal migration to the cortex is impeded. Other theories espoused as to etiology include toxin exposure, viral infections, and genetic factors. Schizencephaly is often associated with focal cortical dysplasia (polymicrogyria), gray matter heterotopias, agenesis of the septum pellucidum (80% to 90%), and pachygyria. Some believe that focal cortical dysplasias are a form of schizencephaly or vice versa—just that the “cleft” never reaches the ventricle in the former. The lining of the cleft with gray matter, best seen on

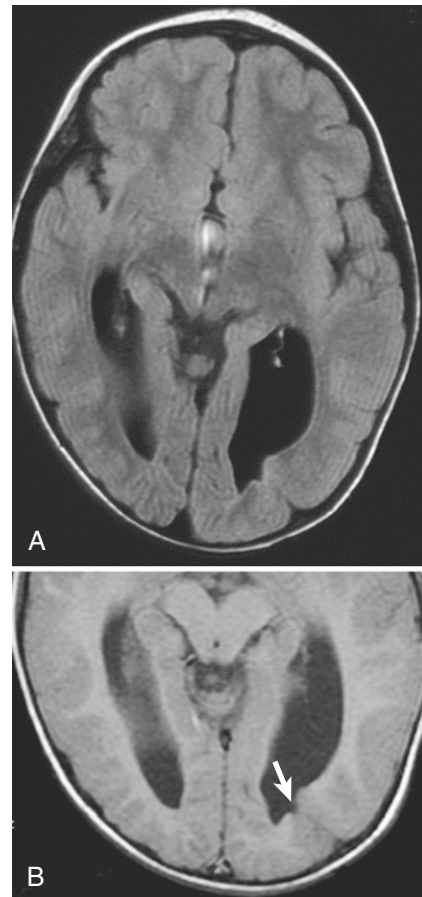


FIGURE 9-15. Schizencephaly. **A**, Can you find the evidence of the closed-lipped schizencephaly on this FLAIR scan? **B**, The nipple at the ventricular surface (arrow) on the T1-weighted image should eliminate any doubt.

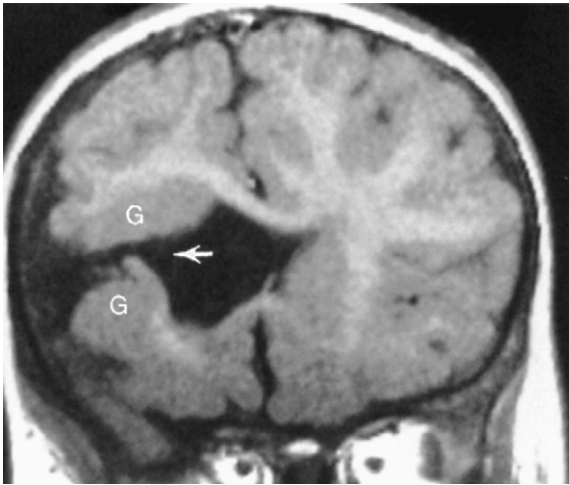


FIGURE 9-16. Schizencephaly. Coronal T1-weighted image reveals an open-lipped schizencephaly (*arrow*) connecting to the lateral ventricle. Note the gray matter-lined lips (G) of the cleft.

MR, is the differential point in this lesion and distinguishes it from encephalomalacic abnormalities (porencephaly), which are usually lined by white matter (Fig. 9-16). The inner surface of the cleft is pia-lined and communicates with the ependyma of the ventricle, which differentiates the lesion from an enlarged sylvian fissure seen in premature infants.

Agenesis of the Corpus Callosum

Agenesis of the corpus callosum is one of the more common congenital abnormalities (occurring in 0.7% of all births). Patients with this anomaly often present with refractile seizures or mental retardation. The corpus callosum develops from anterior genu to posterior splenium, accounting for splenial absence in partial agenesis of the corpus callosum. The rostrum is the last portion of the corpus callosum to form, so the combination of absence of the splenium with rostrum agenesis should not put the neuroradiologist into a quandary. MR is ideal for the visualization of the corpus callosum because a midline sagittal image demonstrates all the portions of the corpus callosum (Box 9-3). Various degrees of corpus callosum agenesis may occur after complete agenesis; loss of the splenium is the next most common manifestation of this disorder (Fig. 9-17). If the splenium is absent, colpocephaly, dilation of the occipital horns of the lateral ventricles caused by a decrease in the posterior white matter mass, is seen. With complete agenesis, a high-riding, posteriorly oriented, dilated third ventricle; parallel and widely spaced orientation of the lateral ventricles; and impression on the medial aspect of the lateral ventricles because of Probst bundles are seen. The longitudinal Probst bundle is a parallel track of white matter that runs anteroposteriorly and is due to the alternative white matter tract development when the corpus callosum is absent

Box 9-3. Findings in Agenesis of Corpus Callosum

- Colpocephaly
- High-riding enlarged third ventricle
- Incomplete development of hippocampal formation
- Interhemispheric cyst or lipoma
- Medial impingement of Probst bundle on ventricles
- Missing portions of corpus callosum
- No cingulate sulcus with radially oriented fissures (eversion of cingulate gyri) into the high-riding third ventricle
- Pointed, crescent-shaped frontal horns
- Septum pellucidum absent or widely separated

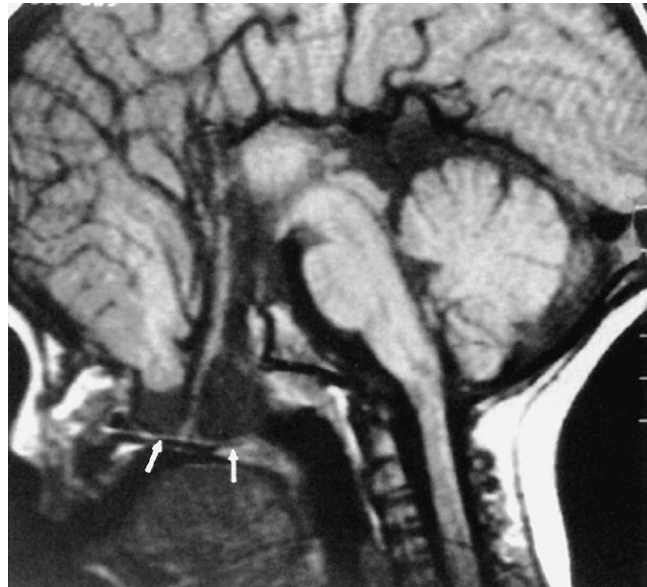


FIGURE 9-17. Agenesis of the corpus callosum. Sagittal T1-weighted image shows complete absence of the corpus callosum. Associated encephalocele in the basal region is identified by *arrows*.

(Fig. 9-18). As the fibers cannot cross, they redirect. The lateral ventricles (especially the occipital horns) are usually moderately dilated and concave medially, as is the third ventricle. Eversion of the cingulate gyrus is also present and the cingulate sulci are therefore not formed. This leads to a picture on the sagittal midline image where the medial hemispheric sulci extend down to the third ventricle. The third ventricle, in turn, extends into the interhemispheric fissure.

Other midline abnormalities may be associated with agenesis of the corpus callosum (see Box 9-3), such as an interhemispheric arachnoid cyst in the expected location of the corpus callosum or a pericallosal lipoma. A cyst would have low density on CT and signal intensity comparable to CSF on T1WI and T2WI. This can be distinguished from a lipoma (Fig. 9-19), which has fat intensity.

Associated congenital abnormalities include agyria, pachygyria, heterotopias, Dandy-Walker syndrome, holoprosencephaly, septo-optic dysplasia, cephaloceles, and Chiari I and II malformations. Trisomy 13, 15, and 18; fetal alcohol syndrome; and Meckel syndrome (occipital encephalocele, microcephaly, polycystic kidneys, polydactyly) are also associated with agenesis of the corpus callosum (and also with holoprosencephaly).

Aicardi syndrome is seen in female patients and consists of the triad of agenesis of the corpus callosum, epilepsy, and choroidal abnormalities. Abnormal myelination, neuronal migrational abnormalities, colobomas, posterior fossa cysts, and microphthalmia may coexist.

Hamartomas

Hamartomas represent an abnormal proliferation of normal brain tissue in an abnormal location. Whereas the heterotopias are due to anomalous neuronal migration, hamartomas are a non-neoplastic proliferation of well-organized brain tissue. There is a propensity for hamartomatous formation in the hypothalamus (see Fig. 11-39). The patients typically present with precocious puberty; however, occasionally, visual disturbances may be present, because the hypothalamic hamartoma involves the optic pathways. Boys are more commonly affected than girls, and symptoms may also include seizures or laughing spells (gelastic seizures). Because the tissue that makes up a hamartoma is essentially normal brain substance, the hamartoma is isodense to gray matter on CT. On MR, the hamartoma is isointense to gray matter on T1WI and variable on T2WI. The abnormality is

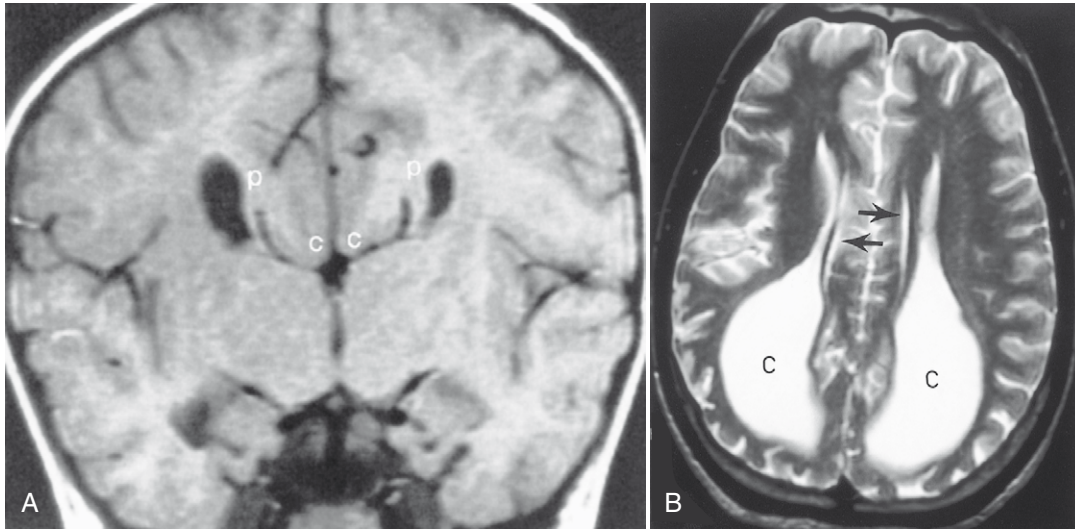


FIGURE 9-18. Agenesis of the corpus callosum. **A**, Probst bundle in agenesis of corpus callosum. Coronal T1-weighted image shows the Probst bundle (P) causing lateral displacement of the frontal horns of the lateral ventricles. Cingulate gyri (C) are malformed. **B**, The shape of the ventricles suggests agenesis of the corpus callosum with colpocephaly (c). Probst bundles account for the inward bowing of the lateral wall of the lateral ventricle. Evagination of the cingulate sulcus (arrows) accounts for the high signal intensity medial to the lateral ventricles.

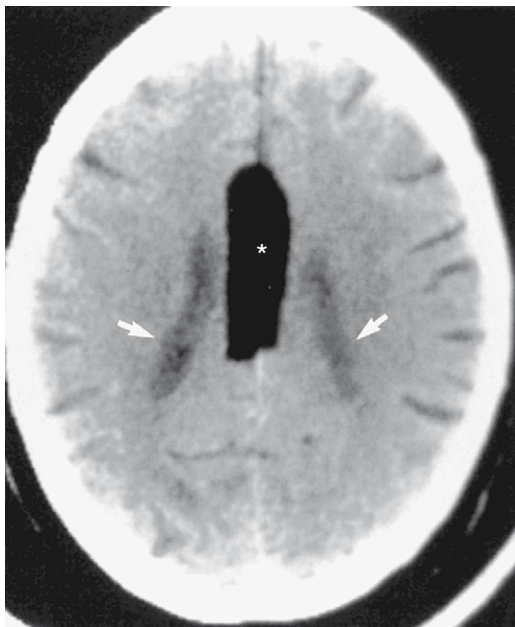


FIGURE 9-19. Agenesis of the corpus callosum with a fatty lipoma. Axial computed tomography reveals a low-density lipoma in the midline (asterisk) associated with agenesis of the corpus callosum. Lateral splaying of the lateral ventricles (arrows) is the tip-off to the agenesis.

identified as a bulbous protrusion of the hypothalamic region in the midline. The hamartomas do not have an abnormal blood-brain barrier and are not expected to show enhancement on either CT or MR. Occasionally, mass effect may be associated with the hamartoma, as evidenced by displacement of the inferior portion of the third ventricle.

Hamartomas may occur in other locations. After the hypothalamic region, the next most common location for hamartomas is the cerebral cortex-subcortical region. Occasionally hamartomas may be seen in a periventricular location.

Fetus in fetu refers to duplication of brain structures, usually seen as an extra-axial frontal region mass. The signal intensity approaches that of normal brain. Case studies of ectopic brain in the nasopharynx or pterygopalatine fossa have also been reported.

— ABNORMALITIES OF NEURONAL MIGRATION

Heterotopias

Heterotopic brain is disorganized brain tissue, usually gray matter, that is located in the wrong place because of a premature arrest in neuronal migration from the germinal matrix to the cerebral cortex (Fig. 9-20). Patients usually have seizures, weakness, spasticity, hyperreflexia, or developmental delay. Heterotopias form as a result of an abnormality in neuronal migration at the seventh to sixteenth week of gestation, when migration of the neuroblasts from the periventricular region to the pia is thwarted, possibly because of damage to the radial glial fibers, which orient migrating neurons. The classification of heterotopias is usually divided



FIGURE 9-20. Brain tumor ... NOT! The first-year fellow read the case as a low-grade glioma. No wonder our program is a two-year fellowship. The absence of edema and the isodensity to gray matter actually suggests a gray matter heterotopia. That is an OK miss in August (1 month into fellowship), but a May reprimand for a first-year fellow, and a “see you next year” at the CAQs.

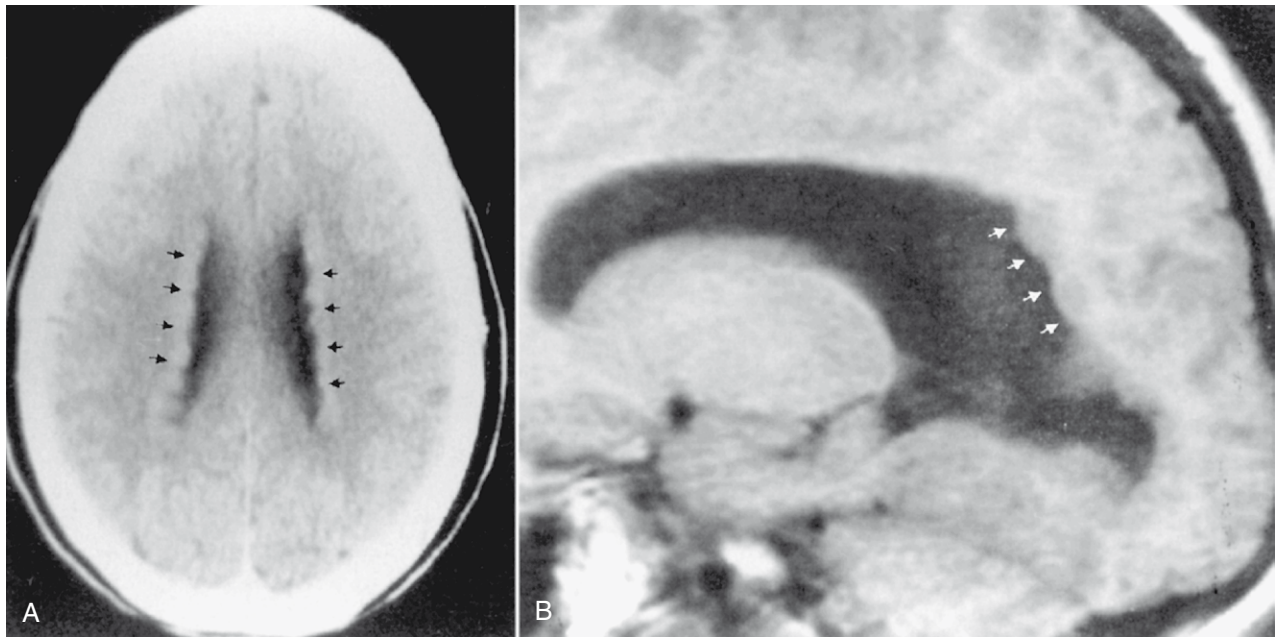


FIGURE 9-21. Heterotopia. **A**, Axial unenhanced computed tomography shows nodular subependymal heterotopia (*arrows*) bilaterally lining the lateral ventricle. This patient did not have tuberous sclerosis. **B**, Sagittal T1-weighted image shows indentation of the lateral ventricle by gray matter nodules (*arrows*) from subependymal heterotopia. Tuberous sclerosis nodules have intensity similar to white matter.

into two varieties: nodular and band types. Under nodular types, you will find subependymal/periventricular and subcortical variants. A subependymal location is very common, and these gray matter heterotopias are usually truly nodular in appearance (Fig. 9-21) and have the same signal intensity as gray matter. If there is hyperintensity on T1WI, it may be due to dystrophic microcalcifications, and these may show hyperdensity on CT. They may occur as an isolated anomaly or in association with other congenital lesions. A gene, responsible for the protein filamin-1, on the long arm of the X chromosome, has recently been implicated in some cases of nodular subependymal heterotopia. The favored sites are at the trigone or occipital horns of the lateral ventricles. They are bilateral in a high rate, but favor the right side over the left.

Patients with subcortical heterotopias often have abnormal sulcation patterns superficial to the heterotopia. The hemisphere ipsilateral to the site of the subcortical heterotopia may be smaller with thinning of the overlying cortex. Subcortical heterotopias may be nodular or curvilinear in shape. The nodular variety of subcortical heterotopias is usually identified in a periventricular or subcortical location, whereas the diffuse (or laminar) heterotopias are seen more commonly in or close to the cortex. These lesions do not enhance and do not elicit edema.

The band type of heterotopias is associated with severe developmental delay and earlier onset of seizures than the focal type (Fig. 9-22). The X-linked gene doublecortin (*DCX*) predisposes to lissencephaly in men and band heterotopia in women (protected by two X chromosomes). Band heterotopias are isointense with cortical gray matter with well-defined smooth margins. A thin interface of white matter is located between the band (laminar) heterotopia and the cortex, creating the double-cortex sign. The heterotopic tissue may demonstrate mass effect and distort deep gray or white matter structures. The overlying cortex may be abnormal as well due to abnormal sulcation/gyration/migration. Band heterotopias are explained as anomalies arising because of arrest of neuronal migration in the intermediate zone between the germinal matrix and the outer cortex (where the cells belong).

The abnormality is difficult to diagnose by CT but may be suggested when one identifies an island of higher density, non-enhancing tissue suggestive of gray matter in a white matter

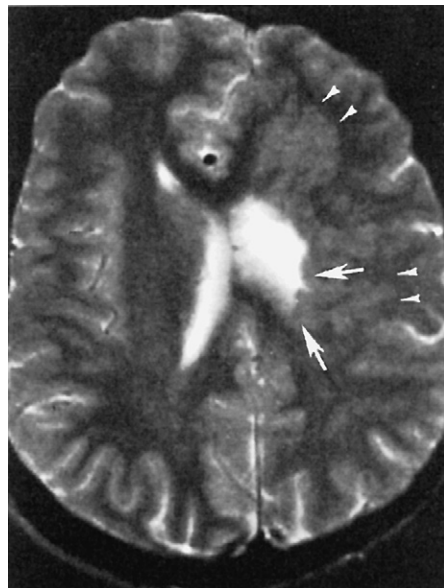


FIGURE 9-22. Subcortical heterotopia. Axial T2-weighted image delineates gray matter signal intensity within the centrum semiovale and corona radiata on the left side (*arrowheads*). Note the distortion of the left lateral ventricle at the interface with heterotopic gray matter (*arrows*).

location. These abnormalities are much better demonstrated with MR, where one can distinguish the gray matter from the white matter on T2WI with a high degree of accuracy. Within the dark myelinated white matter, one typically finds a higher signal intensity island of irregular tissue representing the heterotopia. Look for gray, white, gray, white, ventricle as the pattern for band heterotopias—it is the second gray that is the rub.

Encephaloceles, holoprosencephaly, schizencephaly, Chiari malformations, and agenesis of the corpus callosum may coexist with gray matter heterotopias.

Pachygyria

Pachygyria (incomplete lissencephaly) is a condition of short, broad, fat gyri caused by abnormal sulcation and gyration of the cortical mantle. It is a congenital abnormality that occurs relatively late in gestation, at 12 to 24 weeks, because of neuroblastic migration not proceeding completely to the superficial layers of the cortex (Fig. 9-23). At its most extreme, no sulcation at all may occur, creating a smoothly outlined hourglass configuration to the brain. No sylvian fissures are formed. This condition is termed *agyria* or *complete lissencephaly* and is due to abnormal formation of the superficial cortex of the brain, where incomplete neuroblastic migration to the six-layered cortex has occurred, possibly from cortical laminar necrosis of the third cortical layer. A bright rim around the cortex may be seen on T2WI because of this laminar necrosis in the “cell-sparse layer” of the cortex (Fig. 9-24). Patients with congenital cytomegalovirus (CMV) infection have

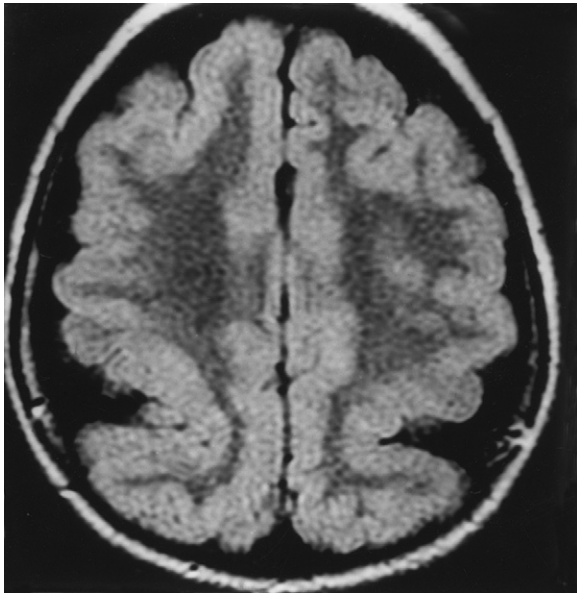


FIGURE 9-23. Pachygyria. Bilateral symmetric pachygyric brain is seen in the parietal lobes on this FLAIR image. The white matter does not arborize in these regions.

high rates of pachygyria. As opposed to hemimegalencephaly, white matter volume will be decreased; in both, gray matter appears thicker because of poor sulcation. Abnormal myelination may coexist.

Two chromosomes have been associated with lissencephaly. With those from the X chromosome (*DCX* gene), you tend to see more severe involvement with a frontal lobe predominance, most commonly in females. Classic lissencephaly (type 1) associated with the *LIS1* gene on chromosome 17 affects the parietal lobe more than the frontal lobe. Classic lissencephaly shows a smooth cortical surface with or without rudimentary gyral formation in the inferior frontal and temporal lobes and is due to arrest of cellular migration. High-intensity bands representing the cell-sparse layer are seen in the parieto-occipital regions. An hourglass configuration due to incomplete opercularization of the temporal lobes is representative.

Cobblestone lissencephaly (type 2) is seen in association with Fukuyama muscular dystrophy and Walker-Warburg syndrome. In this entity, you see nodular surface irregularities, ocular anomalies, and muscular disorders. The neuroblasts have migrated beyond the expected confines of the superficial cortex to protrude into the subarachnoid space. Walker-Warburg syndrome is characterized by macrocephaly, posterior encephaloceles, absent myelination, cerebellar hypoplasia, and microphthalmos.

Microlissencephaly and microcephaly with a simplified gyral pattern present with a small head, a smooth cortical surface, and thickening of the cortex with and without other associated anomalies.

Polymicrogyria

It is believed that polymicrogyria is due to ischemic laminar necrosis of the fifth cortical layer after the twentieth week of gestation, by which time the neurons have reached the cortical surface. CMV infection has been implicated as a cause, but other infections or vascular insults in utero may also lead to polymicrogyria. This disorder is frequently seen in patients with Chiari malformation and schizencephaly. Patients usually have developmental delay, spasticity, or seizures.

Grossly, one can see excessive numbers of small, disorganized cortical convolutions usually in the cortex subjacent to the sylvian fissures. The cortex appears thickened. The white matter thickness is normal (remember that it is increased in hemimegalencephaly and smaller in agyria). On MR, one may be able

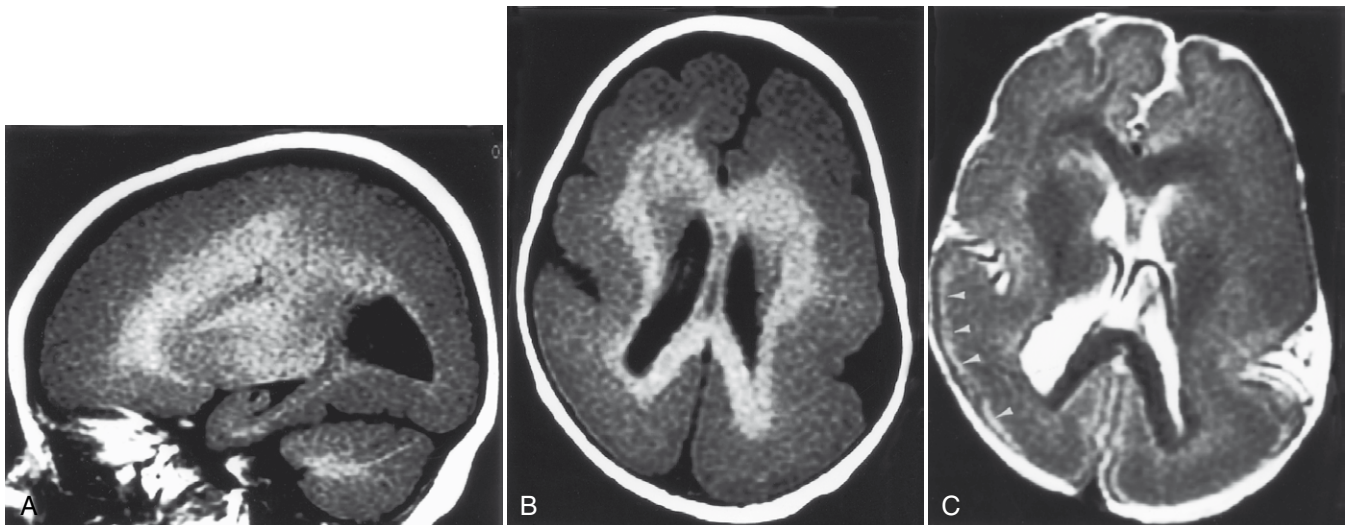


FIGURE 9-24. Classic lissencephaly. A, On this sagittal T1-weighted image (T1WI) incomplete lissencephaly includes areas of agyria (more often parieto-occipital) and pachygyria (frontotemporal). B, On axial T1WI, the sylvian fissures are shallow and maloriented, causing a figure-eight appearance (in this case a bit topheavy). C, On this T2WI, one can identify posteriorly the unmyelinated white matter of the cell sparse layer (arrowheads) that separates the thin cortex from the deeper thickened gray matter in lissencephaly.

to distinguish pachygyria from polymicrogyria; the cortex is less thick with polymicrogyria (5 to 7 mm) than with true pachygyria (8 mm). On thin section images polymicrogyria is “bumpier” than pachygyria. Another distinguishing feature between pachygyria and polymicrogyria is the possible presence of abnormally bright white matter on T2WI deep to the latter. An association with developmental venous anomalies (anomalous venous drainage) is noted with polymicrogyria. When focal, some people use the term *cortical dysplasia* for polymicrogyria.

Congenital bilateral perisylvian (opercular) syndrome is recognized as an entity in which there is polymicrogyria involving the opercular cortex associated with abnormal sylvian fissure sulcation. Patients with congenital bilateral perisylvian syndrome disorder have seizures, congenital pseudobulbar paresis, and developmental delay. The abnormal sylvian fissure may have cortical thickening on either side. Schizencephaly and anomalous venous drainage may also be present. There are rarer bilateral frontal and bilateral frontoparietal polymicrogyria variants as well.

Cerebellar polymicrogyria, lissencephaly, and clusters of intraparenchymal cerebellar cysts may occur in Fukuyama muscular dystrophy. When one sees disordered cerebellar folia and small cysts in the cerebellum in a Japanese patient, one should consider this diagnosis. The cysts may predominate in the semilunar lobule. Cerebral polymicrogyria or pachygyria, absent or delayed myelination, thickened meninges, vermian hypoplasia, fused folia, and hydrocephalus may coexist. The polymicrogyria tends to involve the frontal and parietotemporal lobe, whereas pachygyria involves the temporo-occipital lobes. The polymicrogyria, sometimes called *cobblestone lissencephaly*, can affect the frontoparietal regions with a smooth lissencephaly of the temporo-occipital zone. Other forms of congenital muscular dystrophy are also associated with polymicrogyria and cortical dysplasias.

Type 1 Focal Cortical Dysplasia (Without Balloon Cells)

Cortical dysplasia may be a source of seizures both for the patient and for the unwary neuroradiologist trying to find the entity. It is said that such developmental anomalies are present in 11% to 23% of specimens from surgical procedures performed for epilepsy. The findings may be very subtle, manifested as mild focal volume loss, thickening of cortex, abnormal sulcation, or blurring of cortical margins, without signal intensity variation from gray matter.

The CSF cleft overlying a cortical dimple is a specific sign of cortical dysgenesis. The cortex buckles inward away from the brain surface, leading to a dilated subarachnoid space overlying

it. This is seen in more than 80% of patients with nonballoon cell focal cortical dysplasia, 100% of cases of polymicrogyria, and all cases of schizencephaly.

Other MR findings suggesting dysplasia rather than tumor include the presence of homogeneous hyperintense T2WI signal in the subcortical white matter that tapers as it extends to the lateral ventricle (Fig. 9-25). This signal may be due to hypomyelination or wallerian degeneration. Most clinical manifestations are motor, with spastic hemiplegia.

Microdysgenesis is a term used for a situation where there are too many cells in the cortex with clusters of ectopic neurons in the molecular layer, an excess of neurons in the white matter, and alterations in the cortical laminar architecture without balloon cells. It is a cause of generalized seizures. One etiology may be from hypoglycemia. On imaging, look for abnormal white matter signal with volume loss.

Balloon Cell Focal Cortical Dysplasia of Taylor

Disorders of abnormal neuronal proliferation include balloon cell focal cortical dysplasia of Taylor, in which the number of neurons are increased in number and maloriented. This entity manifests cortical thickening, hyperintense subcortical white matter on T2WI, indistinct gray-white borders, and radial bands from the ventricle to the cortex, usually affecting the frontal lobe. These bands may be of white or gray matter intensity. The appearance is similar to a cortical tuber. In focal gray transmantle dysplasia, gray matter extends from the subependymal zone to the cortex with associated pachygyria, heterotopia, polymicrogyria, and schizencephalic defects. A frontal lobe location favors a balloon cell dysplasia, whereas a temporal lobe (especially medial temporal lobe) location is more suggestive of a neoplasm. Clinical presentation is that of seizures and sensory motor deficits.

Rarely, one may see anomalous venous drainage from areas of cortical dysplasia. Other associations include dysembryoplastic neuroepithelial tumors, gangliogliomas, gangliocytomas, and mesial temporal sclerosis.

Megalencephaly

Megalencephaly is defined as enlargement of all or part of the cerebral hemisphere. Bilateral causes (Box 9-4) and unilateral causes (Box 9-5) may have some overlap and account for various head shapes. Often polymicrogyria (associated with increased hemispheric size) or agyria (associated with less severe hemispheric enlargement) is found on the affected side. MR demonstrates a distorted, thickened cortex with ipsilateral ventricular dilation (Fig. 9-26). This unique feature, that of ventricular dila-

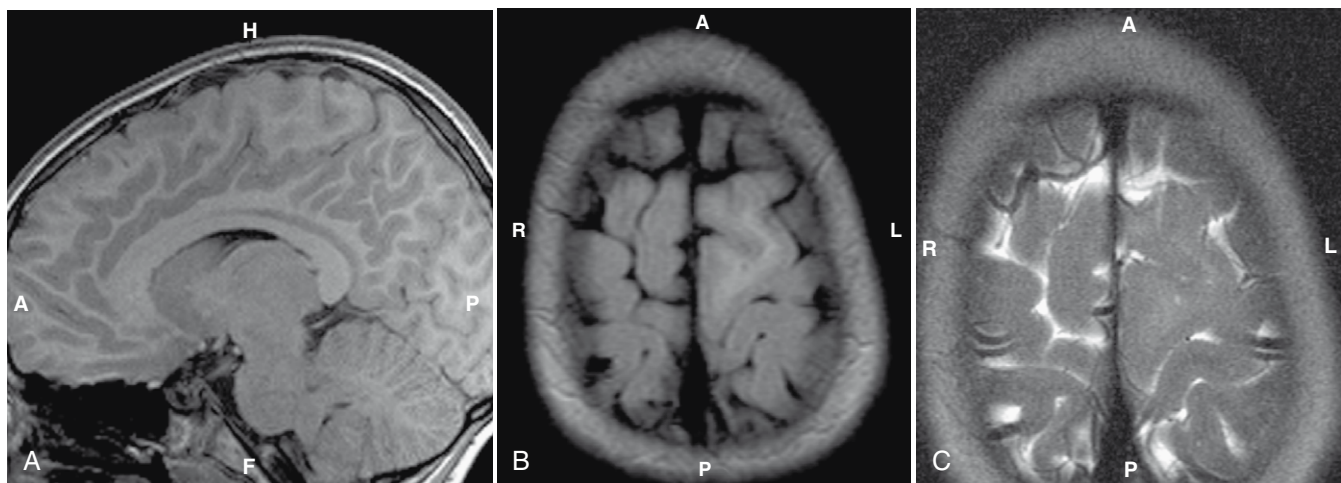


FIGURE 9-25. Cortical dysplasia. Notice the thickened cortex, dimpled surface with mildly expanded cerebrospinal fluid space, and abnormal subcortical signal in the white matter on T1-weighted (A), FLAIR (B) and T2-weighted image (C).

Box 9-4. Bilateral Megalencephaly

- Neurofibromatosis type 1
- Neuronal migrational anomaly
- Achondroplasia
- Mucopolysaccharidoses
- Tuberous sclerosis
- Acromegaly
- Proteus syndrome
- Tay-Sachs disease
- Canavan disease
- Alexander disease

Box 9-5. Unilateral Megalencephaly

- Hemimegalencephaly (neuronal migrational anomaly)
- Neurofibromatosis type 1
- Dyke-Davidoff-Masson syndrome/Sturge-Weber association
- McCune Albright syndrome
- Tuberous sclerosis
- Klippel-Trenaunay-Weber syndrome
- Proteus syndrome
- Epidermal nevus syndrome



FIGURE 9-26. Hemimegalencephaly. Axial T2-weighted image discloses enlargement of the left hemisphere with disorganized brain tissue and a neuronal migrational anomaly. Note the lack of sulcation and the abnormal white matter formation in this child. Big brain, big ventricle.

tion on the side of the enlarged hemisphere, separates congenital hemimegalencephaly from other infiltrative lesions. This disorder results from too many neurons and decreased apoptosis. Heterotopias and cortical thickening are characteristic. Myelination is delayed, but overall white matter volume is increased. Alternatively, megalencephaly may be an isolated finding. Patients have seizures, hemiplegia, developmental delay, and abnormal skull configurations.

Interestingly, a patient with hemimegalencephaly of one hemisphere in infancy may actually show hemimicrocephaly of the hemisphere in later life due to retarded growth of the

dysmorphic brain, causing the contralateral hemisphere to seem larger. Hemimegalencephaly may occur in a variety of syndromes, including neurofibromatosis type 1, Soto syndrome, proteus syndrome, epidermal nevus syndrome, tuberous sclerosis, and Klippel-Trenaunay-Weber syndrome.

Proteus syndrome, which has cutaneous manifestations similar to neurofibromatosis and encephalocraniocutaneous lipomatosis, may present with hemimegalencephaly, subependymal calcified nodules, and periventricular cysts. Irregularly shaped vertebrae may accompany the intracranial findings. Macrocephaly, macrodactyly, hemihypertrophy, cutaneous nevi, soft-tissue tumors, and lipomatosis may make for one unusual-looking patient.

Lipomas

It is now generally accepted that most intracranial lipomas represent congenital abnormalities rather than neoplasms. Lipomas occur because of persistence or maldevelopment of the meninx primitiva, the neural crest tissue that ultimately forms the neural tube. The most common sites of lipomas are the interhemispheric fissure (50%), quadrigeminal plate cistern, pineal region, hypothalamic region, and cerebellopontine angle cistern. These lesions do not grow and are symptomatic only because of other associated congenital anomalies or mass effect on neighboring structures. Many (up to 50%) are associated with agenesis of the corpus callosum. Treatment tends to be conservative because vessels often course through the lipoma, making surgical removal that much harder.

Lipomas have attenuation values on CT that are in the negative range, usually -30 to -100HU, and are isodense to subcutaneous fat (see Fig. 9-19). High in intensity on T1WI, intermediate to low in intensity on conventional T2WI, and bright on fast spin-echo T2WI, the fat of the lipoma can be corroborated by the presence of a chemical shift artifact along the frequency-encoding direction. This causes one edge of the lesion to be highlighted as very bright on T2WI and the other edge along the frequency-encoded axis to be darkened. Alternatively, a fat-suppression pulse sequence can verify the fat by demonstrating signal diminution after it is applied. Calcification may be seen.

Aqueductal Stenosis

Aqueductal stenosis, causing lateral and third ventricular enlargement without fourth ventricular dilation, is usually seen in boys as part of an X-linked recessive hereditary disorder. This is thought to be due to an abnormality of proliferation and differentiation of the periaqueductal gray matter of the mesencephalon, leading to the stenosis. Acquired causes of aqueductal stenosis are numerous and include clots from subarachnoid hemorrhage and fibrosis after bleeds or infections. The congenital causes occur in the setting of enlarged head circumference in infant boys and may be due to webs, septa, or membranes. This entity is covered in greater depth in Chapter 8.

— INFRATENTORIAL ABNORMALITIES

Dandy-Walker Syndrome (Table 9-4)

Classically, the Dandy-Walker malformation is described as partial or complete absence of the vermis, dilation of the fourth ventricle into a large cystic mass in an enlarged posterior fossa, hydrocephalus, and torcular-lambdoid inversion (elevation of the torcular above the lambdoid suture) (Fig. 9-27). The etiology that has been proposed for the Dandy-Walker malformation is obstruction of outward flow of the CSF at the foramina of Magendie and Luschka. This leads to ballooning upward of the fourth ventricle between the cerebellar hemispheres, preventing their fusion to form the cerebellar vermis and changing the osseous configuration of the posterior fossa. The cerebellar vermis is the missing part in the picture of Dandy-Walker anomalies. Patients

TABLE 9-4. Dandy-Walker Complex

Feature	Dandy-Walker Malformation	Dandy-Walker Variant	Giant Cisterna Magna
Posterior fossa size	Enlarged	Normal	Normal or enlarged
Vermis	Absent or very hypoplastic	Hypoplastic	Normal
Hydrocephalus	75%	25%	Unusual
Supratentorial anomalies	Common (68%)	Uncommon (20%)	Rare (6%)
Torcular-lambdoid inversion	Yes	No	No
Hypoplastic cerebellar hemisphere	Yes	Rare	No
Prognosis	Poor	Good	Good
Falx cerebelli	Absent	Present in 32%	Present in 63%
Fourth ventricle	Opens into cyst	Cyst dilatation	Normal

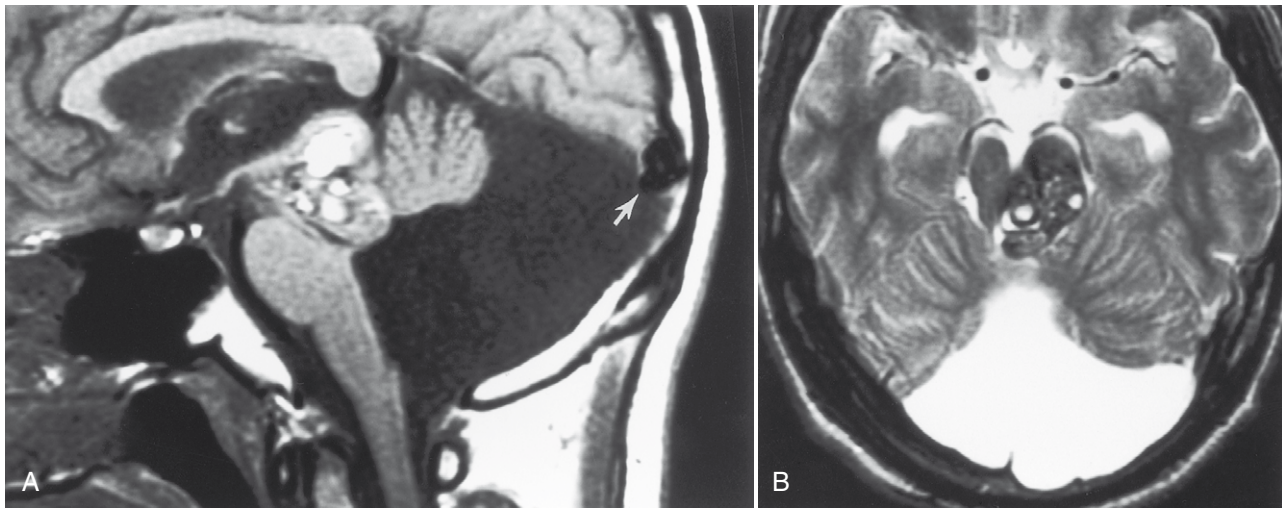


FIGURE 9-27. Dandy-Walker syndrome and occult cerebrovascular malformation (OCVM). **A**, Classic sagittal T1-weighted image (T1WI) showing the cystic expansion of the fourth ventricle, lifting of the torcular (*arrow*), inferior vermian absence, and enlarged posterior fossa. But wait, what is going on at the collicular plate? (Extra credit for this one!) **B**, The axial T2WI shows the ballooned-out fourth ventricle and the heterogeneous hemorrhagic mass in the posterior midbrain. The absence of edema associated with the brain stem lesion and its signal intensity leads to the diagnosis of a cavernous hemangioma or OCVM.

with Dandy-Walker malformation have a high incidence (68%) of other syndromes (Box 9-6) and other congenital CNS abnormalities, including agenesis of the corpus callosum, holoprosencephaly, schizencephaly, polymicrogyria, meningoencephaloceles, lipomas, infundibular hamartomas, malformed olives (the pits), hydromyelia, and cerebral heterotopia. Patient's functional status is more directly correlated with these supratentorial anomalies.

Box 9-6. Associations with Dandy-Walker Syndrome

- Walker-Warburg syndrome
- Aicardi syndrome
- TORCH infection
- Trisomy 9, 13, 18
- Klippel Feil syndrome
- Meckel-Gruber syndrome (occipital encephalocele, microcephaly, polycystic kidneys, polydactyly)
- Fetal alcohol syndrome
- Warfarin embryopathy
- X-linked cerebellar hypoplasia
- Ellis-van Creveld syndrome
- Facial hemangiomas

The CT findings in patients with manifestations of Dandy-Walker malformation include (1) a large cystic structure in the posterior fossa, which represents the ballooned-out fourth ventricle; (2) hydrocephalus; (3) torcular-lambdoid inversion; and (4) inferior vermian hypoplasia or aplasia.

Again, because of the prevalence of midline abnormalities, MR is the ideal study for examining patients with Dandy-Walker syndrome. With this technique, one can identify the communication of the posterior fossa cyst with the fourth ventricle. In addition, one may identify the straight sinus entering the torcular in a high location. The posterior fossa cyst typically has signal intensity exactly that of CSF elsewhere. In the midline MR section you should appreciate the degree of vermian hypoplasia and the presence of concomitant agenesis or lipoma of the corpus callosum.

The Dandy-Walker variant is a less severe form of the Dandy-Walker complex in which there is better development of the vermis and the fourth ventricle posterior fossa cyst is smaller. Neither significant enlargement of the posterior fossa nor torcular-lambdoid inversion is present (Fig. 9-28). Hydrocephalus is variably present since one or more foramina from the fourth ventricle are presumed to be open. Heterotopias and callosal dysgenesis occur in about 20% of cases of Dandy-Walker variant.

The Dandy-Walker malformation should be differentiated from the arachnoid cyst of the posterior fossa, which is located behind the cerebellum, does not communicate with the

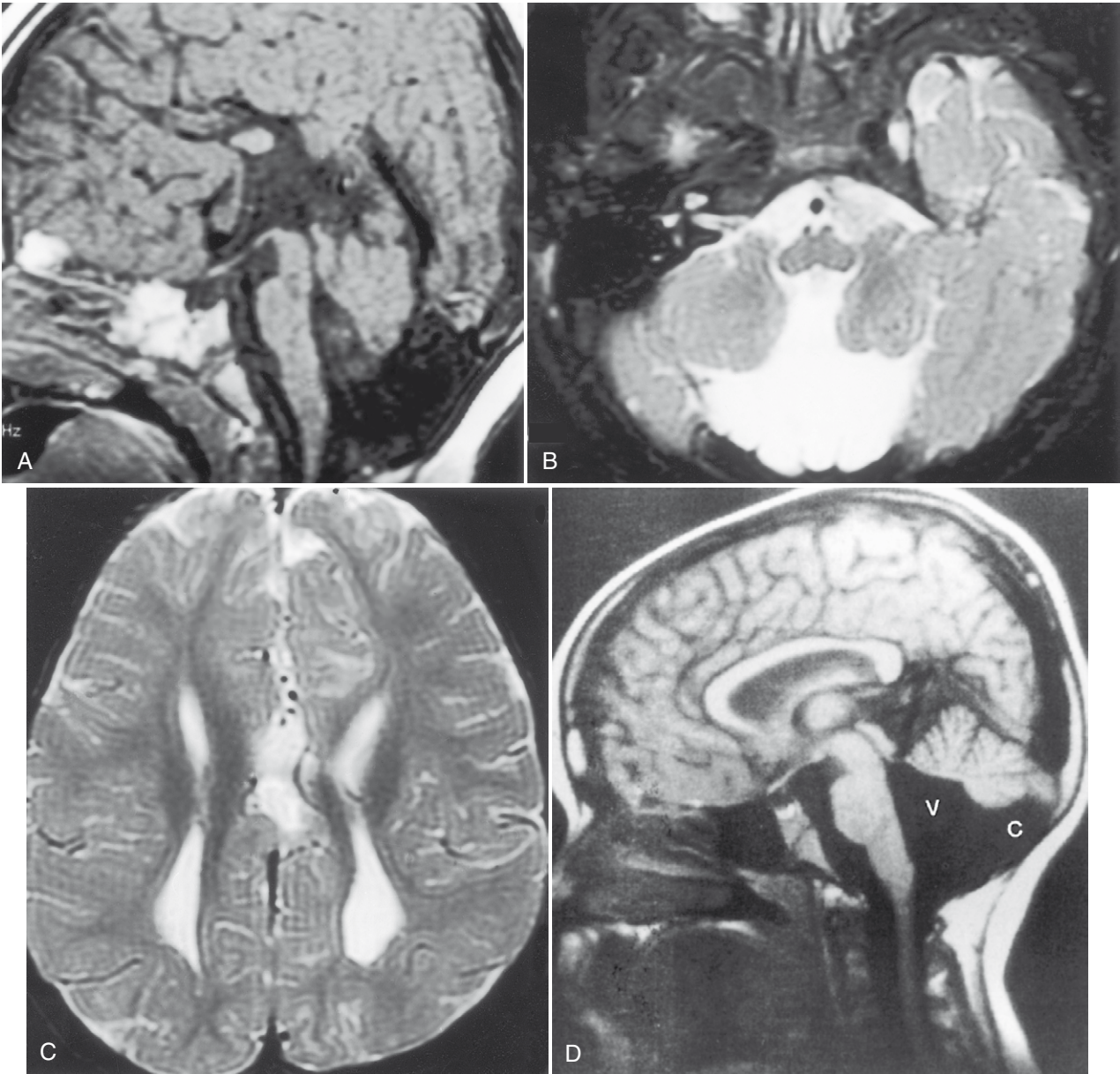


FIGURE 9-28. Dandy-Walker variant. **A**, There is a large cystic structure in the posterior fossa that communicates with the fourth ventricle, but the posterior fossa is not particularly enlarged, nor is there hydrocephalus, judging from the appearance of the third ventricle. Agenesis of the corpus callosum coexists. **B**, There is little inferior vermis left on this axial T2-weighted image, but the cyst replaces the space. **C**, The shape of the ventricles is indicative of agenesis of the corpus callosum, not hydrocephalus. **D**, Dandy-Walker variant. A large cyst (c) communicating with the fourth ventricle (v) and causing partial inferior vermal hypoplasia is seen on this sagittal T1WI. Note that there is no hydrocephalus and the torcular Herophili is not elevated. These findings suggest Dandy-Walker variant. (Courtesy of Altman NR, Naidich TP, Braffman BH: Posterior fossa malformations, *AJNR Am J Neuroradiol* 13:691–724, 1992, Figure 19, © *AJNR*.)

fourth ventricle, and is not generally associated with hydrocephalus or vermian hypoplasia (Fig. 9-29). In addition, the giant cisterna magna is a normal variation, with dilatation of the subarachnoid space posterior to the cerebellum. It is not associated with fourth ventricular abnormalities, hydrocephalus, or torcular-lambdoid inversion. The vermis is usually normal but if compressed early in development may yet be small. As opposed to Dandy-Walker syndrome, patients with a giant cisterna magna or arachnoid cyst of the posterior fossa have a normal (giant cisterna magna) or compressed (arachnoid cyst) fourth ventricle. Compression of the fourth ventricle by the arachnoid cyst may lead to hydrocephalus, further confusing the picture, but this is rare. You may identify vessels coursing

through the subarachnoid space of the giant cisterna magna. The arachnoid cyst demonstrates displacement of those vessels but without associated congenital malformations as described in the Dandy-Walker syndrome. Septations within the subarachnoid space of the cisterna magna and infoldings of the meninges are frequently seen. The falx cerebelli may be bifid and show infoldings as well. Because of this, one may see stranding fibers normally within the posterior fossa CSF spaces even with a giant cisterna magna.

Dandy-Walker syndrome is the most common CNS anomaly associated with PHACES syndrome (posterior fossa malformations, hemangiomas, arterial anomalies, cardiac defects, eye abnormalities, and sternal defects).

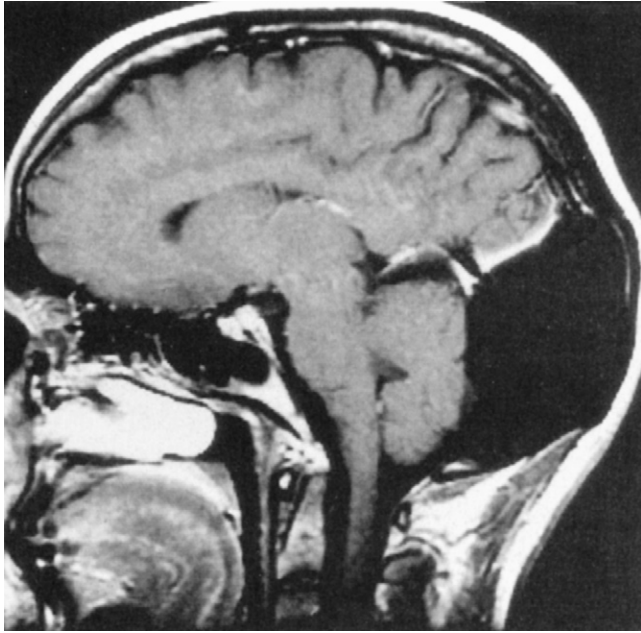


FIGURE 9-29. Retrocerebellar arachnoid cyst. Enhanced sagittal T1-weighted image shows a large arachnoid cyst behind the cerebellum. Note that, although the straight sinus is elevated, this cerebrospinal fluid collection does not communicate with the fourth ventricle and no hydrocephalus is present.

Vermian Dysgenesis/Hypoplasia

Some have said that all forms of vermian dysgenesis fall within the Dandy-Walker syndrome. We do not agree. Inferior vermian hypoplasia may occur in isolation and in patients with congenital ocular motor apraxia syndrome (Fig. 9-30). Patients with Walker-Warburg syndrome have vermian hypoplasia, diffuse cerebral cobblestone cortex, absence of cerebral and cerebellar myelin, cerebellar polymicrogyria (with or without cysts), hydrocephalus,

Box 9-7. Causes of Vermian Dysgenesis

- Down syndrome
- Chiari malformations
- Dandy-Walker syndrome
- Retrocerebellar cysts (Blake pouch cyst)
- Olivopontocerebellar degeneration
- Joubert syndrome
- Congenital ocular motor apraxia syndrome
- Meckel-Gruber syndrome
- Walker-Warburg syndrome
- X-linked hypoplasia of vermis

and variable callosal hypogenesis. There are many metabolic and drug causes of vermian atrophy. Although we discuss metabolic and toxic lesions that cause cerebellar atrophy in Chapter 8 it behooves us to remind our dedicated readers that Dandy-Walker malformations, Chiari malformations, and Down syndrome are associated with vermian dysgenesis. These and other more obscure entities may be found in Box 9-7.

Joubert Syndrome

The imaging findings in Joubert syndrome are virtually pathognomonic. One sees parallel, enlarged, horizontally oriented superior cerebellar peduncles, which, coupled with the elongated pontine-midbrain junction, have the appearance of a molar tooth (Fig. 9-31). Hypoplasia of the vermis brings the two cerebellar hemispheres in virtual contact with each other and a nodulus is not seen. The fourth ventricle develops a “bat wing” appearance from middle cerebellar peduncle, superior cerebellar peduncle, and pyramidal decussation maldevelopment. Associations, including dysgenesis of the corpus callosum, retinal dysplasia, and cystic renal disease, coexist and lead to a poor prognosis.

Clinically, the patients have developmental delay, poor visual development with oculomotor disturbances, colobomas, and abnormal respirations (neonatal tachypnea or apnea). Inheritance is autosomal recessive.

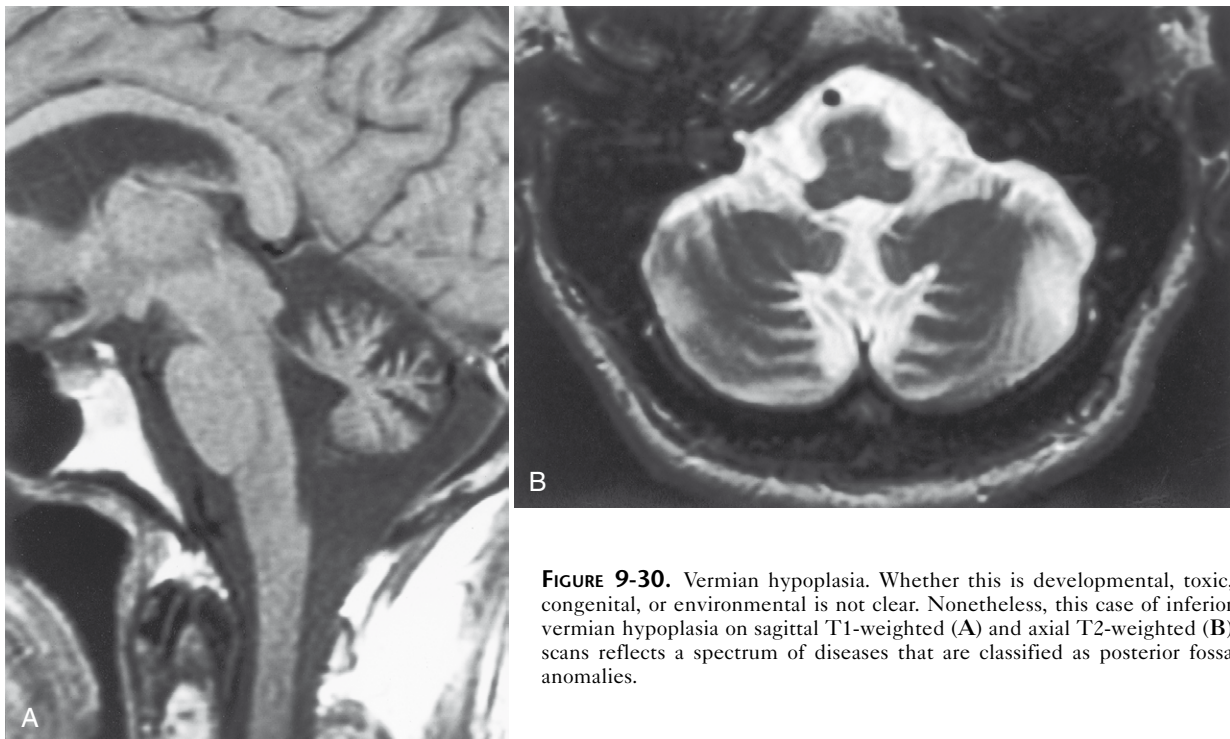


FIGURE 9-30. Vermian hypoplasia. Whether this is developmental, toxic, congenital, or environmental is not clear. Nonetheless, this case of inferior vermian hypoplasia on sagittal T1-weighted (A) and axial T2-weighted (B) scans reflects a spectrum of diseases that are classified as posterior fossa anomalies.



FIGURE 9-31. The molar tooth sign. Note how the brain stem and the elongated superior cerebellar peduncles simulate a molar tooth. Couple this with the vermian hypoplasia evident by the dilated subarachnoid space posteriorly and it will make Aunt Minnie cry out, “Joubert, Whazzup?”

Rhombencephalosynapsis

Rhombencephalosynapsis is a rare entity in which the cerebellar hemispheric separation is lost and there is fusion across midline of the cerebellum. There appears to be an absence of the anterior vermis, fusion of the dentate nuclei and middle cerebellar peduncles, and a deficiency of the posterior vermis. Agenesis of the septum pellucidum may coexist.

Arachnoid Cysts

As described previously, arachnoid cysts are common in the infratentorial space. The posterior fossa sites of the arachnoid cyst are the regions of the cisterna magna and the cerebellopontine angle cistern. The signal intensity within the posterior fossa arachnoid cysts duplicates that of CSF in most cases. One should be cognizant of the association of the arachnoid cyst with acoustic schwannomas in the cerebellopontine angle cistern. Arachnoid cysts occasionally cause hydrocephalus, leading to a clinical presentation.

Chiari Malformations

The spectrum of congenital anomalies labeled the Chiari malformation spans almost as wide a range as the Dandy-Walker syndrome. The fundamental problem in Chiari malformation appears to be underdevelopment of the posterior fossa from para-axial mesoderm that forms the occipital somites (a cranial base dysplasia). CSF and posterior cranial fossa volumes are decreased compared with controls, but overall brain volumes are the same. Chiari I malformations are diagnosed when the cerebellar tonsils alone are below the foramen magnum. Tonsils less than 5 mm below the foramen magnum are very common, but that is the current lower limit of normal most people cite in the literature. In its pure form, a Chiari I malformation shows tonsils down to the C1–C2 region but with normal brain stem location. The incidence of cervical syringohydromyelia in these flagrant cases has been reported to be between 20% and 73% (Fig. 9-32) and the incidence of syrinxomyelia in symptomatic patients with Chiari I malformations and tonsillar herniation greater than 5 mm is reported to be 53% in the surgical literature. No hydrocephalus is present, and the fourth ventricle is normal in location. There is an association with



FIGURE 9-32. Chiari malformation with a syrinx. The sagittal T1-weighted image shows the low tonsils (*white arrow*), the low cervicomedullary junction, and the cervical syrinx (fading into the distance with *black arrow*). It is our policy that, even with a classic congenital syrinx, the first study of a syrinx should include an enhanced study to exclude a neoplastic cause, rare though that may be.

Klippel-Feil syndrome (C2–C3 fusion), short clivus, odontoid or C1 abnormalities, compression of CSF spaces posterior and lateral to the cerebellum, and reduced height of the supraocciput.

The symptoms that are most commonly reported in patients with Chiari I malformations are suboccipital headaches, retro-orbital pressure or pain, clumsiness, dizziness, vertigo, tinnitus, paresthesias, muscle weakness, and lower cranial nerve symptoms (i.e., dysphagia, dysarthria, sleep apnea, tremors). The entity usually presents in the second or third decade of life (mean age of 25 years \pm 14 years), and women outnumber men by a 3:1 ratio.

There has been a lot of focus lately on the issue of CSF, spinal cord, and medullary movement in patients with Chiari malformations. Foramen magnum obstruction may lead to increased systolic spinal cord motion, impaired spinal cord recoil, and impaired diastolic CSF motion anteriorly at the C2–C3 level and in the posterior fossa. Impaired systolic and unimpaired diastolic flow may also be seen just below the foramen magnum. Some neurosurgeons perform suboccipital decompression procedures on patients with a variety of clinical symptoms, including headaches, vertigo, weakness, and fibromyalgia, who have imaging findings of abnormal CSF motion with tonsillar ectopia. It is true that one will often see reduced CSF flow posteriorly at the foramen magnum with low tonsils. Others have reported hyperdynamic movement of the tonsils with posterior movement of the medulla in patients with Chiari malformations.

Dramatic tonsillar herniation through the foramen magnum may be present in patients with osteopetrosis owing to decreased intracranial volume secondary to the thickened calvarium and increased intracranial pressure (ICP). This forces the tonsils down, down, down.

Chiari II (the original Arnold-Chiari malformation) anomalies occur in 0.02% of births and affect girls twice as often as boys. The cerebellar tonsils, vermis, fourth ventricle, and brain stem are herniated through the foramen magnum, and the egress from the fourth ventricle is obstructed (Box 9-8 and Fig. 9-33). A kink may be present at the cervicomedullary junction. Hydrocephalus occurs. The frontal horns of the lateral ventricles are squared off, the fourth

Box 9-8. Findings in Chiari II Malformation**INFRATENTORIAL FINDINGS**

Tonsils and medulla below foramen magnum
 Beaking of tectum
 Bullet-shaped towering cerebellum
 Cerebellum wrapped around brain stem
 Petrous bone scalloping
 Myelomeningocele, syringohydromyelia
 Fourth ventricle compressed, elongated, trapped, and low
 enlarged foramen magnum
 Cervicomedullary kinking
 Small posterior fossa
 Low torcular
 Dysplastic tentorium
 Scalloping of clivus posterior
 Absent hypoplastic arch of C1

SUPRATENTORIAL FINDINGS

Falx hypoplasia
 Hydrocephalus
 Callosal hypogenesis
 Fused, enlarged massa intermedia
 Colpocephaly
 Abnormal gyral patterns
 Caudate hypertrophy, bat-wing lateral ventricles
 Interdigitation of gyri along widened interhemispheric
 fissure
 Lückenschädel skull
 Biconcave third ventricle

ventricle is compressed, and the aqueduct is stretched inferiorly. The tectum of the midbrain is beaked, and the massa intermedia is abnormally enlarged (Fig. 9-34). The superior cerebellum towers superiorly through a widened tentorial incisura because the whole posterior fossa is too small. The rest of the cerebellum may literally wrap around the brain stem. Associated complete agenesis of the corpus callosum occurs in one third of cases, and partial abnormalities occur in 75% to 90%, predominantly affecting the splenium. Heterotopias and abnormal gyral patterns are common.

A tethered cord with a lumbosacral myelocele (Fig. 9-35) or meningomyelocele protruding through the skin is seen in nearly all patients with Chiari II malformations. A lipoma of the filum may coexist. The anchoring of the distal portion of the cranio-spinal axis may account for the downward herniation of intracranial contents in this disorder. Rarely the tonsils may necrose secondary to compression of critical vessels at the foramen magnum. The evidence of this crime is fragments of cerebellar tissue floating in a sea of cervical CSF.

Chiari III malformations are associated with herniation of posterior fossa contents in an occipital or high cervical encephalocele with other features of Chiari II malformations. Nearly all Chiari III encephaloceles contain brain tissue, usually cerebellum, although even the brain stem can herniate outward (Fig. 9-36). Heterotopias, agenesis of the corpus callosum, anomalies of venous drainage, and syringohydromyelia are commonly associated.

Symptoms of Chiari II and III malformations are ataxia, vertical nystagmus, headache, cranial nerve VI through XII findings and, occasionally, central canal syndromes caused by syringohydromyelia. At autopsy, disordered neuronal tissue is present in the brain stem and cerebellum. Thus, it is not clear whether the symptoms are entirely due to compression at the foramen magnum or to dysplastic neurons. Decompression of the foramen magnum often does not improve symptoms in most individuals with Chiari II, suggesting that disorganized medullary tissue may be etiologic in some cases.



FIGURE 9-33. This patient has the Chiari II malformation, cord syrinx, and a treated myelomeningocele, all shown on this 48 field-of-view T2-weighted image. Is that great tectal beaking, or what?

SKULL ANOMALIES**Craniostenosis**

At birth, the sagittal, coronal, lambdoid, and metopic sutures are open. Occasionally, one will see a suture that crosses from one lambdoid suture to the other, the persistent mendosal suture. *Craniostenosis*, or *craniosynostosis*, refers to abnormal early fusion of one or more of the sutures of the skull. In 75% of cases, only one suture or part of a suture is fused; in 25% of cases, more than one suture is affected. This leads to abnormal head shapes and a palpable ridge at the site of fusion. Males are affected much more often than females. These disorders, if severe and early in development, can cause abnormal growth of the brain. Microcephaly may occur. Syndromes associated with early sutural closure include Crouzon syndrome, Apert syndrome, hypophosphatasia,

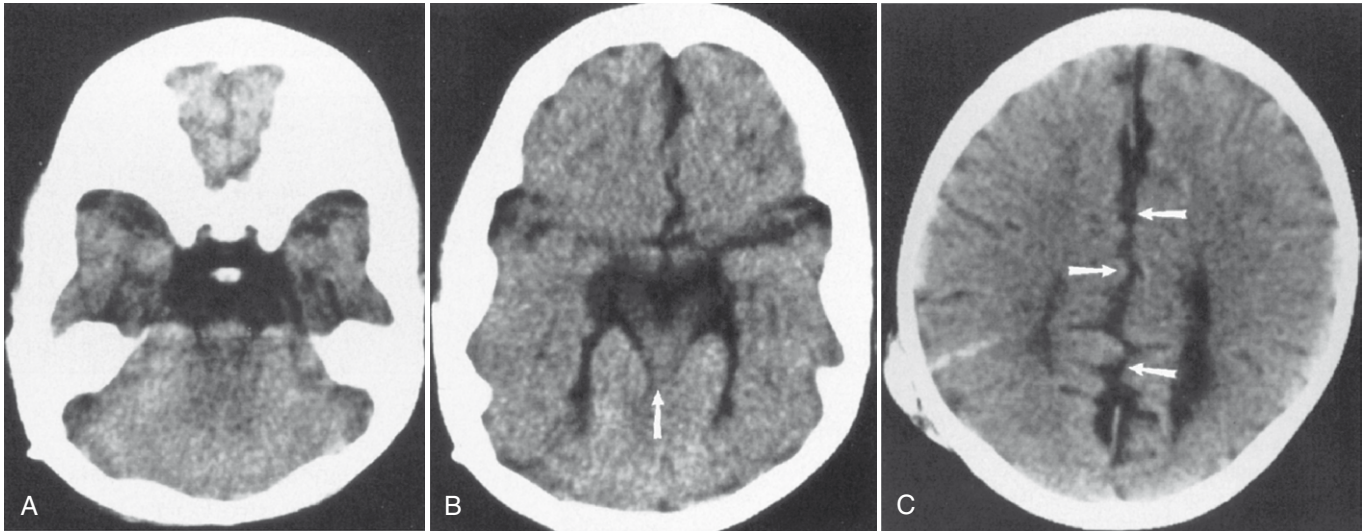


FIGURE 9-34. Imaging findings with Chiari II malformation. **A**, Axial computed tomography (CT) through the posterior fossa shows absence of the fourth ventricle. Posterior fossa seems small. **B**, Axial scan through the level of the midbrain reveals tectal beaking (*arrow*) with the cerebellum wrapping around the posterior lateral aspect of the midbrain. Cerebellum is towering between the leaves of the tentorium. **C**, Axial CT through the supraventricular region shows interdigitation of the gyri (*arrows*) with hypoplasia of the falx. This patient has a right shunt tube in place. Do you think the corpus callosum is present? Are those ventricles parallel?

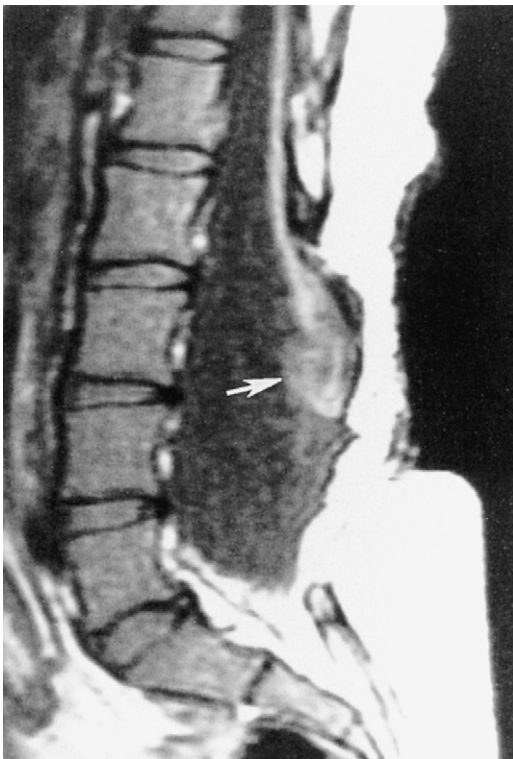


FIGURE 9-35. Myelomeningocele. Sagittal T1-weighted image shows spinal dysraphism with herniation of the spinal cord, neural placode (*arrow*), and cerebrospinal fluid through the gap of the bony anomaly.

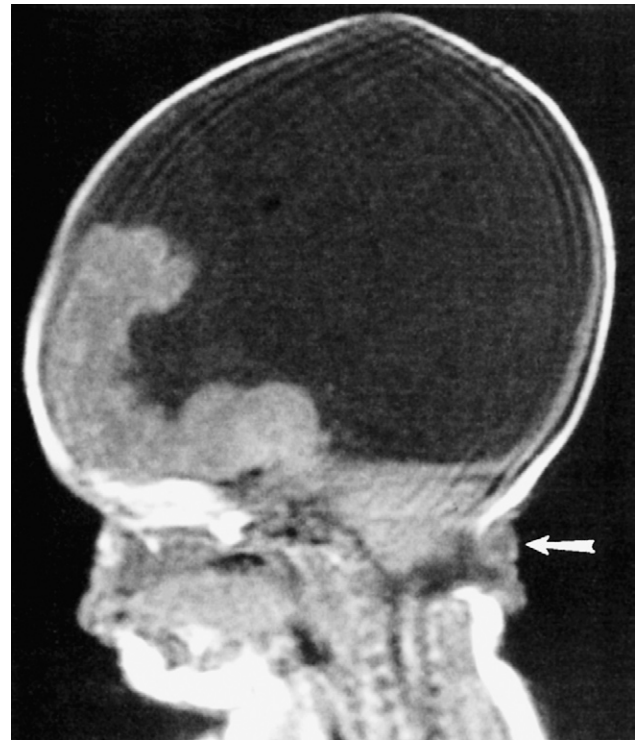


FIGURE 9-36. Chiari III abnormality. Sagittal T1-weighted image shows downward herniation of the cerebellar tonsils associated with an occipital encephalocele (*arrow*). Patient has associated agenesis of the corpus callosum and maximal hydrocephalus.

and Carpenter syndrome (Fig. 9-37). Endocrinologic abnormalities, including rickets, hyperthyroidism, and hypophosphatasia, can cause craniosynostosis. Premature closure of the sagittal suture, the most common variety, produces a head that cannot grow side to side, so the head looks long and thin, or scaphocephalic, also termed *dolichocephalic* (Table 9-5). The incidence of sagittal synostosis is approximately 1 in 4200 births. If the coronal suture fuses early, the head is short and fat, or brachycephalic.

Sometimes only one portion of a coronal or lambdoid suture fuses too early, leading to an asymmetric skull with plagiocephaly. The forehead and orbital rim (eyebrow) have a flattened appearance on that side. This gives a harlequin “winking” eye. Lambdoid suture closure can lead to turricephaly, with a high-riding vertex. Unilateral lambdoid suture fusion results in a posterior flattened plagiocephaly. Metopic sutural closure causes trigonocephaly with a ridge that runs down the forehead like a triceratops.

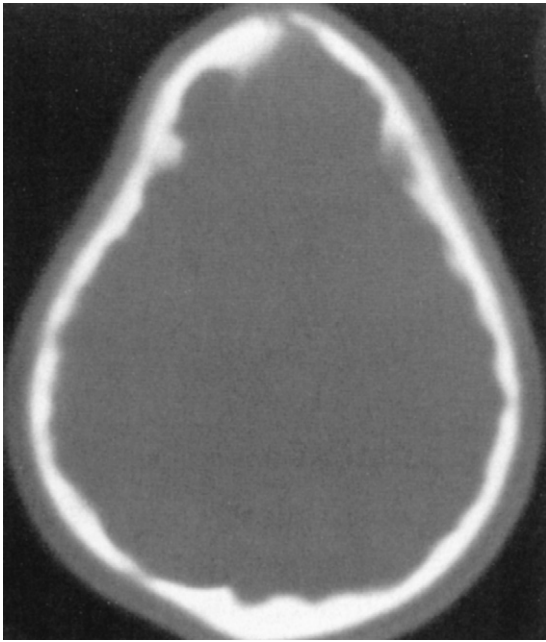


FIGURE 9-37. Cloverleaf skull. Multiple fused sutures, in a patient with Crouzon syndrome, produced anterior beaking and a cloverleaf shape.

TABLE 9-5. Craniostenosis

Type	Suture Involved	Head Shape
Dolichocephaly	Sagittal	Long and thin
Brachycephaly	Coronal	Round and foreshortened
Turricephaly	Lambdoid	High-riding top
Plagiocephaly	Any unilateral suture	Asymmetric
Trigonocephaly	Metopic	Anteriorly pointed head
“Harlequin eye”	Unilateral coronal	One eye points upward

Surgery is attempted for cosmetic reasons or when elevations of ICP are dangerous secondary to the growth of the brain against the noncompliant calvarium. The elevated ICP may lead to reduction in brain perfusion. If brain growth is stunted because of craniostenosis, operative intervention is also indicated. Chronic venous hypertension due to jugular foramen stenosis has been proposed as an etiology for the increased ICP, communicating hydrocephalus, and tonsillar herniation seen in some patients with complex craniosynostosis. This can be seen with Crouzon syndrome.

Osteopetrosis

Osteopetrosis may be inherited as an autosomal dominant or recessive condition, with the latter being the more virulent form. Calvarial involvement is frequent in both types, with clinical manifestations mostly relating to involvement of skull base foramina. Therefore, cranial nerve palsies, optic atrophy, and stenoses of the carotid and jugular vessels may be present. One may see diffuse bone thickening and increased density (or decreased intensity) on imaging studies. MR may depict optic nerve sheath dilation, tonsillar herniation, ventriculomegaly, and meningoencephaloceles (especially through craniotomy sites).

Achondroplasia

Achondroplasia is the most common cause of dwarfism and is characterized by a small foramen magnum but a large head. The macrocephaly may be secondary to hydrocephalus. The

hydrocephalus may be due to venous outflow obstruction at the jugular foramen level, leading to elevated venous pressure and reduced flow in the superior sagittal sinus. The lack of resorption in the arachnoid villi because of these pressure effects produces larger CSF volume in the ventricles, increased ICP, maintenance of widened calvarial sutures, and an enlarged head.

Other features of achondroplasia include a short clivus, platybasia, and a J-shaped sella. Congenital spinal stenosis due to short pedicles is another feature of this disease.

Increased Wormian Bones

Increased wormian bones (secondary ossification centers within sutural lines) are seen in osteogenesis imperfecta, cleidocranial dysplasia, cretinism, pyknodysostosis, Down syndrome, hypothyroidism, progeria, and hypophosphatasia.

Basilar Invagination and Platybasia

Basilar invagination refers to upward protrusion of the odontoid process into the infratentorial space. Two lines must be memorized: (1) McGregor’s line, extending from the posterior margin of the hard palate to the undersurface of the occiput, and (2) Chamberlain’s line, from the hard palate to the opisthion (the midportion of the posterior margin of the foramen magnum) (Fig. 9-38). If the dens extends more than 5 mm (or half its height) above these lines, basilar invagination is present. Paget disease, rickets, fibrous dysplasia, osteogenesis imperfecta, hyperparathyroidism, osteomalacia, achondroplasia, cleidocranial dysplasia, and Morquio syndrome are among the causes of this finding. In adults think rheumatoid arthritis (Fig. 9-39). *Basilar impression* is the term sometimes used when the finding is found secondary to bone-softening diseases.

Basilar invagination should not be confused with platybasia. *Platybasia* literally means “flattening of the base of the skull” and is said to be present when the Wencke basal angle formed by intersecting lines from the nasion to the tuberculum sellae and from the tuberculum along the clivus to the anterior aspect of the foramen magnum (basion) is greater than 143 degrees (see Fig. 9-38). Platybasia is seen with Klippel-Feil anomalies, cleidocranial dysplasia, and achondroplasia.

— CONGENITAL INFECTIONS

In utero infections with toxoplasmosis, rubella, CMV, and herpes simplex (TORCH infections) can cause brain injury (Fig. 9-40). Congenital syphilis is also frequently included with this group. In many instances, when the infection is transmitted hematogenously from the mother or ascends from the vagina through the cervix to the placenta, these infections lead to in utero death. Other infants are seen in the perinatal period with failure to thrive, hydrocephalus, or seizures (Table 9-6). Transmission may be at the time of passage through the vaginal canal during delivery.

On CT, these infections most commonly manifest as periventricular calcifications and leukomalacia with cerebral atrophy. CMV is the most common of the TORCH infections and is usually transmitted hematogenously from maternal infection. In addition to periventricular calcifications, porencephaly, delayed myelination, polymicrogyria, and pachygyria may also be seen with CMV infection. Microcephaly caused by atrophy is common with CMV infections. Periventricular cysts, usually around the occipital poles, may also be present. Echogenic basal ganglia vasculature has been reported on sonograms of infants with CMV and rubella infections.

Of the congenital infections, toxoplasmosis calcifies most frequently (71% of the time in one series). With treatment of congenital toxoplasmosis, 75% of cases show diminution or resolution of the intracranial calcifications by age 1 year. If treatment does not occur, is delayed, or is inadequate the intracranial calcifications may increase. The status of the calcifications often mirrors neurologic function. On

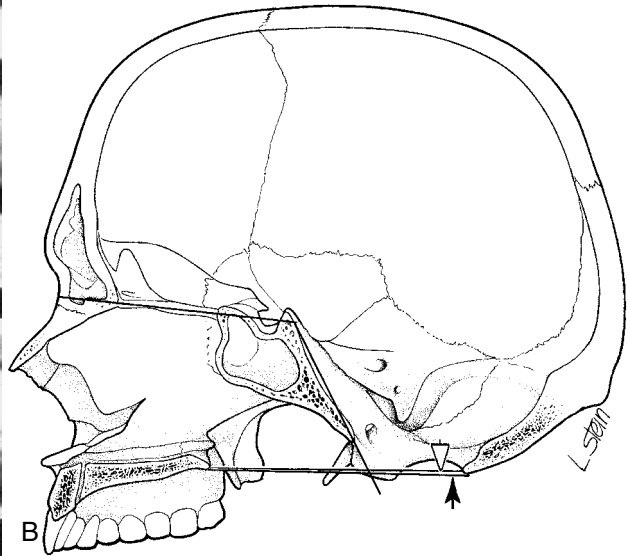
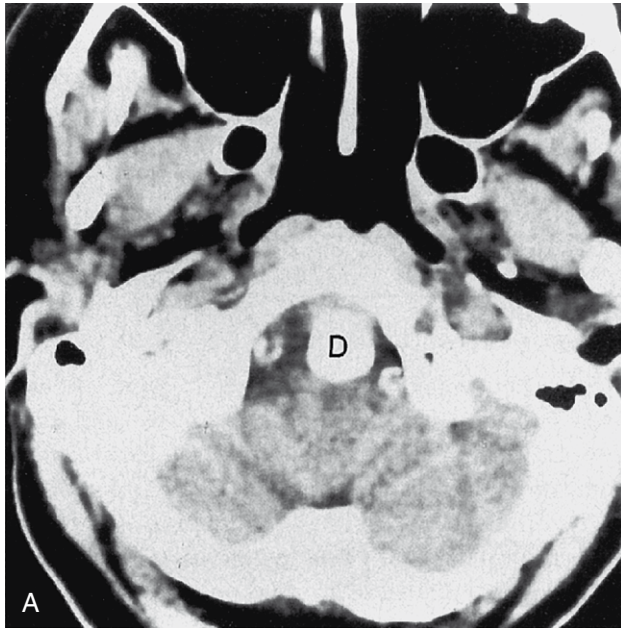


FIGURE 9-38. Basilar invagination. **A**, Computed tomography demonstrates basilar invagination with dens (D) impinging on medulla. This has been likened to a pumpkin rotting on a fence post. **B**, Diagram of McGregor's (*black arrow*) and Chamberlain's (*open arrow*) lines. Note the basal angle from the nasion to tuberculum sellae to basion.

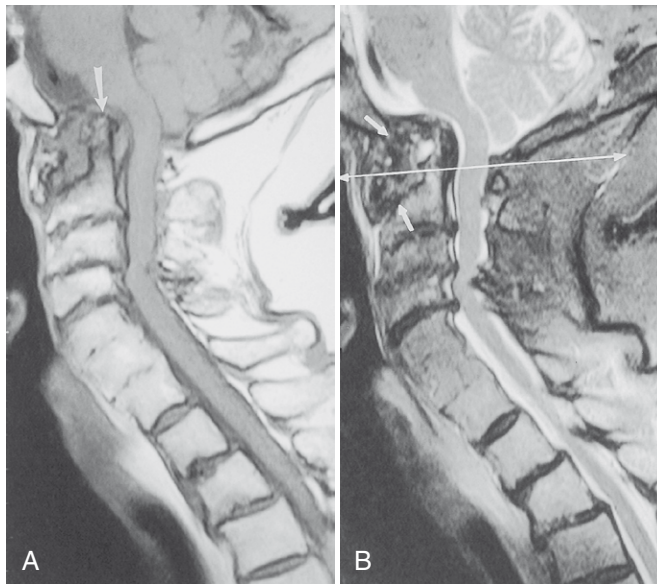


FIGURE 9-39. Rheumatoid arthritis producing basilar invagination. **A**, Sagittal T1-weighted image (T1WI) showing penciling (*arrow*) of the odontoid process and pannus formation around it. **B**, Pannus is dark on T2WI (*arrows*). Observe that there is no high intensity within the spinal cord; however, the foramen magnum and high cervical region do appear to be compressed. Obvious basilar invagination is present by eyeball (and criteria, with McGregor's line depicted by a *double-headed arrow*).

MR, periventricular and subcortical white matter injury is seen as high signal intensity on T2WI. Obstruction of the ventricular system with resultant hydrocephalus may occur because of synechiae at the aqueduct or foramina of Monro, Magendie, or Luschka.

Herpes simplex may have a similar appearance to CMV, but microcephaly and microphthalmia are more prevalent. Marked cystic encephalomalacia is the finding in end-stage herpes infection. Hemorrhagic foci may be present in the basal ganglia, and cortical laminar necrosis may be seen as high signal on T1WI. This virus is usually transmitted during delivery from mothers with genital herpes.

Rubella infection may lead to cataracts, chorioretinitis, glaucoma, and cardiac myopathies. Deafness caused by sensorineural injury is very common. Microcephaly and seizures may lead to medical attention. Calcifications in the periventricular white matter and basal ganglia can develop on CT, as a sequela to the ischemia from vasculopathy.

Congenital HIV infection can cause a diffuse pattern of calcification throughout the brain, not limited to the periventricular region or the basal ganglia. Microcephaly may develop. More often, the disease manifests in early childhood with hemorrhagic diathesis caused by thrombocytopenia, severe nonopportunistic infections, and seizures. On imaging, the findings include intracranial hemorrhages, infections, atrophy, and calcifications. Congenital HIV infection is also associated with arteritis, fusiform aneurysms, and arterial sclerosis with vascular occlusion. One can see diffuse dilation of circle of Willis vessels in these children. Ninety percent of HIV-infected infants get AIDS within the second year of life; thus, they may develop AIDS encephalitis, infections, and lymphoma at an early age. AIDS encephalitis is characterized by atrophy, diffuse white matter hyperintensity on T2WI, and basal ganglia vascular calcification. Progressive multifocal leukoencephalopathy, toxoplasmosis, and tuberculosis are rare in kids with AIDS.

Congenital syphilis leads to seizures and cranial nerve palsies in infancy. Radiologic manifestations include optic atrophy, tabes dorsalis, meningitis, and vasculitis with enhancing meninges and perivascular spaces. Vasculitis may lead to infarctions.

See also Chapter 6 for more information on congenital infections.

— VASCULAR DISEASES OF INFANCY

Hypoxic-Ischemic Encephalopathy

Hypoxic-ischemic disease in neonates is often found in the setting of fetal distress leading to or from placental abruption, meconium-stained amniotic fluid, prolapsed umbilical cord, uterine rupture, or severe placenta previa. Apgar scores are diminished at birth with neonatal acidosis, hypotonia, lethargy, and seizures. One can find a variety of patterns of injury in neonates who experience hypoxic-ischemic injury. Four patterns of injury have

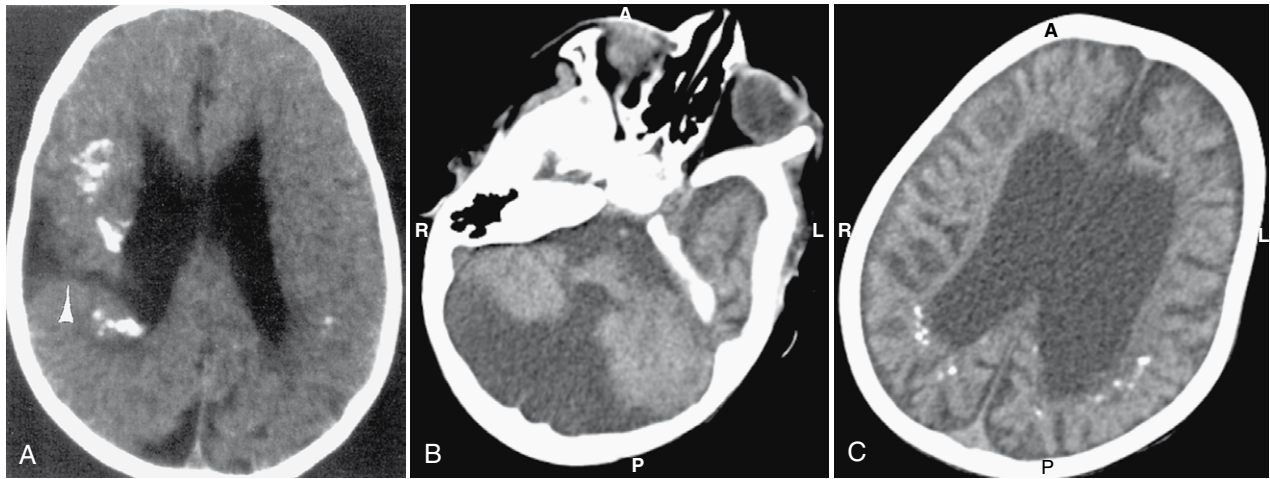


FIGURE 9-40. Congenital cytomegalovirus (CMV) infection. **A**, Axial computed tomography demonstrates calcifications in a periventricular location and in the cortex. Note that the patient also has ventricular dilation and what appears to be a schizencephalic cleft (*arrowhead*). Pachygyria is also associated with CMV infections. **B** and **C**, In this patient with congenital rubella, cerebellar atrophy and periventricular calcifications are seen.

TABLE 9-6. In Utero Infections

Characteristic	Rubella	Herpes Simplex Virus (Type 2 > 1)	Toxoplasmosis	CMV	HIV
Frequency	0.0001% of neonates	0.02% of neonates	0.05% of neonates	Most common; 1% of neonates	Growing exponentially
Clinical manifestations	Hearing loss, mental retardation, autism, speech defects	Skin lesions	Usually fetal death; developmental delay, seizures	Hearing loss, psychomotor retardation, visual defects, seizures, optic atrophy	Asymptomatic at birth, later presentation, developmental delay, late spastic paraparesis, ataxia
Ocular changes	Cataracts, glaucoma, pigmentary retinopathy	Chorioretinitis, microphthalmos	Chorioretinitis	Chorioretinitis	
Neuronal migrational anomaly	Rare	None	None	Frequent (polymicrogyria, heterotopia, hydranencephaly, lissencephaly, pachygyria), cerebellar hypoplasia	
Head size	Microcephaly		Microcephaly unless hydrocephalus	Microcephaly	Microcephaly
Parenchymal changes	Necrotic foci, delayed myelination	Hydranencephaly; patchy areas of low density in cortex, white matter; vast encephalomalacia; cortical laminar necrosis, NO PREDILECTION FOR TEMPORAL LOBE	Hydrocephalus from aqueductal stenosis, intracranial calcifications	Hemorrhage, especially at germinal matrix, loss of white matter, delayed myelination, cortex, subependymal cysts around occipital horns, cerebellar hypoplasia, atrophy	Glial, microglial nodules in basal ganglia, brain stem, white matter; demyelination, atrophy, corticospinal tract degeneration
Vessels	Vasculopathy	Can infect endothelial cells		Infarctions	Vasculopathy, vasculitis with calcifications
Calcifications	Basal ganglia, cortex		71%, periventricular, basal ganglia, parenchyma	Frequent (40%), periventricular, can have cortical calcifications	Perivascular in basal ganglia, cerebellum
Non-CNS	Patent ductus arteriosus, pulmonic stenosis, rash, hepatosplenomegaly		Hepatosplenomegaly rash	Hepatosplenomegaly	Neck adenopathy, oral candidiasis

been described: (1) deep gray matter involvement; (2) cortical involvement in watershed zones or the perirolandic region; (3) periventricular white matter injury without cortical extension; and (4) a mixed injury pattern with or without hemorrhage. These findings are usually bilateral and symmetric.

In the first 24 hours, edema may affect posterior cortical, hippocampal, and basal ganglionic regions. High signal in the thalami, basal ganglia, and central sulcus region on T1WI may then develop followed by subsequent T2-shortening. DWI scans and apparent diffusion coefficient maps may suggest restricted diffusion in the posterior limbs of the internal capsules and thalami. A second pattern with diffuse white matter restricted diffusion in the corona radiata and parietal zones can be seen. The basal ganglia injury is more evident in early life because of its high metabolic rate. These findings may be very subtle the first days of life, so, if possible, find a reason to defer scanning until the end of the first week, early second week. It is very hard to see edema in a watery neonatal brain without myelin. On follow-up studies, loss of the normal cortical T2 hypointensity may suggest the diagnosis of anoxic brain injury. The DWI extent of disease correlates well with short-term neurologic prognosis in these patients.

Patterns of Injury Based on Fetal Age and Degree of Asphyxia

Profound asphyxia from cardiopulmonary arrest or hypotension before 32 weeks' gestational age shows dramatic and often bilateral injury to the thalami, subcortical white matter, basal ganglia, and posterior brain stem. Posterior circulation structures seem to fare more poorly than anterior circulation structures in this scenario. The deep gray structures become hypodense on CT and show increased echogenicity on US. The same areas, especially the thalami early on, are bright on T1WI. If contrast enhancement of the basal ganglia or brain stem is present, the children seem to do worse on follow-up.

Partial (less severe than above) asphyxia in premature infants usually produces the classic pattern of periventricular leukomalacia. The term *periventricular leukomalacia* (PVL) is now being used generically to signify the nonspecific white matter small-vessel ischemic foci seen in elderly patients in the corona radiata and centrum semiovale. However, in the pediatric population, PVL refers to a white matter insult usually seen in premature infants because of watershed ischemia in the perforating arteries. Cystic cavitation and necrotic areas in a periventricular location may be striking. Classically, there is a posterior predominance, with the most severe changes seen around the trigone of the lateral ventricle. In the chronic phase, there is a decrease in the width of white matter between the atria and the parieto-occipital cortex, resulting in gliosis (Fig. 9-41). These findings may be seen on transcranial US, CT, or MR. The ventricles enlarge and are irregular in shape. Clinically the patients have spastic diplegia and visual field deficits.

On US, increased echogenicity of the periventricular white matter is seen in the first 2 days after the hypoxic-ischemic insult, being as echogenic as the normal choroid plexus. After a few weeks this pattern is replaced by cystic cavitated areas amid the echogenic background. Subsequently, the lateral ventricles expand, volume loss is evident, and the intervening tissue is diminished in size but of normal echotexture. The grading of PVL by US consists of grade 1, evanescent periventricular echogenicity lasting shorter than 7 days; grade 2, prolonged periventricular echogenicities lasting longer than 7 days; grade 3, periventricular lesions evolving into small cysts; grade 4, periventricular lesions evolving into extensive periventricular cysts; and grade 5, periventricular lesions involving the subcortical white matter and creating extensive periventricular and subcortical cysts.

The MR scans of patients with sonographic evidence of PVL may show more extensive hemorrhagic foci in the periventricular

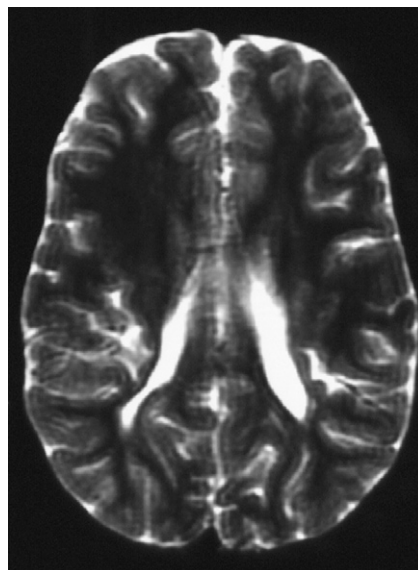


FIGURE 9-41. Periventricular leukomalacia. This child, who was born prematurely, shows the diminution in white matter volume and abnormal configuration of the ventricles indicative of periventricular leukomalacia of prematurity. Note how deep the sulci dive on this T2-weighted image.

and subcortical regions, even when only periventricular echogenicity is evident on US. MR also demonstrates more extensive cyst formation than US. The more areas of hemorrhage, the more likely cyst formation and the worse the long-term outcome. The MR findings of PVL correlate well with clinical evidence of visual loss and spastic paraparesis. Volumetric reduction and signal hyperintensity of the peritrigonal white matter and atrophy of the calcarine cortex correspond to the finding of visual impairment in children. One may even see secondary degeneration of the lateral geniculate bodies.

Partial asphyxia in term infants causes cortical watershed distribution lesions between cerebral arteries. The long-term consequence of partial asphyxia in the term infant is a peculiar-shaped atrophy of the cortex in parasagittal locations termed *ulegyria* (mushroom shaped). The cortex at the depth of the sulci suffers more profound cortical loss than those more superficial in the infant, leading to this unusual shape. This pattern of injury seems to differ from that of partial asphyxia in premature infants (where the damage is predominantly periventricular) and of profound asphyxia in term infants.

Term infants with profound asphyxia have greater involvement of the lateral thalami, corpus striatum, hippocampus, and dentate nuclei of the cerebellum. The cortex is spared except around the central sulcus region. Again, the key to detection is to note the low density of the deep gray matter structures on CT and high signal on T1WI 2 to 3 days postpartum.

Subdural hematomas in the brains of asymptomatic term infants after uncomplicated deliveries are not unusual. The incidence of supratentorial subdural hematomas ranges from 26% to 46%, usually located in the posterior extra-axial spaces, especially parafalcine, and measuring less than 4 mm in thickness. Twenty percent also have a posterior fossa subdural hematomas. These collections resolve within 1 month. Cephalhematomas occur in 22%. Subdural hematomas are more common in neonates delivered by vaginal routes rather than by cesarean sections and when there is prolongation of the second stage of labor. Assisted deliveries (vacuum extraction and forceps deliveries) have a higher rate as well.

Cerebral Palsy

The development of cerebral palsy in premature infants is most closely related to early MR findings of subependymal

TABLE 9-7. Grading of Germinal Matrix Hemorrhage

Grade	Location of Hemorrhage, Findings
1	Limited to germinal matrix
2	Germinal matrix and intraventricular
3	Germinal matrix and intraventricular with hydrocephalus
4	Germinal matrix, intraventricular, and intraparenchymal

hemorrhage associated with parenchymal destruction, periventricular signal alteration with irregularity of the ventricular wall, and widespread cerebral infarction (usually middle cerebral artery distribution). In term asphyxiated infants, deep gray matter or diffuse involvement of the hemispheres is predictive of a poor prognosis. Parenchymal periventricular encephaloclastic cysts also bode poorly for outcome in premature infants, whereas focal parenchymal damage is less debilitating (perhaps because of the plasticity of the brain). In term asphyxiated infants, T2 signal alterations of the deep gray matter rather than T1-shortening and diffuse involvement of the hemispheres are predictive of long-term deficits. Focal hemispheric parenchymal lesions alone are not predictive of cerebral palsy.

Germinal Matrix Hemorrhages

Germinal matrix and caudate-thalamic junction hemorrhages are also seen in premature infants (usually those that are 32 weeks' gestation or less). Ninety percent of hemorrhages in premature infants occur in the first week of life, hence the screening US that are often ordered. The hemorrhages are thought to be venous in origin. The hemorrhage may track along the venous perivascular space and rupture into the parenchyma. Hydrocephalus caused by intraventricular blood, clots in the aqueduct, or arachnoid villi plugging occurs in 70% of premature infants with intraventricular hemorrhage (Table 9-7). Grade IV hemorrhages may actually be bleeds into venous infarctions secondary to occlusions of thalamostriate veins.

Arteriovenous Anomalies

The arteriovenous malformations are described fully in Chapter 4. The only "congenital" malformation that presents in infancy is the so-called *vein of Galen aneurysm*. This is really a central arteriovenous malformation or fistula. The tremendous arteriovenous shunting may lead to congestive heart failure in a newborn infant. To make matters worse, congenital cardiac anomalies may coexist. We are able to make this diagnosis in utero by US or MR (Fig. 9-42) and plan for treatment immediately after birth. Intrauterine therapy has not been contemplated by neuroradiologists just yet, but may be described in the next edition of this book, no doubt.

Miscellaneous Insults

Parry-Romberg Syndrome

In Parry-Romberg syndrome, or progressive facial hemiatrophy, one can find unilateral focal infarctions in the corpus callosum, diffuse deep and subcortical white matter signal changes, mild cortical thickening, and leptomeningeal enhancement with dense mineral deposition. The pathogenesis of this process is thought to be a chronic vasomotor/ischemic one related to sympathetic nervous system inflammation.

Maternal Cocaine Abuse

Another scenario where neonatal ischemia may be present is in children of women abusing cocaine. "Normal" neonates with a maternal history of cocaine use are more likely to have focal infarctions in their basal ganglia. They also have a higher rate of

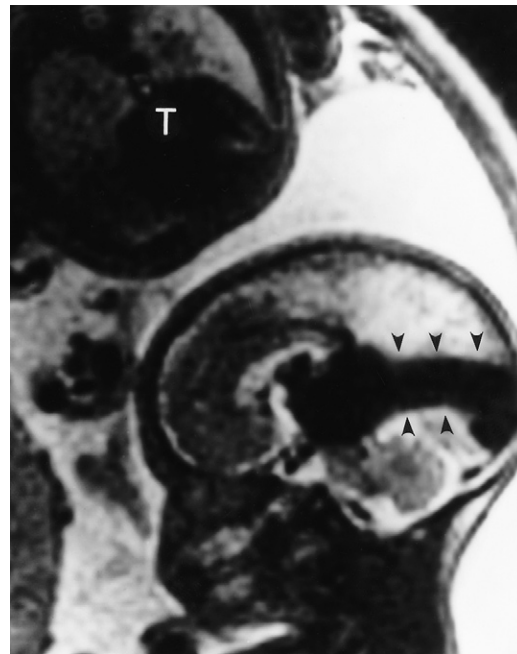


FIGURE 9-42. In utero demonstration of vein of Galen malformation on magnetic resonance. Note the very large flow void (arrowheads) in the expected location of the vein of Galen in this fetus. The large size portends a bad prognosis. Shhhhhhh! Don't wake up the twin (T) seen sharing the sac.

neural tube closure defects. The mechanism for these abnormalities is probably due to vasospasm caused by cocaine when used in pregnancy.

Neonatal Hypoglycemia

Neonatal hypoglycemia (glucose <30 mg/dL) secondary to hyperinsulinemia can cause seizures and altered mental status. The cause may range from maternal diabetes to hypoxic-ischemic injury, to sepsis, gestational immaturity or malnutrition, or glucose dysmetabolism (Beckwith-Wiedemann syndrome, endocrinopathies). Brain damage in the parieto-occipital region is most common. High signal on T2WI is understandable, but high signal on T1WI may coexist, secondary to hemorrhage, calcification, or myelin breakdown.

Kernicterus

Kernicterus (bilirubin encephalopathy) is associated with high signal intensity in the globus pallidus, which resolves with normalization of the bilirubinemia.

Attention Deficit Hyperactivity Disorder

No definite structural lesions have been identified in patients with attention deficit hyperactivity disorder (ADHD), though some interesting functional work has been done. ADHD is thought to represent dopamine dysfunction localized to the frontal lobes and striatum. Medications that increase the availability of dopamine receptor sites affect the core behaviors that define ADHD. Functional brain imaging shows that frontal lobe abnormalities in children with ADHD worsen with concentration exercise and are reversible following stimulant administration. Children with ADHD show frontal lobe deactivation during concentration tasks. They show decreased left prefrontal lobe and dorsal frontal lobe activity at rest compared with controls as well as with concentration.

— MESIAL TEMPORAL SCLEROSIS

The search for mesial temporal sclerosis (MTS) is like the Holy Grail of neuroimaging because this entity is a common source for seizures in adolescents and young adults. Going from the

Box 9-9. Causes of Temporal Lobe Epilepsy

Mesial temporal sclerosis (hippocampal sclerosis)
 Ganglioglioma
 Astrocytomas of all types
 Cavernous hemangioma
 Cortical dysplasia
 Heterotopia
 Oligodendroglioma

superomedial to inferolateral surface of the hippocampus, one passes from the fimbria to the alveus to the dentate fascia and then Ammon's horn (zones 1 to 4) region (see Chapter 2). After passing around the hippocampal fissure, one proceeds into the subiculum (the superomedial border) to the parahippocampal gyrus medially and the entorhinal and piriform cortex inferiorly. The collateral sulcus separates the parahippocampus above from the occipitotemporal gyrus below. Ammon's horn, or cornu ammonis, has four zones of granular cells. CA1 is also called the vulnerable sector because it is the most sensitive area of the brain (with the globus pallidus) to anoxia. CA2 (dorsal resistant zone) and CA3 (resistant Spielmeyer sector) are thought to be more resistant to anoxic damage. CA4 (end folium) is partially affected by anoxia. Sclerosis of CA1, and to a lesser extent CA4, is the etiology of MTS or hippocampal atrophy and has been linked to cerebral ischemia and febrile seizures. The selective vulnerability of CA1 may be due to overactivity of glutamate receptors and increased concentration of intracellular calcium ions in these granular cells. Hypoglycemia and kainic acid toxicity could also injure hippocampal structures.

Mesial temporal sclerosis accounts for as much as 50% of subjects undergoing temporal lobe surgery, and the main site of disease is CA1. However, the causes of temporal lobe seizures are manifold (Box 9-9).

Temporal lobe seizures are usually partial (that is, there is no loss of consciousness), as opposed to generalized seizures (where there is loss of consciousness). If consciousness is altered the term used is *complex partial seizure*; if no alteration, neurologists call it *simple partial seizure*. Thirty percent of temporal lobe seizures are idiopathic, with no cause, 40% have an underlying visible cause (symptomatic), and 30% are cryptogenic, where the cause may be unknown but a lesion probably exists. MTS is considered the symptomatic variety and often results in poorly controlled

seizures. Although 60% of all seizure disorders are well-managed with medications, MTS often requires surgical intervention.

In those patients with ipsilateral hippocampal atrophy, surgical removal of MTS is 90% effective in eliminating seizures. In adults with temporal lobe epilepsy who have resection of their temporal lobe, 65% of the time, the pathology shows MTS. Twenty percent of cases show normal MR structural scans—hence the potential for magnetic resonance spectroscopy to rear its opportunistic head (see below).

Although most cases present after or in adolescence, the roots of MTS may reside in febrile seizures in infancy. Multiple seizures in early childhood are associated with hippocampal atrophy. Nonetheless, MTS is considered a progressive disease and the imaging findings of selective atrophy may progress with age.

Atrophy of the mesial temporal lobe may affect the amygdala (12%), hippocampal head (51%), hippocampal body (88%), and hippocampal tail (61%) (Fig. 9-43). Hyperintense signal on T2-weighted scans may involve the amygdala (4%), hippocampal head (39%), hippocampal body (81%), and hippocampal tail (49%) or the entire ipsilateral hippocampus (44%). Bilateral involvement occurs in approximately 20% of cases. Another finding in the spectrum of MTS is the loss of the normal cortical interdigitations of the hippocampal head. The sensitivity of this finding is approximately 90%; it may be present even when atrophy and signal intensity changes are absent in the medial temporal lobe. Histopathologically, one sees neuronal loss and gliosis in the patients. The mechanism for congenital, nonfebrile development of MTS is mysterious, but may be due to a perinatal ischemic event due to compression of arteries during delivery, intrauterine hypoxia, hypoxia secondary to status epilepticus, neurotoxic effects of excessive glutamate production, or hypoglycemia.

One can obtain greater and greater layers of sophistication in the analysis of the temporal lobes using quantitative volumetry, T2 relaxometry, magnetic resonance spectroscopy (MRS) (decreased N-acetyl aspartate [NAA], also reported as NAA/choline ratio <0.8 and NAA/creatine ratio <1.0), positron emission tomography, and single-photon emission computed tomography. If patient is scanned during or within 24 hours of acute temporal lobe seizures, one finds lactic acid buildup or lipid peaks on the proton MRS studies of the affected temporal lobe. The bottom line is that simple 512×512 matrix FLAIR or T2WI for signal intensity changes and 512×512 resolution inversion recovery T1-weighted scans (phase-sensitive inversion recovery) for the presence of hippocampal atrophy will tell you which temporal

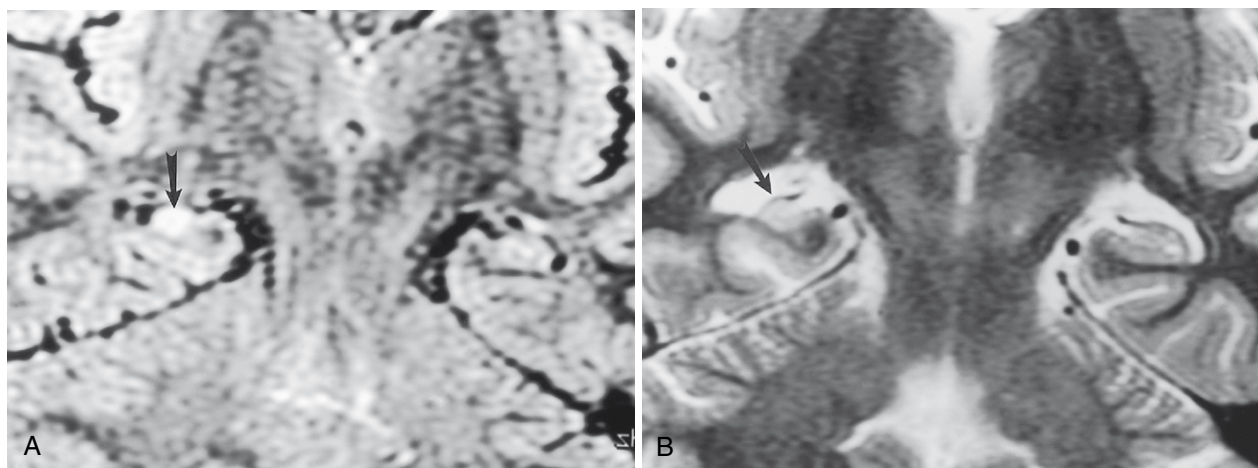


FIGURE 9-43. Mesial temporal sclerosis. **A**, Note the focal area of high signal in the right hippocampus (arrow) on the FLAIR image. **B**, Atrophy of the hippocampus (arrow) and high signal are also apparent on the T2-weighted image.

lobe is abnormal in the vast majority of cases. Or you can call for the electroencephalography (EEG) results and be done with it. For those cases with equivocal EEG findings or bilateral disease, careful scrutiny of the images will stand you in good stead. There is a whole cottage industry of volumetric programs that will determine which hippocampus is smaller—they can be extremely accurate.

The fornix and mamillary body ipsilateral to the side of MTS may be atrophic secondary to the decreased input to crossing fibers and limbic contributions. These findings may also be present in cases of temporal lobe resections, strokes, and tumors.

When the localization of a seizure focus is problematic, the neurosurgeons may place stainless steel or platinum alloy subdural grid contact arrays. This is a last resort when ictal scalp recordings have failed and when functional cortical mapping is required before surgery. The placement of these grids is not without risk; be wary of the reported complications of extra-axial hematomas or effusions, venous thromboses, subfalx or transtentorial herniations, tension pneumocephalus, intraparenchymal hemorrhage, and cerebral infections. Depth electrodes into brain parenchyma is the final stage of invasive localization.

One potential obstacle associated with the workup for seizures should be recognized. If you image the patient immediately after a seizure or even during status epilepticus that is inapparent to the clinicians, you may see meningeal enhancement and high signal intensity in the seizing temporal lobe. This may imply a more diffuse process than is actually there (encephalitis or gliomatosis) and in fact, this “abnormality” may resolve completely on MR in a few days. This is probably due to the increased blood flow to the seizing temporal lobe; that is, a perfusion effect. Even DWI scans may be transiently positive.

Other sources of seizure foci include (in the young patient) neoplasms, vascular malformations, gliotic abnormalities, and malformations of cortical development. Add strokes to this list for older adults. Occipital lobe epileptogenic foci are most often due to developmental abnormalities (e.g., focal cortical dysplasia, heterotopias, hamartomas, migrational anomalies) or tumors (usually gliomas).

PHAKOMATOSES

The phakomatoses are a group of hereditary diseases of the neuroectoderm characterized by cutaneous manifestations and sometimes called *neurocutaneous disorders*. *Phakos* is Greek for “mother-spot,” probably reflecting the cutaneous manifestation. These disorders include neurofibromatosis, tuberous sclerosis, von Hippel-Lindau disease, and Sturge-Weber syndrome. The quintessential lesion is the neurogenic tumor, the tuber, the hemangioblastoma, and the angiomatosis, respectively. Hereditary hemorrhagic telangiectasia, ataxia-telangiectasia, neurocutaneous melanosis, basal cell nevus syndrome, Wyburn-Mason syndrome, and Parry-Romberg syndrome are also classified as phakomatoses.

Neurofibromatosis

Neurofibromatosis Type 1

Neurofibromatosis type 1 (von Recklinghausen disease, or NF-1) (Table 9-8) is a disease of childhood that occurs in a hereditary form transmitted by autosomal dominance in 50% of cases and sporadically in the other 50%. Overall, the incidence of NF-1 is approximately 1 in 2000 to 6000 live births. NF-1 is diagnosed if there are two or more of the following findings: (1) six or more café-au-lait spots, (2) two or more Lisch nodules (hamartomas) of the iris, (3) two or more neurofibromas or one or more plexiform neurofibromas, (4) axillary/inguinal freckling, (5) one or more bone dysplasias or pseudarthrosis of a long bone, (6) optic pathway glioma, or (7) a first-degree relative with the diagnosis of NF-1.

Neurofibromatosis type 1 appears to be transmitted on the long arm of chromosome 17 (17q11) and occurs in 1 in 2500

TABLE 9-8. NF-1 versus NF-2

Feature	NF-1	NF-2
Chromosome involved	17	22
Optic gliomas	Yes	No
Acoustic schwannomas	No	Yes
Meningiomas	No	Yes
UBOs in deep gray matter, cerebellum	Yes	No
Incidence	1/4,000	1/50,000
Skin findings	Many	Few
Spinal gliomas	Astrocytoma	Ependymoma
Skeletal dysplasias	Yes	No
Lisch nodules (iris hamartomas)	Yes	No, but sublenticular cataracts
Dural ectasia	Yes	No
Age at presentation (yr)	<10	10–30
Vascular stenoses	Yes	No
Plexiform neurofibromas	Yes	No
Malignant change	Yes	No
Sphenoid wing absence	Yes	No
Hydrocephalus	Yes, obstructed/stenotic aqueduct	No
CNS hamartomas	Yes	No
Paraspinal neurofibromas	Yes	Yes
Meningocele	Yes, lateral thoracic	No

UBOs, unidentified bright objects.

to 4000 live births. In NF-1 the patients have many café-au-lait spots and have a preponderance of optic pathway pilocytic astrocytomas. These optic gliomas present in childhood yet may have little effect on vision until they are large. From 10% to 38% of patients with optic gliomas have NF-1, and 15% to 40% of patients with NF-1 have optic pathway gliomas (Fig. 9-44). Cerebellar, brain stem, and cerebral astrocytomas are also seen with NF-1. In addition, as noted on MR, the patients have high signal intensity foci that appear in the peduncles or deep gray matter of the cerebellum, the brain stem (especially the pons), the basal ganglia (especially the globus pallidus), and the white matter of the supratentorial space (Fig. 9-45). There is considerable debate concerning what these areas of high signal intensity on T2WI represent, as described in this chapter in the section Hamartomas. At this time most people believe that they are due to myelin vacuolization or hamartomas, focal areas of gliosis, Wallerian degeneration, dysplastic white matter or, less likely, preneoplastic lesions. These basal ganglia foci may also be bright on T1-weighted scans.

Follow-up studies of these high-intensity foci in neurofibromatosis patients suggest that, though present in the basal ganglia and brain stem in younger patients with relatively high frequency, they often decrease in size with age. Lesions in the cerebellar white matter and dentate nuclei are found in younger patients and are rare after the third decade. Rarely they may enlarge in adulthood.

Astrocytomas may arise within the previously described locations in the basal ganglia, optic radiations, cerebellar gray or white matter, or brain stem. When the high-intensity foci enhance or grow after adolescence, the specter of neoplasm must be raised. Short follow-up scans are indicated. Patients with NF-1 also have increased incidence of astrocytomas of the spinal cord.

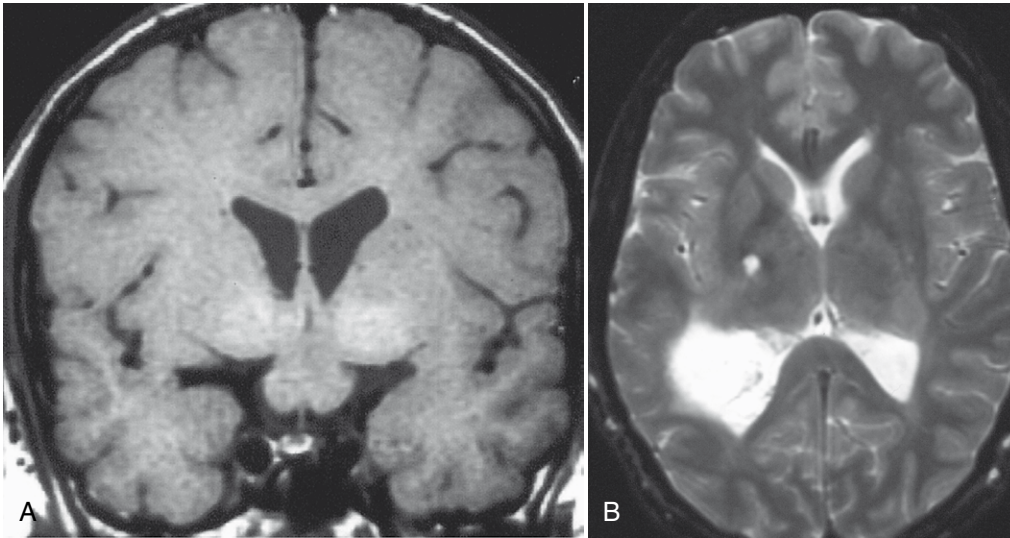


FIGURE 9-44. Optic pathway glioma. **A**, There is marked enlargement of the optic chiasm in this individual. **B**, The optic fibers adjacent to the right occipital horn of the lateral ventricle are involved. The tiny deep gray matter focus is indicative of neurofibromatosis type 1.

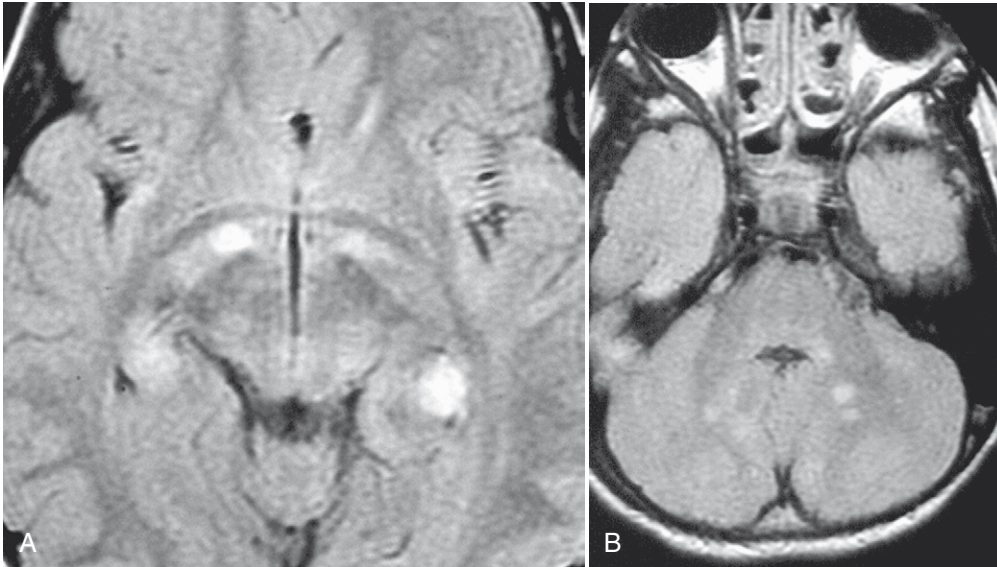


FIGURE 9-45. Unidentified bright objects (UBOs) of neurofibromatosis type 1 (NF-1). **A**, This FLAIR scan epitomizes the vexing lesions of the basal ganglia in patients with NF-1. Histopathologically, these UBOs have yet to be well-characterized. **B**, They are also seen in the thalami and the cerebellar white matter tracts.

On imaging, one may see enlargement of the optic nerves or chiasm. These tumors are generally low-grade pilocytic astrocytomas and slow growing and are usually watched; treatment is withheld until the patient becomes progressively symptomatic. Enhancement is variable.

The presence of a plexiform neurofibroma strongly suggests NF-1. A plexiform neurofibroma consists of sheets of collagen and Schwann cells that spread in an aggressive manner, insinuating themselves in a cylindrical fashion around a nerve. These lesions tend to involve the scalp, neck, mediastinum, retroperitoneum, cranial nerve V, and orbit (Fig. 9-46). The lesions are soft and elastic, and probably account for the “elephantiasis” of neurofibromatosis.

Sarcomatous degeneration of neurofibromas occurs in approximately 5% of patients with peripheral nerve sheath neural tumors. The more neurofibromas one has, the higher the likelihood of malignant degeneration, but this usually occurs in midadulthood. Plexiform neurofibromas have a higher rate of malignant change, much more so than schwannomas.

Additional findings that one might see in patients with neurofibromatosis include spinal dural ectasia (Fig. 9-47), lateral thoracic meningoceles, posterior vertebral body scalloping, aqueductal stenosis, pachygyria, polymicrogyria, syringomyelia, and other heterotopias. Neuroradiologists can have a field day with neurofibromatosis (note: this, too, is a favored topic for board examinations).

Neurofibromatosis Type 2

Neurofibromatosis type 2 (NF-2) appears to be transmitted on chromosome 22q12 and is approximately one tenth as common as NF-1. The patients have fewer skin lesions, but the pathognomonic sign of NF-2 is bilateral cranial nerve VIII vestibular schwannomas (Fig. 9-48). Diagnosis is made if the patient has one of the following features: (1) bilateral vestibular acoustic schwannomas or (2) a first-degree relative with NF-2 and either a single acoustic schwannoma or any two of the following: schwannomas, neurofibromas, meningiomas, or gliomas. A posterior

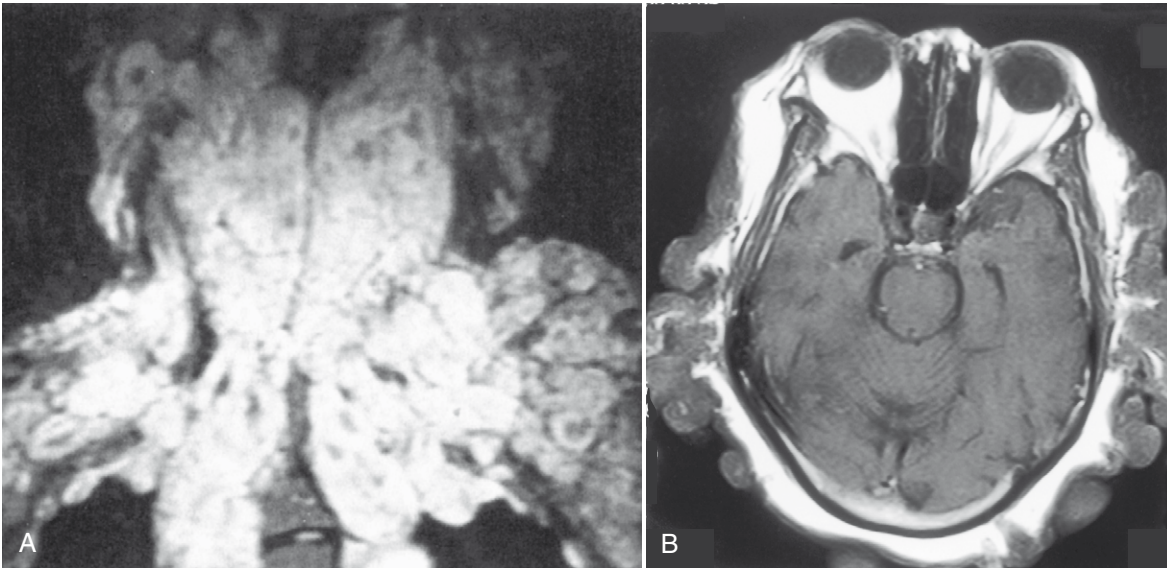


FIGURE 9-46. Plexiform neurofibroma. **A**, Coronal magnetic resonance depicts an enormous plexiform neurofibroma of the spine, shoulders, and neck. **B**, Multiple cutaneous neurofibromas. Despite the numerous cutaneous neurofibromas, which extended into the subcutaneous tissue bilaterally, this patient's brain was normal. Which would you rather have, the cosmetic deformity of multiple cutaneous neurofibromas or the potential danger of intracranial (optic pathway) manifestations? (Case courtesy of Stuart Bobman.)

FIGURE 9-47. Neurofibromatosis type 1 (NF-1). **A**, Sagittal T1-weighted image (T1WI) with posterior scalloping of the T10 vertebral body. **B**, After intrathecal contrast a fluid level is observed in the lateral meningocele. The pedicle is thinned and the left posterior margin of the vertebral body is scalloped. **C**, T2WI in another patient demonstrating a large lateral thoracic meningocele. Marked scalloping is noted in the posterior aspect of the vertebral body.

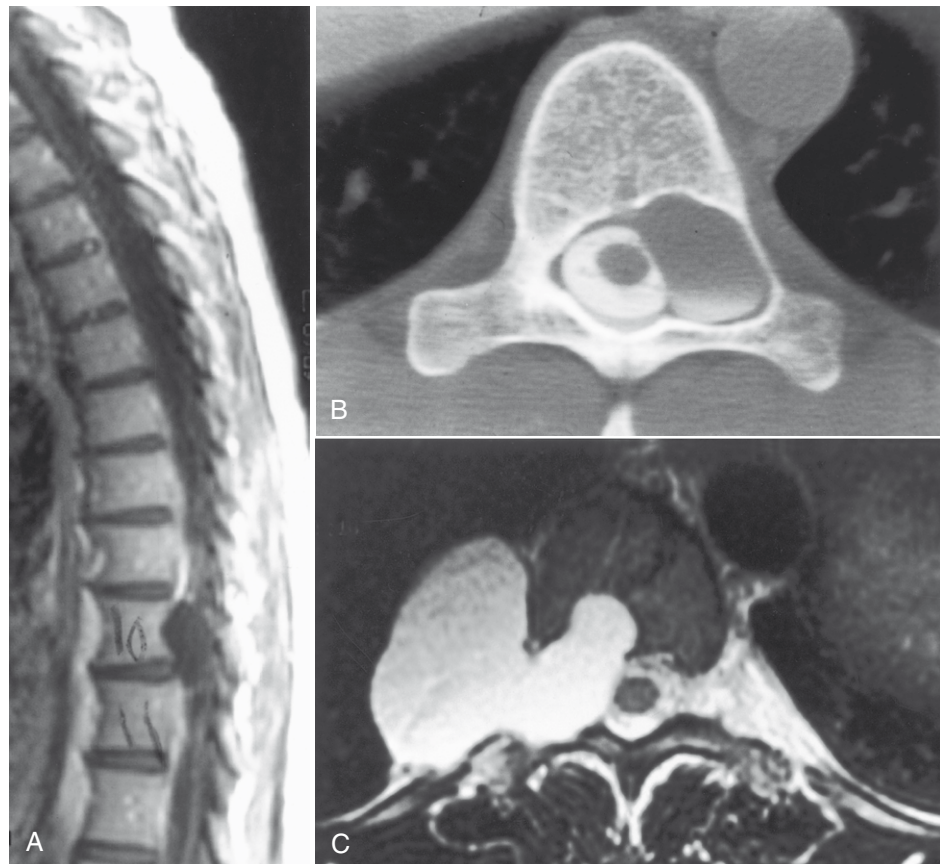




FIGURE 9-48. Neurofibromatosis type 2 (NF-2). Axial enhanced T1-weighted image shows bilateral acoustic schwannomas (*arrows*). This finding is the sine qua non of NF-2. Forget it and you fail your boards.

sublenticular capsular cataract in a young patient is also typical of this disorder. Cranial nerve V is the second most common site of schwannomas in NF-2. Sensory roots are affected more commonly than motor roots. The patients also have increased incidence of meningiomas and rarely have other glial tumors (ependymomas). The nickname MISME (multiple inherited schwannomas, meningiomas, and ependymomas) attests to the fact that neurofibromas are not a feature of NF-2.

Spinal manifestations of NF-2 can be seen in 63% to 90% of cases. Patients with non-sense or frame shift mutations have a higher rate of spinal tumors than those with splice-shift and all other types of genetic mutations. In one report 53% of patients had intramedullary lesions, 55% intradural extramedullary tumors (88% were nerve sheath tumors and 12% meningiomas), and 45% both intramedullary and extramedullary masses. Of those with intramedullary masses, over half had multiple ones. Multiple nerve sheath tumors (both schwannomas [75%] and neurofibromas [25%]) are usually seen in the cauda equina and may be intradural or extradural. Of intramedullary tumors, ependymomas predominate, but astrocytomas and intramedullary schwannomas may occur.

Patients with NF-2 demonstrate enhancing masses located in and around the cerebellopontine angle or extending into the internal auditory canal. The lesions generally are slightly hyperintense on T2WI. (Please see Chapter 3 for typical and atypical features of vestibular schwannomas.) Occasionally, dural ectasia of cranial nerve VIII root sleeve can enlarge the internal auditory canal, producing the same type of bony flaring seen with acoustic schwannomas. Arachnoid cysts may accompany the vestibular schwannomas. In addition, meningiomas may occur at this location, although the parasagittal regions predominate.

Tuberous Sclerosis

Tuberous sclerosis (Bourneville disease) (Box 9-10) is a disease that most commonly occurs spontaneously (60%) but is also seen in an autosomal dominant form transmitted on the long arm of chromosome 9 (9q34) or 16 (16p13). It arises in 1 in 6000 to 15,000 live births. The characteristic findings with tuberous sclerosis are adenoma sebaceum (60% to 90% of cases), mental retardation (50%), and seizures (60% to 80%). All three findings occur in only one third of cases. Patients also may have retinal hamartomas (50%), shagreen patches (20% to 40%), ungual fibromas (20% to 30%), rhabdomyomas of the heart (25% to 50%), angiomyolipomas of the kidney (50% to 90%), cystic skeletal lesions, and the intracranial manifestations. Tuberous sclerosis is like a shotgun blast: It can hit all parts of the body.

Box 9-10. Tuberous Sclerosis Findings

CLINICAL

- Adenoma sebaceum
- Ash-leaf spot
- Café-au-lait spots
- Mental retardation
- Retinal hamartomas
- Retinal phakoma
- Seizures
- Shagreen patches
- Subungual fibromas

RADIOGRAPHIC CNS

- Atrophy
- Calcified optic nerve head drusen
- Cortical tubers
- Giant cell astrocytomas
- Intracranial calcifications
- Neuronal migrational anomalies
- Periependymal nodules
- Radial glial fiber hyperintensity

RADIOGRAPHIC NON-CNS

- Angiomyolipomas of kidneys
- Aortic aneurysm
- Hepatic adenomas
- Pulmonary lymphangiomyomatosis
- Rhabdomyomas of heart
- Renal cell carcinoma
- Renal cysts
- Skeletal cysts, sclerotic densities, periosteal thickening
- Upper lobe interstitial fibrosis, blebs, pneumothorax, chylothorax
- Vascular stenosis

The intracranial manifestations include periventricular subependymal nodules (candle gutterings) (90% to 100%), cortical and subcortical peripheral tubers (94% of patients on MR), white matter hamartomatous lesions, and subependymal giant cell astrocytomas (6% to 16%) (Fig. 9-49). Patients may have cortical heterotopias and ventriculomegaly as well. Eighty-eight percent of periventricular subependymal nodules are calcified, whereas only 50% of the parenchymal hamartomas are calcified. The frequency of cortical tubers and white matter lesions is highest in the frontal lobes, followed by the parietal, occipital, temporal, and cerebellar regions. Tubers may expand gyri or show central umbilication and are bright on long repetition time (TR) sequences. Patients with cerebellar tubers are older than those with cerebral tubers, have more extensive disease, and may have focal cerebellar atrophy associated with those tubers. White matter lesions may appear on MR as curvilinear or straight thin bands radiating from the ventricles (88%), wedge-shaped lesions with apices near the ventricle (31%), or tumefactive foci of abnormal intensity (14%). Subependymal nodules (31%), cortical tubers (3%), and white matter lesions (12%) may show enhancement on MR. FLAIR imaging is particularly good at spotting subcortical small tubers, even more so than T2-weighted scans. It should be noted, however, that the number, size, and location of tubers seems to be unrelated to the neurologic symptoms in adults. A greater number of tubers occur in children with infantile spasms, seizures before age 1 year, and mental disability. The pathogenesis of the various lesions of tuberous sclerosis is thought to be due to abnormal radial-glial migration of dysgenetic giant cells that are capable of astrocytic or neuronal differentiation—multipotential cells with multiproblems.

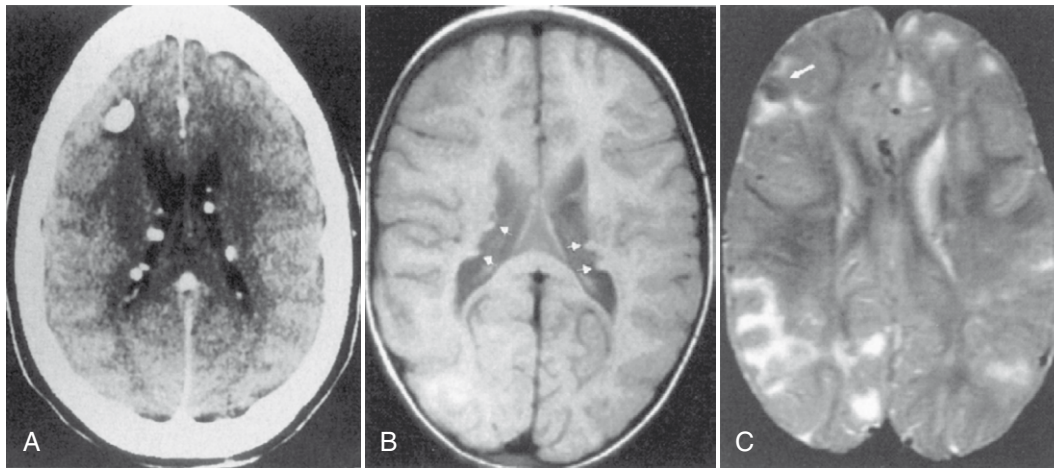


FIGURE 9-49. Tuberous sclerosis. **A**, Note the periventricular calcified subependymal nodules on this computed tomography scan. Cortical calcified tuber is also located in the right frontal region. **B**, Axial T1-weighted image (T1WI) shows the subependymal nodules (*small arrows*) lining the lateral ventricles bilaterally isointense to white matter. **C**, Axial T2WI demonstrates foci of abnormal signal intensity throughout the subcortical white matter and in the cortex corresponding to areas of abnormal myelination and cortical tubers. Right frontal cortical tuber (*arrow*) is probably calcified (because it is very low in intensity on T2WI). Calcified subependymal nodules are present; find them.

In infants, the subependymal nodules of tuberous sclerosis are hyperintense on T1WI and hypointense on T2WI, the opposite of what is seen in adults. They are not isointense to gray matter and therefore should not be confused with subependymal nodular heterotopias. White matter anomalies are more visible in infants. However, cortical tubers are more difficult to identify in infants. In utero demonstration of periventricular subependymal nodules and cardiac rhabdomyomas has been reported in a fetus of 28 weeks' gestational age.

Tuberous sclerosis has an association with subependymal giant cell astrocytomas (SGCA) that generally occur around the foramina of Monro (see Chapter 3) (Fig. 9-50). As opposed to subependymal tubers, these lesions enhance commonly and uniformly, are large, grow with time, cause obstructive hydrocephalus, and have a lower rate of calcification. Nonetheless,

it is believed that these tumors arise from subependymal nodules. They occur in approximately 1.7% to 15% of patients who have tuberous sclerosis. Their malignant potential is small.

On CT, the periventricular calcified nodules are seen easily; however, the more peripheral tubers are harder to detect. Calcification obviously would be difficult to detect on MR without gradient-echo scans. Nonetheless, the tubers are well seen by MR, showing up as increasing intensity on T2WI. The subependymal tubers may be better seen on T1WI. The SGCAs are increased in signal intensity on T2WI and demonstrate moderate enhancement. CT may be more specific than MR for SGCA because enhancement on CT implies a SGCA whereas enhancement on MR (because of the sensitivity) may be seen with tubers and subependymal nodules.

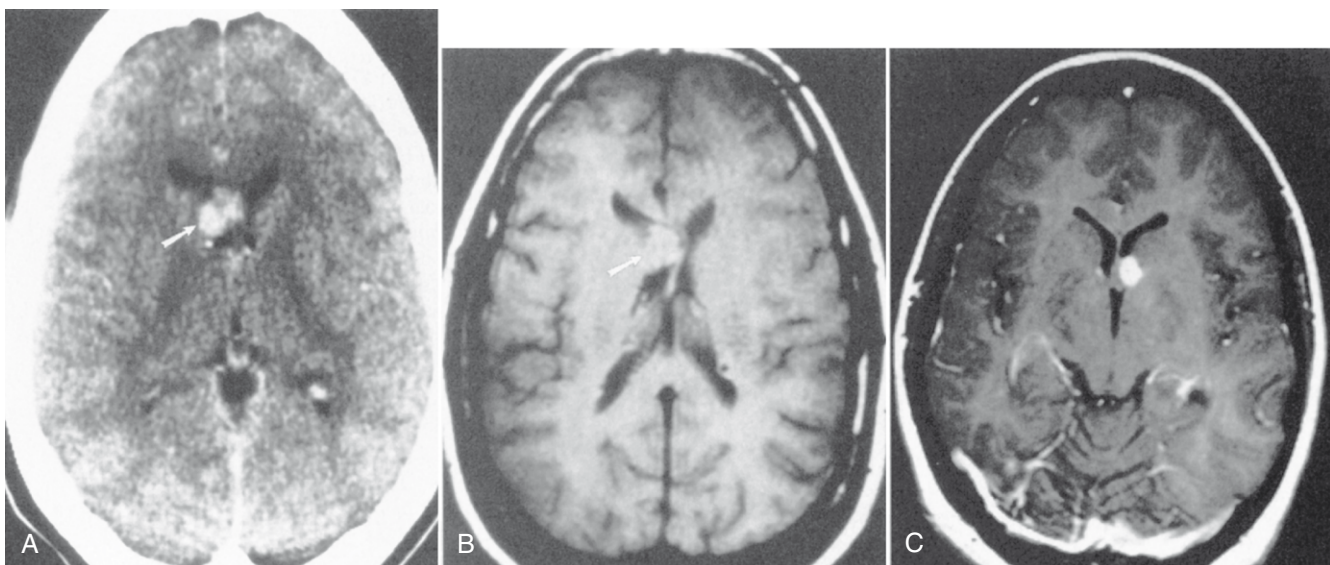


FIGURE 9-50. Subependymal giant cell astrocytoma in tuberous sclerosis. **A**, Enhanced computed tomography (CT) demonstrates high density (*arrow*) in this patient with tuberous sclerosis. On the basis of the CT we cannot tell whether the lesion enhances or is calcified. This would be important because on CT subependymal giant cell tumors enhance, whereas tubers usually do not. **B**, T1-weighted image (T1WI) without contrast also shows the isointense subependymal mass (*arrow*). Unfortunately, the patient left before contrast could be given to go to an Ozzy Osborne reunion. However, on magnetic resonance this does not help in distinguishing subependymal giant cell tumor from a subependymal nodule because both have been reported to enhance. **C**, Another case shows enhancement on T1WI of a subependymal giant cell astrocytoma.

Box 9-11. Findings in Sturge-Weber Syndrome**CLINICAL**

Accelerated myelination
 Choroidal angioma
 Glaucoma-buphthalmos
 Hemiparesis, hemiplegia
 Mental retardation
 Scleral telangiectasia
 Seizures
 Trigeminal angioma (capillary telangiectasia); port wine nevus in cranial nerve V-1 distribution
 Visceral angioma

RADIOGRAPHIC

Anomalous venous drainage to deep veins
 Choroid plexus angioma or hypertrophy ipsilateral to angiomatosis
 Dyke-Davidoff-Masson syndrome
 Elevated petrous ridge, sphenoid wing
 Enlarged frontal sinuses
 Hemihypertrophied skull
 Hemiatrophy
 Intracranial calcification (tram-tracks)
 Pial angioma

Sturge-Weber Syndrome

Sturge-Weber syndrome (encephalotrigeminal angiomatosis) (Box 9-11) is associated with facial port wine stain (nevus flammeus), hemiplegia, and seizure disorder. Other manifestations include congenital glaucoma and buphthalmos, choroidal or scleral hemangiomas, and mental retardation. This disease usually occurs sporadically with equal male and female incidence. The cutaneous vascular nevus in the face is usually in the V-1 distribution. There are rare cases reported in which the patient has Sturge-Weber syndrome without the facial nevus. Ipsilateral to the vascular angioma within the brain, one often identifies enlargement and enhancement of the choroid plexus, suggesting an angioma.

Leptomeningeal capillary-venous angiomatosis is also seen in Sturge-Weber syndrome. On CT Sturge-Weber syndrome is usually detected by cortical calcification (tram-tracks) in the ipsilateral occipital, parietal, or temporal lobe underlying the leptomeningeal vascular malformation with associated hemiatrophy (Fig. 9-51). The abnormality is truly a pial vascular abnormality, which demonstrates underlying patchy gliosis and demyelination. Patients usually have a homonymous hemianopsia, contralateral hemiplegia, and hemisensory loss. The calcification is within the cortex and not the meninges, arises in the fourth layer of the cortex, and is thought to be due to anoxia from stasis of flow within the meninges. Calcification, however, is not seen until about the second year of life. CT demonstrates the cortical calcification to best advantage. Atrophy is present on the ipsilateral side, as is enlargement of the choroid of the lateral ventricles. In fact, the size of the choroid plexus and extent of leptomeningeal involvement in children with Sturge-Weber syndrome correlates well.

Magnetic resonance imaging detects a greater extent of disease than CT, particularly on enhanced T1WI. In this instance, the pia enhances dramatically, giving a true demonstration of the degree of the vascular abnormality (Fig. 9-52). Cortical enhancement caused by ischemic injury may also be present. Abnormally low signal intensity within the white matter on T2WI is probably related to abnormal myelination from

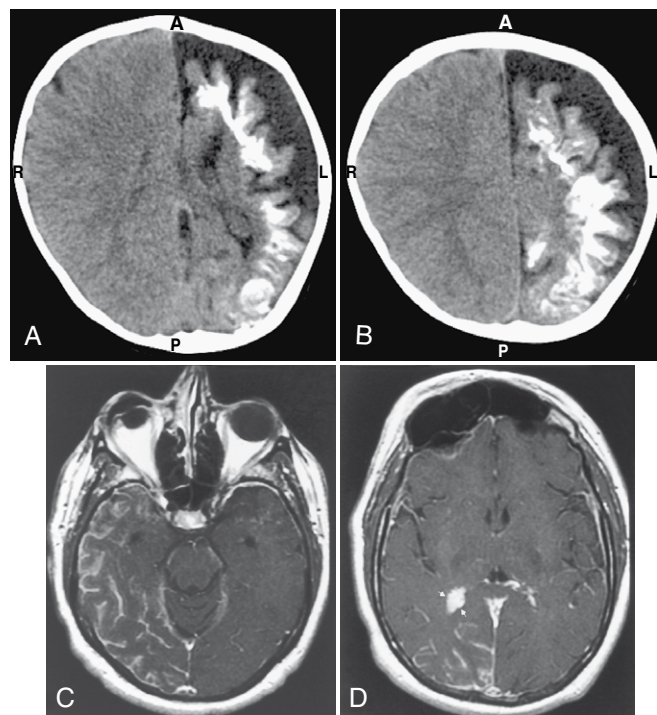


FIGURE 9-51. Sturge-Weber syndrome. **A**, This computed tomography scan shows gyriform and subcortical calcifications, atrophy of the affected left hemisphere, and an enlarged choroid glomus indicative of Sturge-Weber syndrome. **B**, The gyriform calcification versus subcortical calcification can also be represented higher up. **C**, This enhanced scan in another case shows diffuse meningeal and pial enhancement in the right temporal lobe. Note that the patient has had an enucleation on the right side secondary to a large angioma of the choroid of the right globe. **D**, The ancillary finding of enlargement of the choroid of the right lateral ventricle supports the diagnosis. Is the right frontal sinus enlarged suggestive of Dyke-Davidoff-Masson syndrome?

ischemia. Bilaterality of the vascular lesion is often seen on MR imaging.

On angiography, an increase in the number and size of the medullary veins with decreased cortical veins (anomalous venous drainage) and a capillary stain are usually seen in the parietal and occipital lobes. There is slow cerebral blood flow, and the ipsilateral cerebral arteries are generally small.

Keep your eyes on your patients' eyes! In nearly 50% of patients with Sturge-Weber syndrome you will find abnormal ocular enhancement, be it due to choroidal hemangiomas or inflammation from glaucoma. Visualization of ocular hemangiomas is increased with bilateral intracranial disease, extensive facial nevi, and ocular glaucoma.

The Wyburn-Mason syndrome may be a forme fruste of Sturge-Weber syndrome. Patients have a facial vascular nevus in cranial nerve V distribution, retinal angioma, and a midbrain arteriovenous malformation. The differential diagnosis also includes Klippel-Trenaunay-Weber syndrome (hemihypertrophy, cutaneous angiomas, varices, or anomalous venous drainage).

von Hippel-Lindau Disease

Central nervous system hemangioblastomas combine with retinal hemangioblastomas (67%); cysts of the kidney, pancreas, and liver; renal cell carcinomas; islet cell tumors; and adenomas to form von Hippel-Lindau disease (VHL). Diagnosis

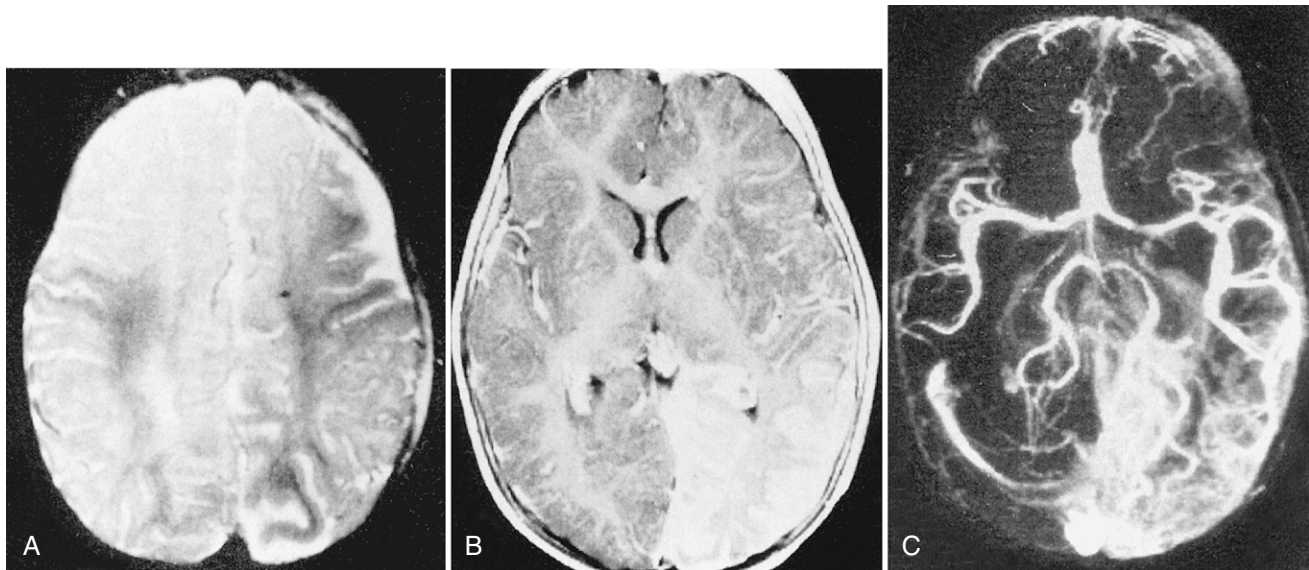


FIGURE 9-52. Sturge-Weber syndrome on magnetic resonance (MR) imaging. **A**, T2-weighted image (T2WI) demonstrates atrophic changes in the left hemisphere. Hypointensity is noted in the left occipital, posterior temporal region. There is also hypointensity on the contralateral side, although the atrophic changes are not as marked. **B**, Enhanced T1WI illustrates dense gyriiform enhancement in the occipital, posterior temporal region. **C**, Enhanced time-of-flight MR angiogram outlines dense vascularity in the lesion.

is based on a capillary hemangioblastoma of the CNS or retina and the presence of one VHL-associated tumor or a previous family history. Pheochromocytomas of the adrenal gland may also be present, linking the multiple endocrine neoplasia syndromes with VHL. Endolymphatic sac tumors have also been described with this entity. There also appears to be a link to neurofibromatosis.

Multiple CNS hemangioblastomas are the sine qua non of this syndrome, and they may arise in the cerebellum (most commonly), the medulla, the spinal cord or, less commonly, supratentorially. The lesions may be cystic, solid, or combined (see Chapter 3, especially Figs. 3-41 and 3-42). The classic description is a highly vascular, enhancing mural nodule associated with a predominantly cystic mass in the lateral cerebellum.

Spinal hemangioblastomas represent about 3% of spinal cord tumors. One third are associated with VHL. Of all spinal hemangioblastomas 80% are single, 20% multiple (almost all associated with VHL), 60% intramedullary, 11% both intramedullary and extramedullary, 21% intradural but purely extramedullary, and 8% extradural. Their location is usually characterized by the surgeons as “subpial.” They are more commonly found in the thoracic cord than the cervical cord. Most hemangioblastomas seen with VHL are 10 mm or less in size and may be intramedullary or along the dorsal nerve roots. It is extremely rare to see flow voids on MR imaging in hemangioblastomas under 15 mm in size—you will have to wait for the tumors to grow. On the other hand, a syrinx may be present in 40% to 60% of cases (often out of proportion to the small size of the tumor).

The disorder appears to be transmitted through autosomal dominant inheritance in 20% of cases on chromosome 3p25. Twenty percent of patients with hemangioblastomas of the cerebellum have VHL. Cerebellar hemangioblastomas ultimately develop in 83% of patients with VHL.

Meningiomatosis

Meningiomatosis, or meningioangiomatosis, refers to a disorder in which there is hamartomatous proliferation of meningeal cells via the intraparenchymal blood vessels into the cerebral

cortex. The leptomeninges are thick, infiltrated with fibrous tissue, and may be calcified. Cortical meningovascular fibroblastic proliferation along the Virchow-Robin spaces is also present with psammomatous calcification, causing a tram-track appearance. The lesion resembles Sturge-Weber syndrome, but no vascular abnormalities are present. Meningioangiomatosis may be considered a forme fruste of neurofibromatosis.

Neurocutaneous Melanosis

Another relatively obscure syndrome put in the classification of the phakomatoses is neurocutaneous melanosis. Melanoblasts from neural crest cells are present in the globes, skin, inner ear, sinonasal cavity, and leptomeninges and are the source of this disorder. It is characterized by cutaneous nevi and melanotic thickening of the meninges. Diffuse enhancement of the meninges of the brain and spine (20%) is seen; the melanin may (Fig. 9-53) or may not be detected on the pre-enhanced T1WI. Hydrocephalus, cranial neuropathies, and syringohydromyelia may develop.

Although malignant degeneration of the skin lesions is very uncommon, malignant transformation of CNS melanosis occurs in up to 50% of cases. When this occurs, parenchymal or intramedullary infiltration is the hallmark.

Neurocutaneous melanocytosis is usually a sporadic disease discovered in children due to hydrocephalus from gummed-up arachnoid villi. Multiple cranial neuropathies may develop.

Hereditary Hemorrhagic Telangiectasia

Hereditary hemorrhagic telangiectasia, also known as HHT or Osler-Weber-Rendu syndrome, is an entity consisting of mucocutaneous telangiectasias and visceral AVMs. One of the many presenting symptoms may be epistaxis secondary to sinonasal mucocutaneous telangiectasias. However, one should not forget that 5% of patients with HHT have a cerebral AVM and 2% of AVMs are associated with HHT. When a patient with HHT has one cerebral AVM, there is a 50% chance of a second AVM of the brain elsewhere. The AVMs may have a nidus (seen more frequently in adults) or may actually represent a fistula (more common in kids).

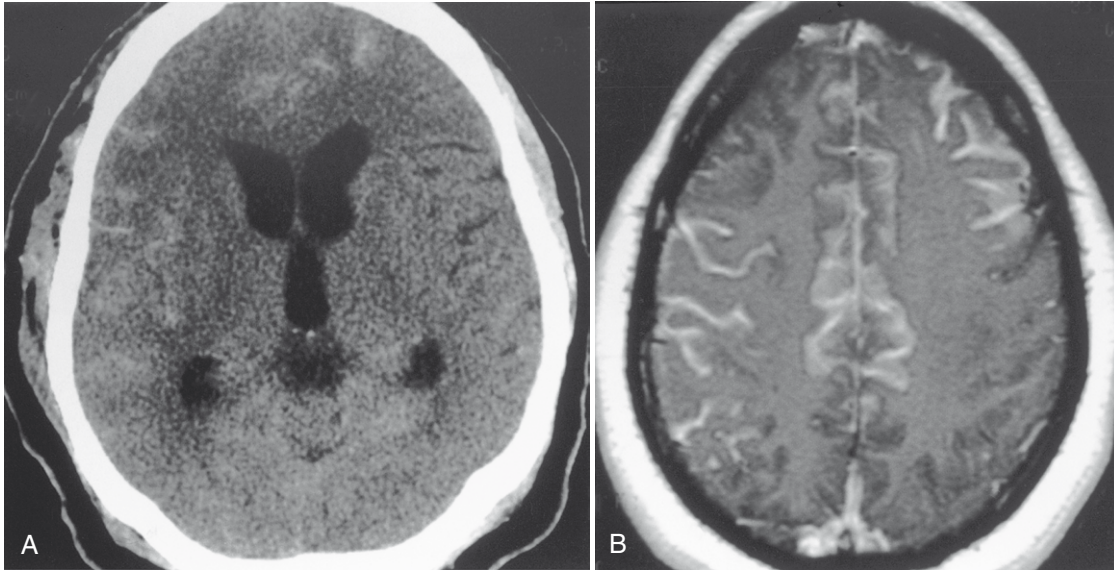


FIGURE 9-53. Neurocutaneous melanosis. **A**, This computed tomography scan shows hyperintensity to the sulci. First diagnosis is subarachnoid hemorrhage, but there was no blood in the basal cisterns. Next thought—meningitis? **B**, Precontrast T1-weighted image showed high intensity to the pia arachnoid. Hemorrhagic meningitis? No, neurocutaneous melanosis!

— CONGENITAL SPINAL ANOMALIES

Bony Disorders (see Chapter 17)

Many bony disorders are associated with spinal anomalies. Hypoplasia or incomplete development of the C1 arch or odontoid process is a common occurrence and may be asymptomatic. Occipitalization of the C1 vertebral body may be associated with atlantoaxial destabilization, however.

The Klippel-Feil anomaly refers to fusion of multiple cervical spine bodies. It may be associated with the Chiari malformations and syringohydromyelia. The C2–C3 and C5–C6 levels are the most common sites of fusion.

Meningoceles, Myeloceles, and Meningomyeloceles

The latest classification scheme for sorting among various congenital outpouchings of the spine separates the lesions into those that have an open defect to the skin surface versus those that are closed by a covering of skin. The closed defects are also separated into whether or not there is an associated mass. **Box 9-12** details this classification, which is useful also to radiologists.

The mechanism for development of spinal dysraphic conditions is a lack of folding of the primordial neural tissue into a tube. Thus, the skin remains lateral to the unfolded superficial neural ectoderm, leaving a midline defect. Although no bone is induced directly over the neural tissue, it may develop laterally where skin ectoderm and neural ectoderm are in continuity. The neural ectoderm is uncovered at birth. The size of the pia-arachnoid and CSF over the neural tissue is variable. Many of these disorders will be detected prenatally by serologic tests or amniocentesis (elevated α -fetoprotein level) and US (**Fig. 9-54**). Folate and multivitamin administration in prenatal vitamins has led to a decrease in the incidence of these lesions in the United States.

Meningocele, *myelocele*, *myelomeningocele*, and *lipo(myelo)meningocele* are terms used to describe the tissue extending through the bony spinal canal defect in a person with spinal dysraphism (**Fig. 9-55**). Together with the bony defect in the spine (usually seen in the lower lumbar or sacral region), there may be an opening in the skin, a dimple at the skin surface, or a hairy patch on the back. A *meningocele* refers to herniation of meninges alone without spinal cord or nerve roots into the defect in the bony spinal canal. This is an uncommon type of spinal anomaly (**Fig. 9-56**). Even rarer is the anterior sacral meningocele, where the mass protrudes into the pelvis, causing compression on the rectum or bladder. The anterior meningocele may be inapparent at the skin surface. Currarino’s triad refers to (1) anorectal malformation, (2) bony sacral defect, and (3) presacral mass (e.g., anterior sacral meningocele). These meningoceles are more common in NF-1 and Marfan syndrome.

A *myelocele* refers to herniation of the neural placode (a flat plate of unneurulated neural tissue) through the bony defect such that it lies flush with the surface of the skin of the back (see **Fig. 9-35**). The neural placode may also be evident with myelomeningoceles and is the “working part” of the now-opened lower spinal cord. Very little CSF is evident, and only a layer of arachnoid is present over the myelocele. A myelomeningocele contains meninges and either spinal cord or nerve root structures. The myelomeningocele is the most common form of open spinal dysraphism, dwarfing myeloceles; these entities are usually associated with Chiari II malformations and with syringohydromyelia,

Box 9-12. Classification of Spinal Defects

OPEN SPINAL DEFECTS

- Myelomeningocele (99%)
- Myelocele (1%)

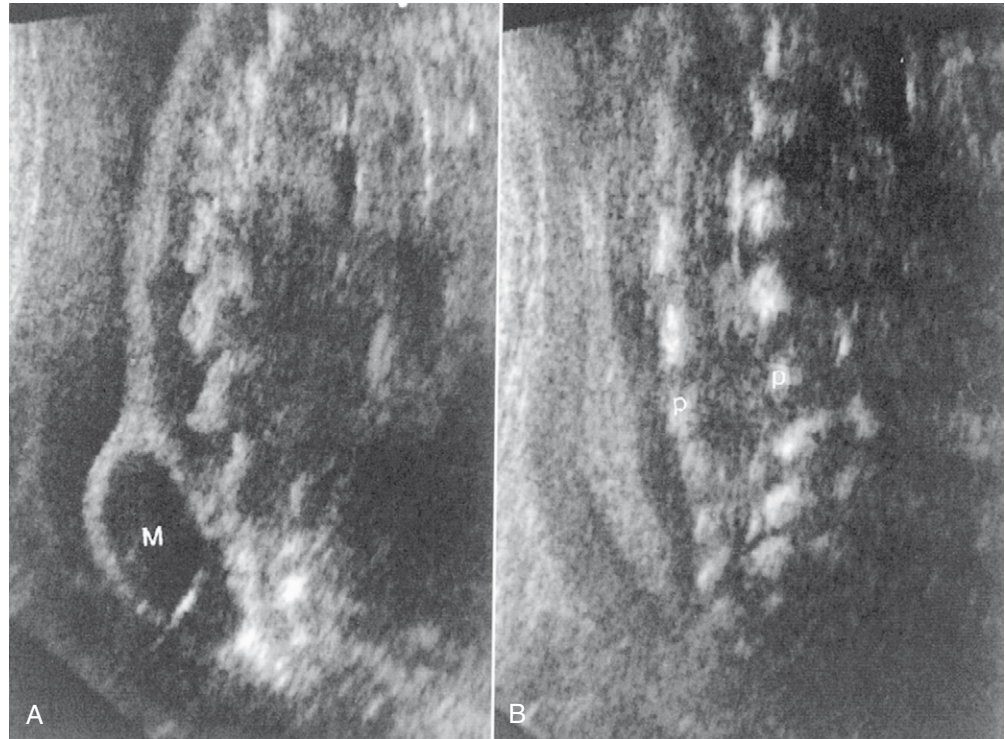
CLOSED SPINAL DEFECTS WITHOUT MASSES

- Lipomas
- Tight filum syndrome

CLOSED SPINAL DEFECTS WITH MASSES

- Lipomyelocele
- Lipomyelomeningocele
- Meningocele
- Myelocystocele

FIGURE 9-54. Meningocele. **A**, Ultrasound (US) reveals a cerebrospinal fluid collection (M) herniating through the spinal canal in this 20-week fetus. **B**, Coronal US through the spinal canal shows widening of the interpediculate distance (P) from the meningocele. (Compliments of Peggy Brennecke, MD.)



and the cord is tethered low. Myelomeningoceles are repaired quickly after birth, often without any preoperative imaging based on prenatal ultrasounds. Hydrocephalus coexists in 75% of cases, and the intracranial congenital defects may impact morbidity and mortality, more so than the spinal anomalies.



FIGURE 9-55. Myelomeningocele. It is rare to actually obtain a magnetic resonance image in an infant with a myelomeningocele because the child is usually sent right to surgery. Note the neural placode, enlarged spinal canal, and spinal dysraphism. Can you see the distal syrinx? Could that be the terminal ventricle (ventriculus terminalis) in a tethered, low conus (*arrow*)?

Meningoceles are one tenth as common as myelomeningoceles. In the lumbosacral region they are usually midline defects (80%), but they can also occur in the thoracic region laterally and may be associated with NF-1 or Marfan syndrome. They may progressively increase in size, causing posterior scalloping or enlarged foramina, and may even present as a presacral mass. All of these entities are usually associated with a low-lying, tethered conus medullaris below the L2–L3 disk. The normal termination of the conus after age 3 months is above the L2–L3 disk level; less than 2% of normal humans have a conus below the L2–L3 disk level. The clinical presentation of myelomeningoceles, meningoceles, or lipomyelomeningoceles that are not detected at birth includes hyperreflexia, bladder and bowel difficulties, and spasticity (Fig. 9-57).

The goal of therapy is to (1) enclose the defect into the intraspinal structures so that infection is prevented and (2) free up the distal end of the neural tube so that tethering does not occur as the patient grows. If tethering does occur, downward herniation of intracranial contents through the foramen magnum is a possibility. One of the complications of the surgery is production of fibrous tissue, which may rethether the dysraphic tissue (Fig. 9-58). On postoperative examination, you may not see a difference in the location of the conus medullaris from the preoperative location. Nonetheless, symptomatic improvement usually occurs even with no change in the site of the bottom of the cord. Presumably, CSF pulsations return to normal and the cord and hindbrain can move again.

Recall that, as opposed to meningoceles, myeloceles, and meningomyeloceles, which are lesions of absence of separation between cutaneous and neural ectoderm and are associated with Chiari malformations, lipomyeloceles and intradural lipomas are due to premature separation of these two types of ectoderm (abnormal neurulation). The abnormal migration of primitive mesenchymal cells to the neural placode leads to fat formation that connects superficial subcutaneous fat to the fat-containing neural placode via a midline defect in the posterior elements. If flat and within the spinal canal, call it a *lipomyelocele*; if protruding beyond the spinal boundaries and expands the CSF space, call it *lipomyelomeningocele*. They are NOT associated with Chiari malformations. Lipomyelomeningoceles have skin covering the dysraphism (closed). The fat may insert into the conus or along the dorsal surface of the conus with nerve roots anterior to the lipoma.

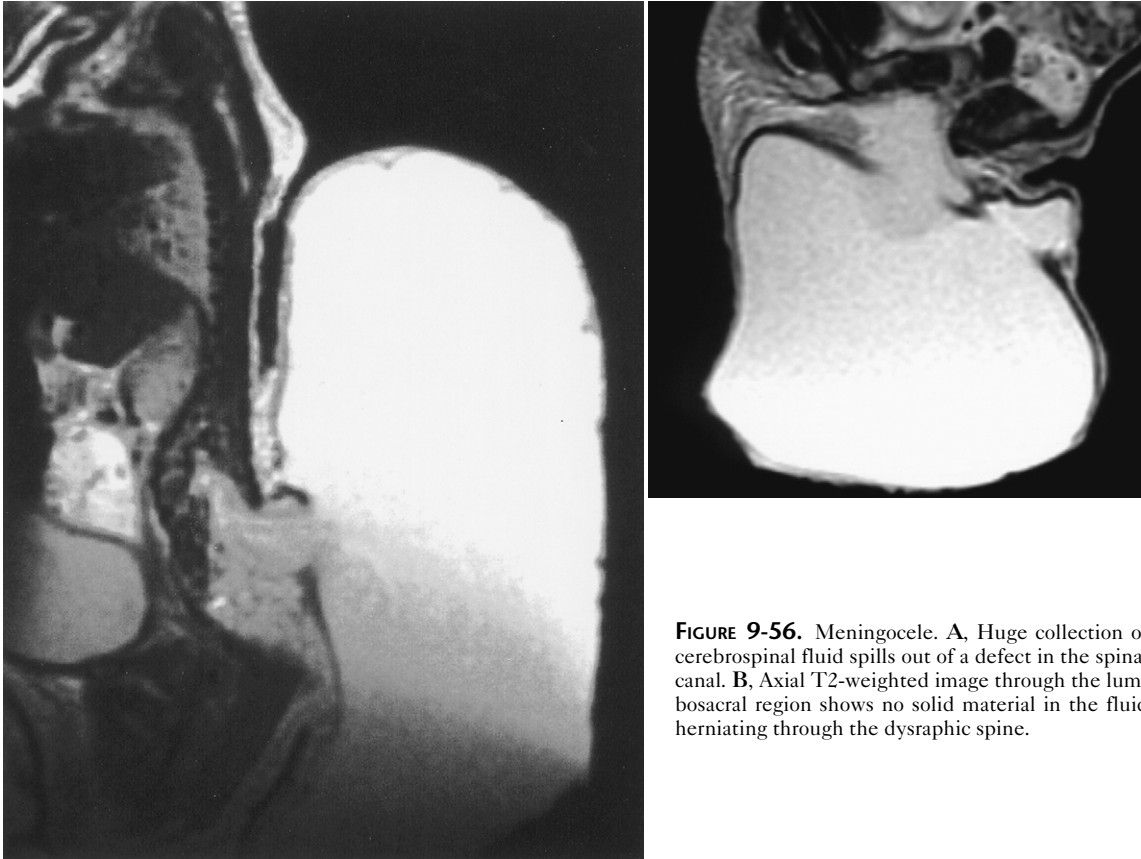


FIGURE 9-56. Meningocele. **A**, Huge collection of cerebrospinal fluid spills out of a defect in the spinal canal. **B**, Axial T2-weighted image through the lumbosacral region shows no solid material in the fluid herniating through the dysraphic spine.

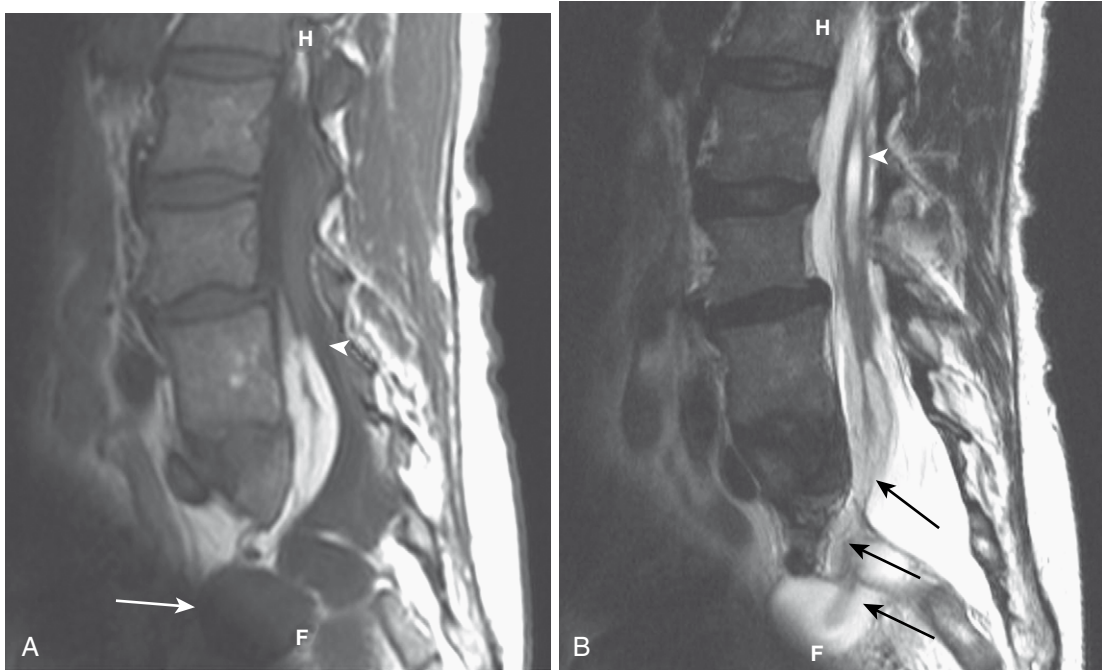


FIGURE 9-57. Lipomyelomeningocele. **A**, This is an unusual case because the defect in the spinal canal was anteriorly placed rather than posteriorly seen. Note the cystic component of the meningocele (*arrow*) as well as the tethering fat anteriorly (*arrowhead*). **B**, One gets a better appreciation of the neural elements (*arrows*) going through the anterior opening (myelocele) as well as the co-existent terminal syrinx (*arrowhead*).



FIGURE 9-58. Postoperative meningocele repair, now an adult. The sagittal T1-weighted image shows the postoperative defect from the myelomeningocele repair. The thickened filum extends to the operative defect and the conus termination is probably at the L3–L4 disk level, a bit low. The patient had spasticity and was losing bladder function. Could this be a normal postoperative appearance? The answer is yes, unfortunately.

Spina Bifida Occulta

With isolated spinal bifida occulta the skin surface of the back is normal; however, a cleft in the posterior elements of the vertebrae is seen. No myelomeningocele is present; however, this defect may be seen with tethered cords or diastematomyelia. Rarely one may have a skin-covered myelocystocele in which dura, arachnoid, and hydromyelic spinal cord are encysted under the skin, superficial to the spina bifida occulta. This entity is seen in patients with cloacal exstrophy. The hydromyelia communicates with the conus and the cyst communicates with the subarachnoid space.

Diastematomyelia

Diastematomyelia refers to a longitudinal split in the cord. The split may also involve the dura so that there may be two dural sacs (Type II) or, more commonly, two hemicords within one enlarged sac (Type I). In this case, two is not better than one. Usually this abnormality occurs in the lower thoracic-upper lumbar region and is associated with bony abnormalities 85% of the time, including spina bifida, widened interpediculate distances, hemivertebrae, tethered cord, and scoliosis. Hairy skin patches occur in 75% of cases. The separation of the spinal cord into two hemicords may be due to a bony spur, cartilaginous separation, or fibrous bands (Fig. 9-59). When this occurs, generally the cord reunites below the cleft. There often is some asymmetry in the size of the hemicords. A bony spur causing the diastematomyelia is more commonly associated with two separate dural sacs than a fibrous split. The cleft is between T8 and T12 25% of the time; 60% of the time it is in the lumbar region. Associated tethering of the conus medullaris, Chiari II malformations, myelomeningoceles (31% to 46%), and hydrosyringomyelia are common.

All of these neural tube defects are best evaluated with MR imaging in conjunction with CT. Although CT is useful in detecting the bony canal abnormalities and the bony spur between the diastematomyelia, MR imaging is superior in locating the distal portion of the conus medullaris and identifying the thickening of the filum terminale, the fatty component to the dysraphic state, and the presence of hemicords. Obviously, the presence or absence

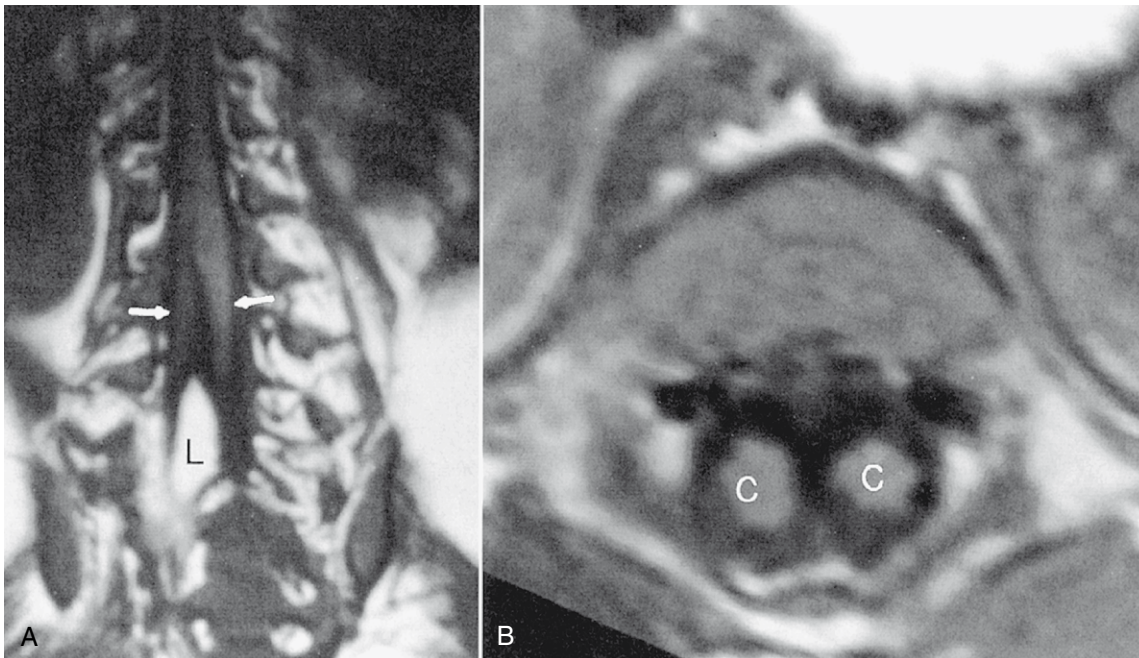


FIGURE 9-59. Diastematomyelia. **A**, Separation of two hemicords (arrows) with intervening cerebrospinal fluid is seen on coronal T1-weighted image (T1WI). Note the lipoma (L) below the level of the split. Spinal canal is markedly widened at the level of the diastematomyelia. **B**, Axial T1WI shows the two cords (C) with an enlarged thecal sac. A thin bony separation or fibrous band would not be readily detectable on magnetic resonance imaging and might be better seen with intrathecal contrast and axial computed tomography.

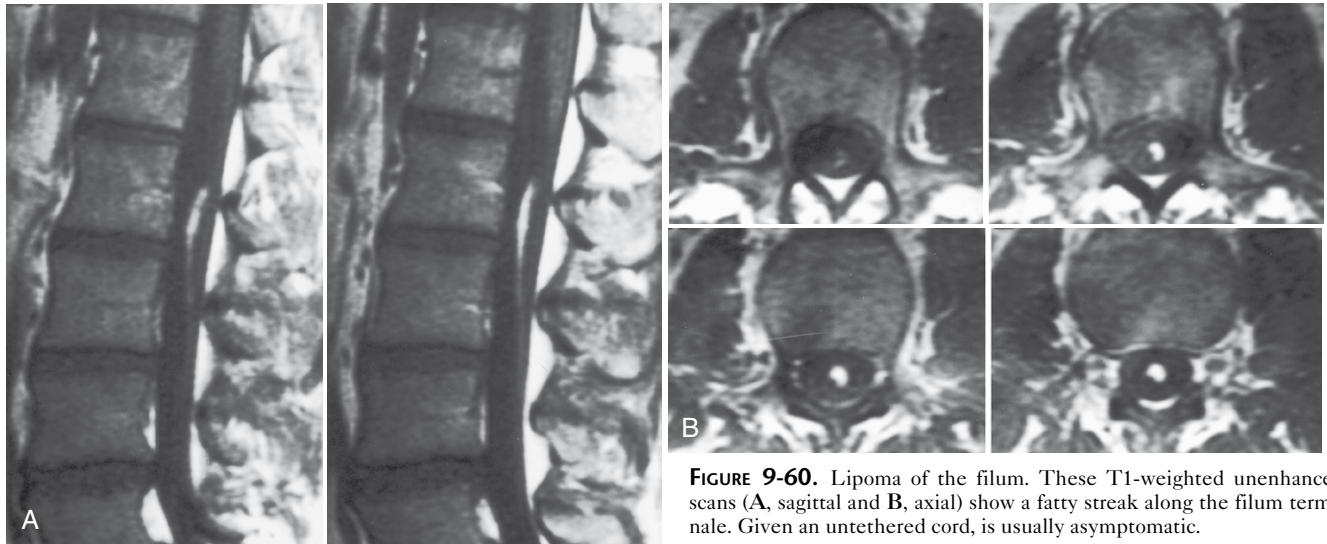


FIGURE 9-60. Lipoma of the filum. These T1-weighted unenhanced scans (A, sagittal and B, axial) show a fatty streak along the filum terminale. Given an untethered cord, is usually asymptomatic.

of a hydromyelic cavity within the spinal cord is better identified with MR imaging than with CT (see Chapter 17). A full examination of the patient who has spinal dysraphism should include MR evaluation of the skull base to assess for a Chiari malformation, the cervical spine to detect the hydromyelic cavity, the thoracolumbar portion of the spine to evaluate for the position of the conus medullaris and the identity of the structures protruding through the bony defect, and CT or plain films of the spine to evaluate for block vertebrae or hemivertebrae in other locations.

An extremely rare condition is diplomyelia, which in the strictest sense is a duplication of the spinal cord with a full set of motor and sensory roots emanating from each cord. Thus, two ventral and two dorsal roots are at each affected level. Most cases reported as diplomyelia are in fact cases of diastematomyelia where the two hemicords together provide a single set of nerve roots.

Abnormalities of the Filum Terminale

Lipomas of the filum terminale are another form of spinal dysraphism that may cause tethering of the cord. These lesions are identified as having fat density on CT or intensity on MR imaging (Fig. 9-60). Small amounts of fat in the filum are usually asymptomatic in kids and may be termed *fibrolipomas* or *filar lipomas*. As adults a small percentage of patients with filar lipomas have tight filum syndrome, which results in tethering. Here the filum terminale may be markedly thickened and tethered with or without fatty infiltration (Fig. 9-61). The conus medullaris may be dragged downward by the thick filum. The normal filum is less than 2 mm in cross-sectional diameter. Associated findings with a taut filum terminale (adult tethered cord syndrome) are kyphoscoliosis, midline bony defects in the lumbosacral part of the spine, and fatty infiltration

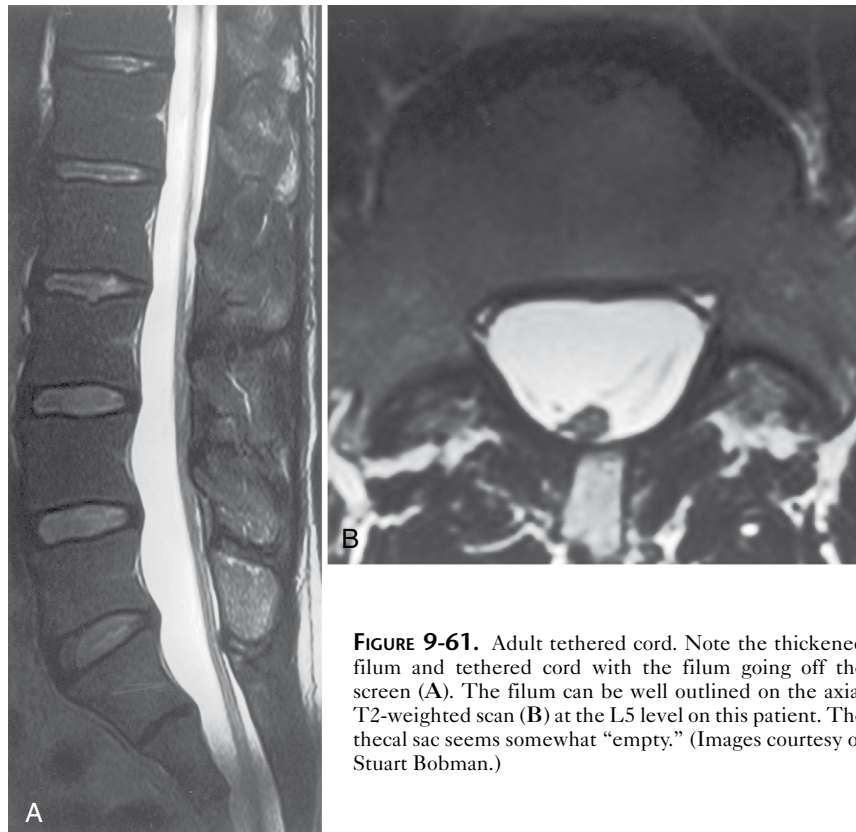


FIGURE 9-61. Adult tethered cord. Note the thickened filum and tethered cord with the filum going off the screen (A). The filum can be well outlined on the axial T2-weighted scan (B) at the L5 level on this patient. The thecal sac seems somewhat “empty.” (Images courtesy of Stuart Bobman.)

of the filum. Patients may develop conus ischemia, the dreaded sphincteric dysfunction, foot deformities, and abnormal gait.

Remember, intradural thoracic lipomas outnumber lumbosacral ones.

Caudal Regression Syndrome

In caudal regression syndrome you may see a truncated, blunt spinal cord in the lower thoracic level associated with incomplete formation of the sacrum, let alone the genitourinary-rectal tract. This entity is most commonly seen in children of diabetic mothers. Variable amounts of vertebral body fusion and stenoses may be seen, but the Aunt Minnie is the wedged-shaped distal cord terminating at the T12 region (Fig. 9-62). The cord may be tethered despite being high. The filum is thick. One can have myelocystoceles also.

Pilonidal Cysts

Pilonidal cysts are the most benign form of spinal dysraphism. The cord and thecal sac and vertebral column are normal. A tuft of hair with a small subcutaneous cyst is seen at the level of the coccyx. When a dermal sinus coexists, it is usually seen at a higher level. A dermal sinus has the potential to communicate with the thecal sac (Fig. 9-63). This is a nidus for spread of infection and must be removed in its entirety. It is caused by failure of separation of cutaneous ectoderm from neuroectoderm. Lumbosacral dermal sinus tracts outnumber occipital, thoracic, and cervical, in that order. The tract may be seen on MR, and dimpling of the thecal sac at the site of entry may be present. A dermoid or epidermoid tumor may coexist and may be intramedullary or extramedullary (see Fig. 17-14). Tethering may occur.

Marfan Syndrome

Dural ectasias can be seen in Marfan syndrome. If one measures the diameter of the dural sac and corrects for vertebral body

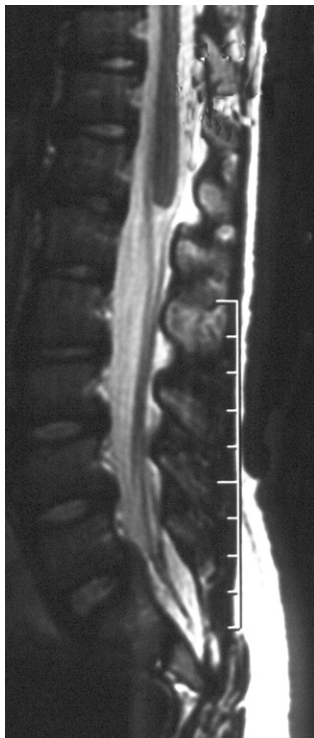


FIGURE 9-62. Caudal regression syndrome. Note the truncated appearance to the cord, rounded off like a pencil eraser. This, in association with sacral dysplasia, suggests caudal regression syndrome.

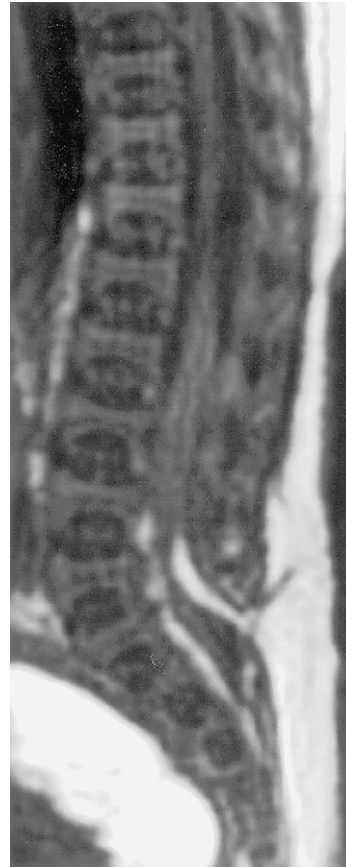


FIGURE 9-63. Dermal sinus tract. Follow the high-intensity fat on the T1-weighted image from the subcutaneous region into the spinal canal in this patient with a patent dermal sinus tract. The lumbosacral spine is dysraphic.

diameters, one finds that the dural sac ratios in patients with Marfan syndrome are increased compared with controls, particularly at L3 and S1. The sensitivity and specificity of dural ectasia for Marfan syndrome at either of these levels is 95% and 98%, respectively, using cutoff values of 0.47 for L3 and 0.57 for S1. Dural ectasia, after excluding neurofibromatosis as a cause, is considered a principal criterion for Marfan syndrome (see Fig. 16-33). Associated findings include widening of the canal, thinning of adjacent bone, enlargement of neural foramina, increased interpediculate distance, scalloping of the posterior vertebral body, and meningocele formation.

Genetic mutations associated with Marfan syndrome have been mapped to the long arm of chromosome 15 (*fibrillin-1* gene). Other manifestations include aortic dilation, dissection, or coarctation; lens dislocation (up and out); arachnodactyly; pectus excavatum; tall stature; osteopenia; dolichocephaly; pes planus; scoliosis; ligamentous laxity; glaucoma; mitral valve regurgitation; pulmonary cysts; and blue sclerae.

Lateral thoracic meningoceles are most commonly seen with NF-2, but can be seen in Marfan syndrome. Lehman syndrome includes wormian bones, hypoplastic atlas, and malar hypoplasia with lateral meningoceles. Ehlers-Danlos syndrome can also be associated.

Syringohydromyelia

A cavity in the cord may be due to central canal dilation (hydromyelia) or a cavity eccentric to the central canal (syrinx) (see Fig. 17-15). Because the resolution of most CT and some MR studies is not sufficient to distinguish these two entities, most neuroradiologists hedge and call the cavities *syringohydromyelia*.

Most hydromyelic cavities are associated with congenital spinal and hindbrain anomalies, such as Chiari malformations and myelomeningoceles. Most syringes are also congenital but may arise as a result of spinal cord trauma, ischemia, adhesions, or neoplasms (see Chapter 17). Be aware that at the conus medullaris level in neonates one may see the “fifth ventricle,” also called the *ventriculus terminalis*. This appears as an ovoid, non-enhancing, smooth dilation of the central canal with the signal intensity of CSF on all pulse sequences. This is a normal variant and is asymptomatic.

Although it used to be thought that syringomyelic cavities form in association with Chiari malformations due to transmitted pressures down the central canal from the fourth ventricle, most researchers now believe that the obstruction of CSF flow at the foramen magnum is to blame. The pulsatile systolic CSF flow from the spinal canal is driven into perivascular and interstitial spaces of the cord and then into the central canal.

Neurenteric Cysts

Neurenteric cysts are a form of congenital cyst in which the signal intensity on T1WI may be bright due to high protein. This is a cyst arising from failure of cleavage between the endodermic bronchial or gastrointestinal tract and the spinal system. The persistent connection (via the canal of Kovalsky) may be manifest as an intradural extramedullary cyst in the spinal canal (most commonly), but in some cases (<20%) may have a coexistent thoracic bronchoenteric cyst. More than 50% have vertebral segmentation anomalies, including but not limited to hemivertebrae, block vertebral bodies, Klippel-Feil syndrome, butterfly vertebrae, and fused vertebrae. Bony remodeling from the long-standing cyst may be present. The cyst is usually bright on T2WI and variable in signal intensity on T1WI. Fat is not present. Neurenteric cysts may lie anterior to the spinal canal as well as in the posterior mediastinum.

Dermal/Epidermal Cysts

When ectoderm persists within the infolding neural placode you can have epidermal and dermal rests, which may or may not communicate with the skin as dermal sinus tracts or dermoid/epidermoid cysts. The epidermoid cysts arise most commonly between T5 and T8, but the dermal sinus tracts occur most commonly in the lower lumbar-sacral regions (see Fig. 16-33). Although they may isolate intradurally or extradurally, they may span both compartments. Fat in the dermal lineage of lesions is characteristic, whereas restricted diffusion in epidermoid cysts is the *sine qua non*. A dermal sinus tract has an associated cyst intradurally in 50% of cases.

Remember that whereas epidermoids and dermoids are congenital rests containing epithelial rests or skin appendages, respectively, teratomas are true neoplasms arising from pluripotential stem cells and most commonly found in the sacrococcygeal region of neonates. Teratoma grading is defined in **Box 9-13**. These lesions are typified by cystic, calcified, and lipomatous components.

Box 9-13. Grading of Teratoma by Extent

- I: Protrudes externally with or without presacral component
- II: Protrudes externally and internally with intrapelvic mass
- III: Protrudes internally with pelvic and abdominal mass, minimal external component
- IV: Protrudes only internally in presacral space

SUGGESTED READINGS

Aida N, Nishimura G, Hachiya Y, et al: MR imaging of perinatal brain damage: comparison of clinical outcome with initial and follow-up MR findings, *AJNR Am J Neuroradiol* 19:1909–1921, 1998.

Altman NR, Naidich PP, Braffman BH: Posterior fossa malformations, *AJNR Am J Neuroradiol* 13:619–624, 1992.

Aoki S, Barkovich AJ, Nishimura K, et al: Neurofibromatosis types 1 and 2: cranial MR findings, *Radiology* 172:527–534, 1989.

Ashikaga R, Araki Y, Ono Y, et al: Appearance of normal brain maturation on fluid-attenuated inversion-recovery (FLAIR) MR images, *AJNR Am J Neuroradiol* 20:427–431, 1999.

Barkovich AJ: Analyzing the corpus callosum, *AJNR Am J Neuroradiol* 17:1643–1645, 1996.

Barkovich AJ: Imaging of the cobblestone lissencephalies, *AJNR Am J Neuroradiol* 17:615–618, 1996.

Barkovich AJ: MR of the normal neonatal brain: assessment of deep structures, *AJNR Am J Neuroradiol* 19:1397–1403, 1998.

Barkovich AJ: Neuroimaging manifestations and classification of congenital muscular dystrophies, *AJNR Am J Neuroradiol* 19:1389–1396, 1998.

Barkovich AJ: *Pediatric neuroimaging*, ed 3, Philadelphia, Lippincott Williams & Wilkins, 2000.

Barkovich AJ: Subcortical heterotopia: a distinct clinicoradiologic entity, *AJNR Am J Neuroradiol* 17:1315–1322, 1996.

Barkovich AJ, Edwards MSB, Cogen PH: MR evaluation of spinal dermal sinus tracts in children, *AJNR Am J Neuroradiol* 12:123–129, 1991.

Barkovich AJ, Ferriero DM, Bass N, Boyer R: Involvement of the pontomedullary corticospinal tracts: a useful finding in the diagnosis of X-linked adrenoleukodystrophy, *AJNR Am J Neuroradiol* 18:95–100, 1997.

Barkovich AJ, Fram EK, Norman D: Septo-optic dysplasia: MR imaging, *Radiology* 151:189–192, 1991.

Barkovich AJ, Girard N: Fetal brain infections, *Childs Nerv Syst* 19(7–8):501–507, 2003 Epub 2003 Jun 19.

Barkovich AJ, Gressens P, Evrard P: Formation, maturation, and disorders of brain neocortex, *AJNR Am J Neuroradiol* 13:423–446, 1992.

Barkovich AJ, Hajnal BL, Vigneron D, et al: Prediction of neuromotor outcome in perinatal asphyxia: evaluation of MR scoring systems, *AJNR Am J Neuroradiol* 19:143–149, 1998.

Barkovich AJ, Kjos BO: Nonlissencephalic cortical dysplasias: correlation of imaging findings with clinical deficits, *AJNR Am J Neuroradiol* 13:95–103, 1992.

Barkovich AJ, Kjos BO: Gray matter heterotopias: MR characteristics and correlation with developmental and neurologic manifestations, *Radiology* 182:493–499, 1992.

Barkovich AJ, Kjos BO, Norman D, et al: Revised classification of posterior fossa cysts and cystlike malformations based on the results of multiplanar MR imaging, *AJR Am J Roentgenol* 153:1289–1300, 1989.

Barkovich AJ, Kuzniecky RI, Dobyns WB, Jackson GD, Becker LE, Evrard P: A classification scheme for malformations of cortical development, *Neuropediatrics* 27(2):59–63, 1996.

Barkovich AJ, Kuzniecky RI, Jackson GD, Guerrini R, Dobyns WB: A developmental and genetic classification for malformations of cortical development, *Neurology* 65(12):1873–1887, 2005. Epub 2005 Sep 28.

Barkovich AJ, Rowley H, Bollen A: Correlation of prenatal events with the development of polymicrogyria, *AJNR Am J Neuroradiol* 16:822–827, 1995.

Barkovich AJ, Sargent SK: Profound asphyxia in the premature infant: imaging findings, *AJNR Am J Neuroradiol* 16:1837–1846, 1995.

Barkovich AJ, Westmark K, Partridge C, et al: Perinatal asphyxia: MR findings in the first 10 days, *AJNR Am J Neuroradiol* 16:427–438, 1995.

Barnes PD, Lester PD, Yamanashi WS, et al: Magnetic resonance imaging in infants and children with spinal dysraphism, *AJNR Am J Neuroradiol* 7:465–572, 1986.

Becker LE: Infections of the developing brain, *AJNR Am J Neuroradiol* 13:537–550, 1992.

Becker LE: Lysosomes, peroxisomes, and mitochondria: function and disorder, *AJNR Am J Neuroradiol* 13:609–620, 1992.

Ben-Omran TI, Blaser S, Phillips H, Callahan J, Feigenbaum A: Atypical phenotype in a boy with a maple syrup urine disease, *J Inherit Metab Dis* 29(1):195–200, 2006.

Blaser SI, Jay V: Disorders of cortical formation: radiologic-pathologic correlation, *Neurosurg Clin N Am* 13(1):41–62, 2002.

Braffman BH, Bilaniuk LT, Naidich TP, et al: MR imaging of tuberous sclerosis: pathogenesis of this phakomatosis, use of gadopentetate dimeglumine, and literature review, *Radiology* 183:227–238, 1992.

Bronen RA, Spencer DD, Fulbright RK: Cerebrospinal fluid cleft with cortical dimple: MR imaging marker for focal cortical dysgenesis, *Radiology* 214:657–663, 2000.

Castillo M, Quencer RM, Dominguez R: Chiari III malformation: imaging features, *AJNR Am J Neuroradiol* 13:107–113, 1992.

Davis PC, Hoffman JC Jr, Ball TI, et al: Spinal abnormalities in pediatric patient: MR imaging findings compared with clinical, myelographic, and surgical findings, *Radiology* 166:679–685, 1988.

Epelman M, Daneman A, Blaser SI, et al: Differential diagnosis of intracranial cystic lesions at head US: correlation with CT and MR imaging, *Radiographics* 26(1):173–196, 2006.

Fluss J, Blaser S, Chitayat D, et al: Molar tooth sign in fetal brain magnetic resonance imaging leading to the prenatal diagnosis of Joubert syndrome and related disorders, *J Child Neurol* 21(4):320–324, 2006.

- Ghai S, Fong KW, Toi A, Chitayat D, Pantazi S, Blaser S: Prenatal US and MR imaging findings of lissencephaly: review of fetal cerebral sulcal development, *Radiographics* 26(2):389–405, 2006.
- Ghazi-Birry HS, Brown WR, Moody DM, et al: Human germinal matrix: venous origin of hemorrhage and vascular characteristics, *AJNR Am J Neuroradiol* 18:219–229, 1997.
- Glenn OA, Barkovich AJ: Magnetic resonance imaging of the fetal brain and spine: an increasingly important tool in prenatal diagnosis, part 1, *AJNR Am J Neuroradiol* 27(8):1604–1611, 2006.
- Hamilton J, Blaser S, Daneman D: MR imaging in idiopathic growth hormone deficiency, *AJNR Am J Neuroradiol* 19:1609–1615, 1998.
- Milhorat TH, Chou MW, Trinidad EM, et al: Chiari I malformation redefined: clinical and radiographic findings in 364 symptomatic patients, *Neurosurgery* 44:1005–1014, 1999.
- Oosterhof T, Groenink M, Hulsmans F-J, et al: Quantitative assessment of dural ectasia as a marker for Marfan's syndrome, *Radiology* 220:514–518, 2001.
- Patronis NJ, Courcoutsakis N, Bromley CM, et al: Intramedullary and spinal canal tumors in patients with neurofibromatosis 2: MR imaging findings and correlation with genotype, *Radiology* 218:434–442, 2001.
- Raghavan N, Barkovich AJ, Edwards M, et al: MR imaging in the tethered spinal cord syndrome, *AJR Am J Roentgenol* 152:843–852, 1989.
- Ramaswamy V, Miller SP, Barkovich AJ, Partridge JC, Ferriero DM: Perinatal stroke in term infants with neonatal encephalopathy, *Neurology* 62(11):2088–2091, 2004.
- Samuelsson L, Bergstrom K, Thuomas K-A, et al: MR imaging of syringohydromyelia and Chiari malformations in myelo-meningocele patients with scoliosis, *AJNR Am J Neuroradiol* 8:539–546, 1987.
- Shah SS, Zimmerman RA, Rorke LB, Vezina LG: Cerebrovascular complications of HIV in children, *AJNR Am J Neuroradiol* 17:1913–1917, 1996.
- Shaw DWW, Cohen WA: Viral infections of the CNS in children: imaging features, *AJR Am J Roentgenol* 160:125–133, 1993.
- Smirniotopoulos JG, Murphy FM: Phakomatoses, *AJNR Am J Neuroradiol* 13:725–746, 1992.
- Takanashi J, Barkovich AJ, Ferriero DM, Suzuki H, Kohno Y: Widening spectrum of congenital hemiplegia: periventricular venous infarction in term neonates, *Neurology* 61(4):531–533, 2003.
- Thompson JE, Castillo M, Thomas D, et al: Radiologic-pathologic correlation polymicrogyria, *AJNR Am J Neuroradiol* 18:307–312, 1997.
- Truwit CL, Barkovich AJ: Pathogenesis of intracranial lipoma: an MR study in 42 patients, *AJR Am J Roentgenol* 155(4):855–864, 1990.
- Truwit CL, Barkovich AJ, Shanahan R, Maroldo TV: MR imaging of rhombencephalosynapsis: report of three cases and review of the literature, *AJNR Am J Neuroradiol* 12(5):957–965, 1991.
- Utsunomiya H, Takano K, Ogasawara T, et al: Rhombencephalosynapsis: cerebellar embryogenesis, *AJNR Am J Neuroradiol* 19:547–549, 1998.
- van der Knaap MS, Linnankivi T, Paetau A, et al: Hypomyelination with atrophy of the basal ganglia and cerebellum: follow-up and pathology, *Neurology* 69(2):166–171, 2007.
- Widjaja E, Blaser S, Miller E, et al: Evaluation of subcortical white matter and deep white matter tracts in malformations of cortical development, *Epilepsia* 48(8):1460–1469, 2007. Epub 2007 Apr 18.
- Widjaja E, Blaser S, Raybaud C: Diffusion tensor imaging of midline posterior fossa malformations, *Pediatr Radiol* 36(6):510–517, 2006. Epub 2006 Apr 21.
- Widjaja E, Nilsson D, Blaser S, Raybaud C: White matter abnormalities in children with idiopathic developmental delay, *Acta Radiol* 49(5):589–595, 2008.
- Wolf RL, Zimmerman RA, Clancy R, Haselgrove JH: Quantitative apparent diffusion coefficient measurements in term neonates for early detection of hypoxic ischemic brain injury: initial experience, *Radiology* 218:825–833, 2001.